UNIVERSITAT POLITÈCNICA DE CATALUNYA

Programa de doctorat:

AUTOMATITZACIÓ AVANÇADA I ROBÒTICA

Tesi doctoral

ACCUMULATION MOMENTS: THEORY AND APPLICATIONS

Judit Martínez

Director: Federico Thomas

Institut d'Organització i Control de Sistemes Industrials

Juny de 1998

Acknowledgements

I wish to express my sincere gratitude to Federico Thomas, whose guidance has shaped this thesis. I especially thank him for being a constant source of help and encouragement.

I also thank my friends and colleagues from the Institut de Cibernètica, and from the Institut de Robòtica i Informàtica Industrial, for so many interesting conversations and great times together.

Finally I cannot fail to mention the moral support I received from my family, and especially from Cèsar who deserves an honorary PhD in patience.

This work has been partially supported by:

- the REST project, from the Spanish CICYT under contract TIC96-0721-C02-01, and
- a grant from the Spanish Government, *Dirección General de Ensenãnza Superior* (PN TAP93-0451).

Contents

List of Figures

List of Tables

Chapter 1

Introduction

1.1 Motivation and background

Any computer vision application requires the selection of adequate features of the image. Since the information contained in these features is used in successive processing steps, their selection, for a specific task, is a relevant problem [120]. Image features can be local or global. Local features provide pixel-based information, that is, knowledge about the behavior of any pixel into its neighborhood. On the other hand, global features provide region-based information, that is, information about all the pixels inside a given region. Choosing either local or global features is task-dependent. Local features are commonly used in those processes requiring contour or region extraction while global features are used to identify and distinguish one region from another.

Deciding which is the appropriate set of global features is not a trivial task. It depends on the specific application; however, common feature requirements can be summarized in two points. On one hand, they have to provide enough task-oriented information. For instance, in pattern recognition, these features should be sufficient to identify and distinguish one region of the image from the others. In other applications, such as compression, they should allow to reconstruct the most significant parts of the image from a reduced set of them. On the other hand, they have to be computable using fast and memory-efficient algorithms, mainly in real-time applications.

The extraction of linear global features consists of projecting the image, defined as a bidimensional function, onto a set of basis functions. A specific type of global features, the geometric moments, sometimes also called standard moments, have been commonly used in computer vision applications [6, 8, 25, 32, 51, 63, 84, 90, 97]. They are obtained as the projection of the image onto a set of monomial functions. Most of the times, their use is motivated either by their straightforward geometrical interpretation or by the fact that some non-linear combinations of them yield invariant parameters to changes of scale, translation, rotation and reflection [2, 5, 9, 14, 21, 31, 40, 60, 83, 91, 92, 96, 99, 111, 112, 118]. Typical examples of applications involving moments are pattern recognition, edge detection, orientation determination, image normalization, image reconstruction,

and texture classification (see [89] for a survey).

However, the geometric interpretation of the so-called geometric moments is limited to moments up to second order, from which most invariants are defined. Hence, no formal interpretation of the information contained in higher order moments has been previously stated and no a priori criteria exist to decide which is the appropriate number of useful moments. Some empirical results can be found in [81] and [108], where the number of useful moments is related to the signal-to-noise ratio of the image.

The interpretation of higher order moments and their use in many applications has led to the analysis of the inverse problem, that is, the reconstruction of the image from a finite set of its moments. In all its instances, the inverse moment problem is universally recognized as a notoriously difficult inverse problem which often leads to the solution of very ill-posed systems of equations that do not have a unique solution [4, 46, 48, 93, 105].

In computer tomography, the X-rays of an object can be used to estimate the moments of the underlying mass distribution and, from these, the distribution itself. Recently, the relationship between the geometric moments of an image and those of its Radon transform has been stated in [70]. The relevance of this relationship is that Radon transform coefficients are physically obtained through tomography, which encompasses a wide variety of applications in such diverse areas as medical imaging, geophysical and oceanographic signal processing, computer vision and astronomy. The reconstruction of an image from its Radon coefficients is an active research field since the very beginning of tomographic applications.

In geophysical applications, the measurements of the exterior gravity field of a region can readily be converted into moment information, and from these, the mass density can be determined. In radiation field applications, an analog relation allows to obtain the moments of an electric charge distribution, and from these, the distribution itself.

Due to the finite number of bytes that any computer uses to represent a number, some numerical restrictions arise with regard to the largest and smallest value able to handle, as well as to the resolution able to handle. Although the former restriction does not normally constitute a problem in moment computation since the computer numerical range – defined as the ratio between its largest and smallest possible value – is large enough for common applications, resolution generates roundoff errors causing numerical instabilities. Because of these numerical instabilities the reconstruction process becomes ill-conditioned [13, 29, 47].

Hence, given the relevance of geometric moments, there has been an active interest in finding efficient algorithms for their computation either for binary [18, 42, 52, 53, 54, 56, 75, 85, 114, 115, 117] or gray-level images [16, 55, 68, 119]; even some hardware implementations have been proposed for real-time applications [33, 16, 103]. Likewise, two methods to solve the inverse problem have been proposed that are based either on Legendre polynomials [106, 61, 81, 82, 108] or on variational techniques [71, 73, 79]. A new approach is introduced in [65] that allows to reconstruct a band-limited or resolution-limited image. Ill-conditioning issues are addressed in [108], where it is experimentally shown for different kinds of noisy functions that, although the approximation error is

supposed to diminish as the number of known moments increases, there exists a limit in the number of useful moments in the reconstruction process.

1.2 Accumulation moments

Besides geometric moments, a number of other moments have been proposed in recent years. In general, any set of coefficients obtained by projecting an image onto a 2D discrete polynomial basis has generally been accepted as moments. Some examples are Legendre, Zernique, rotational and complex moments. These moments exhibit different degrees of noise sensibility, information redundancy, and discrimination power [108].

This thesis introduces a new set of moments to the above family: the accumulation moments [67]. The introduction of this new set of moments is motivated by the following fact. Let us assume a signal, $f(t)$, time-limited to the interval $0 \leq t \leq T$. Then, using the Laplace transform [87], it can be easily proved that its n-th order moment can be calculated as follows:

$$\int_0^T t^n f(t) = \frac{n!}{(-1)^{n+1}} \int_0^T \int_0^{t_n} \cdots \int_0^{t_2} \int_0^{t_1} f(T - t_0) dt_0 dt_1 \ldots dt_{n-1} dt_n. \tag{1.1}$$

Roughly speaking, the result of integrating a signal $n + 1$ times is directly related to its n-th order geometric moment. Also, from this formulation, it seems possible to compute moments of higher order using the intermediate steps required to obtain those of lower order, at least in part. Based on this possibility, a simple iterative algorithm for the efficient computation of grey-level image moments could be envisaged [66, 69], in the same way it was done in the binary domain in [42].

The thesis is essentially devoted to obtain the 2D discrete counterpart of (1.1); use it to reduce the computational complexity of some applications involving geometric moments; and, reconstruct an approximated image from them.

The discrete counterpart of (1.1) leads us to the introduction of what we call accumulation moments. We show how these moments can be obtained as projection coefficients onto a polynomial basis for which reason they can be properly called moments. We prove that this new global features are

- fast and easy to compute,
- easily related to commonly used features,
- interpretable in terms of commonly used image parameters such as bandwidth and spatial resolution, and
- allow the reconstruction of a bandwidth or resolution-limited image from a finite set of them.

The later aspect can be expressed into the more general framework of inverse problems [62, 64, 105] and we will show that it requires:

- solving its ill-posedness and
- solving its ill-conditioning.

1.3 Organization of the thesis

The thesis is structured in two parts. The first part encompasses the accumulation moment definition and their advantageous use, instead of geometric moments, in some applications. The second part refers to the inverse problem, that is, the reconstruction of an image from a reduced set of accumulation moments.

The first part is organized as follows. Chapter 2 introduces the concept of accumulation moments, both direct and reverse, and how they are connected to geometric moments. It is shown that they are obtained by simply accumulating image values along its rows or columns and, subsequently, accumulating the values of the resulting vector to yield a single number. If these accumulations are repeated several times on the already accumulated matrix or vector, the result is a set of numbers that are called accumulation moments. It is proved that sets of geometric and accumulation moments are related through a one-to-one linear transformation. Therefore, the information provided by a set of geometric moments up to a given order is preserved in the same amount of accumulation moments. In chapter 3, real-time computation aspects are considered. A hardware implementation scheme that only requires bit-serial adders and shift registers is proposed. In chapters 4 and 5, the connection between geometric and accumulation moments is exploited to provide computational advantages in three different applications. In particular, chapter 4 analyzes the use of accumulation moments to speed up the computation of geometric moments and their associated invariants. In chapter 5, accumulation moments are used as description parameters in sliding window applications. In general, description vectors obtained in a particular window location can be related to those in previous locations of the window if overlapping occurs. It is shown how the actualization cost drops from $O(m^3)$ to $O(m^2)$, where m refers to the amount of moments, when accumulation moments are used instead of geometric moments. Therefore, any application of this kind that traditionally required geometric moments can benefit from the use of accumulation moments. Finally, in chapter 6, a generalization of the presented concepts and results to higher dimensions is developed.

The second part is organized as follows. In chapter 7, the reconstruction of an image from a finite set of accumulation moments is carried out by accumulated subtractions. This is the most intuitive reconstruction method since it involves the inverse operations used to obtain accumulation moments from an image, using a process that we call backprojection. In chapter 8, the reconstructing problem is expressed in terms of a matrix-based reformulation of the series approximation of an image from a set of projection coefficients. This reformulation provides a geometric interpretation of both the least-squares approximation of the image and the so-called unitary approximation of the image from a reduced

set of projection coefficients. Then, in chapter 9, image reconstruction from a finite set of moments is set into this framework: moments are identified as projection coefficients. Ill-conditioning and ill-posedness of the inverse problem is analized in this context. It is shown how numerical instabilities of the reconstruction process can be explained in terms of the projection basis functions and they can be quantified in terms of the condition number of the Gram matrix, that is, the matrix containing the inner product between all the elements of the basis set. In chapter 10, it is shown how former reconstruction methods, i.e. the Legendre and variational methods, are incorrect because they both assume a continuous domain. The Legendre method is based on the use of orthogonal polynomials to obtain a least-squares approximation of the image. However, the Legendre polynomials are not orthogonal in the discrete domain as shown in this chapter. Variational methods (maximum entropy and minimum divergence methods) rely on optimization. Using Lagrange multipliers it is possible to obtain an explicit form of the reconstructed image in terms of an exponential function. However, this method implicitly assumes a continuous domain of the function to be minimized because it involves continuous derivatives and this is not the case. In chapter 11, two novel reconstructing methods are introduced. The first one is a reformulation of the Legendre method for orthogonal polynomials of discrete variable, that is, the Chebyshev polynomials. A least-squares approximated image is obtained in this case. The second one is called the unitary transform method because it obtains an approximation of the image using its truncated series expansion onto orthonormal basis sets. Depending on particular properties of the chosen basis set, it is possible to obtain a reconstructed image that satisfies some visual properties. In this sense, it allows to obtain a low-pass approximated image, if Fourier coefficients are used, or a low-resolution one, if Haar coefficients are used instead. In chapter 12, computational aspects are considered. Algebraic methods that decompose the whole reconstruction problem into simpler ones, thanks to the fact that the underlying basis functions that we are using are separable, are proposed. Singular value decomposition and iterative algorithms are also proposed to alleviate the ill-conditioning of required matrix inversion. In chapter 13, the particular case of binary images is considered. In this case, the reconstruction problem fits into the context of constraint satisfaction problems. Since the constraints involve all the variables, obtaining a solution is, in most cases, computational unfeasible. Nevertheless, a partial constraint satisfaction problem defined by moments up to first order has been efficiently solved using a sequential algorithm that allows to introduce local constraints in a simple way.

Finally, chapter 14 summarizes the contributions of this thesis, describes open problems and proposes several directions of future research.

1.4 Notation

A simple notation is used throughout this thesis to denote vectors and matrices. Lower case bold letters denote vectors and capital bold letters, matrices. We always use subscripts to denote their dimensions. For example, $\mathbf{v}_n$ denotes a columnwise vector and $\mathbf{v}_n[l]$, one of its elements, where l may range from 1 to n. Likewise, $\mathbf{Z}_{mn}$ denotes a matrix and $\mathbf{Z}_{mn}[k,l]$, its element (k,l), where k and l may range from 1 to m, and from 1 to

n, respectively; $\mathbf{Z}_{mn}[:, l]$ refers to its column l and $\mathbf{Z}_{mn}[k, :]$, to its row k. For simplicity, square matrices will only have one subscript. Superscripts are also used to denote any parameter on which a matrix depends.

Two unary matrix operations are used: $(\cdot)^t$ denotes the transpose of a given matrix and $(\cdot)^{-1}$, its inverse.

Given the vectors $\mathbf{v}_n$ and $\mathbf{w}_n$, $< \mathbf{v}_n, \mathbf{w}_n >= \mathbf{v}_n^t \mathbf{w}_n$ denotes their inner product. For the general case of two matrices $\mathbf{A}_{mn}$ and $\mathbf{B}_{mn}$, $< \mathbf{A}_{mn}, \mathbf{B}_{mn} >$ is defined as the inner product of the vectors constructed by sequentially reading each row of both matrices. If one of the matrices is separable, then $< \mathbf{A}_{mn}, \mathbf{B}_{mn} >=< \mathbf{A}_{mn}, \mathbf{x}_m \mathbf{y}_n^t >= \mathbf{x}_m^t \mathbf{A}_{mn} \mathbf{y}_n$ and, if both are, $< \mathbf{A}_{mn}, \mathbf{B}_{mn} >= < \mathbf{v}_m \mathbf{w}_n^t, \mathbf{x}_m \mathbf{y}_n^t >=< \mathbf{v}_m, \mathbf{x}_m >< \mathbf{w}_n, \mathbf{y}_n >$.

Part I

Obtaining the accumulation moments of an image

Chapter 2

Direct and reverse accumulation moments and how they are connected to geometric moments

There exist different kinds of moments depending on the polynomial basis set used in their definition (see [89] for a survey). In this chapter, we introduce a new set of moments: the accumulation moments [67]; and we show how they are connected to the widely used geometric moments. To this end, we start by defining what is a moment and its order.

Definition 2.0.1 (Moment). Given an image represented by matrix $\mathbf{I}_{ab}$, the coefficient g_{mn} obtained from:

$$g_{mn} = \sum_{x=1}^{a} \sum_{y=1}^{b} p_m(x) q_n(y) \mathbf{I}_{ab}[x, y], \tag{2.1}$$

where $p_m(x)$ and $q_n(y)$ are polynomials of order m and n, respectively, is defined as a *moment*.

Definition 2.0.2 (Moment order). The *order* of moment g_{mn} is defined as the ordered pair (m, n).

Note that this definition of moment order is different from the traditionally accepted one. A set of moments up to order (m, n) encompasses all moments g_{kl}, ranging from $k = 0$ to $m - 1$ and from $l = 0$ to $n - 1$. Then, they can be arranged as the elements of an $m \times n$ matrix. On the contrary, the traditional definition of order would refer to moments up to order $N = m + n$ as the ones contained in the upper-left triangular part of an $(m + n + 1) \times (m + n + 1)$ matrix.

2.1 Geometric moments

Definition 2.1.1 (Geometric moment matrix). The geometric moment of order (m, n) with respect to an arbitrary point (v, w) of a discrete image $\mathbf{I}_{ab}$ is defined as:

$$\mu_{mn}^{vw} = \sum_{x=1}^{a}\sum_{y=1}^{b}(x-v)^m(y-w)^n\mathbf{I}_{ab}[x,y]. \tag{2.2}$$

Then, the geometric moment matrix, $\mathbf{M}_{mn}^{vw}$, is defined as:

$$\mathbf{M}_{mn}^{vw}[k,l] = \mu_{k-1,l-1}^{vw}.$$

Theorem 2.1.1.

$$\mathbf{M}_{mn}^{vw} = (\mathbf{T}_m^v)^t\ (\mathbf{V}_{am})^t\ \mathbf{I}_{ab}\,\mathbf{V}_{bn}\,\mathbf{T}_n^w, \tag{2.3}$$

where

$$\mathbf{T}_p^q[k,l] = \begin{cases} \binom{l-1}{k-1}(-q)^{l-k}, & \text{if} \quad l \geq k, \\ 0, & \text{otherwise}, \end{cases} \tag{2.4}$$

and $\mathbf{V}_{pq}$ *is a non-square Vandermode matrix of general term*

$$\mathbf{V}_{pq}[k,l] = k^{l-1}. \tag{2.5}$$

Proof. The decomposition of the binomials in (2.2) into adding terms leads to:

$$\mu_{m,n}^{vw} = \sum_{x=1}^{a}\sum_{y=1}^{b}\sum_{i=0}^{m}\sum_{j=0}^{n}\binom{m}{i}(-v)^{m-i}x^i\binom{n}{j}(-w)^{n-j}y^j\mathbf{I}_{ab}[x,y].$$

Then, expanding the summatories into a vector-matrix form, one obtains:

$$\mu_{m,n}^{vw} = \begin{pmatrix} \binom{m}{0}(-v)^m \\ \binom{m}{1}(-v)^{m-1} \\ \vdots \\ \binom{m}{m} \end{pmatrix}^t \begin{pmatrix} 1 & 1 & \dots & 1 \\ 1 & 2 & \dots & a \\ \dots & \dots & \dots & \dots \\ 1 & 2^m & \dots & a^m \end{pmatrix} \mathbf{I}_{ab} \begin{pmatrix} 1 & 1 & \dots & 1 \\ 1 & 2 & \dots & 2^n \\ \dots & \dots & \dots & \dots \\ 1 & b & \dots & b^n \end{pmatrix} \begin{pmatrix} \binom{n}{0}(-w)^n \\ \binom{n}{1}(-w)^{n-1} \\ \vdots \\ \binom{n}{n} \end{pmatrix}.$$

Finally, when moments up to order $(m-1, n-1)$ are grouped into the geometric moment matrix, vectors turn into matrices and equation (2.3) is obtained.

□

Corollary 2.1.1.

$$\mathbf{M}_{mn} = (\mathbf{V}_{am})^t \, \mathbf{I}_{ab} \, \mathbf{V}_{bn}. \tag{2.6}$$

Corollary 2.1.2 (Steiner theorem).

$$\mathbf{M}^{vw}_{mn} = (\mathbf{T}^v_m)^t \, \mathbf{M}_{mn} \, \mathbf{T}^w_n. \tag{2.7}$$

Since $\mathbf{T}^q_p$ are triangular matrices, any geometric moment of an image positioned at an arbitrary point can be obtained from the geometric moments of the same order and lower of the image positioned at the origin. Note also that each matrix $\mathbf{T}^q_p$ accounts for a translation along either x or y axes.

Property 2.1.1.

$$(\mathbf{T}^q_p)^{-1} = \mathbf{T}^{-q}_p. \tag{2.8}$$

2.2 Direct accumulation moments

Definition 2.2.1 (Direct accumulation moment matrix). The direct accumulation moment of order $(k-1, l-1)$ of matrix $\mathbf{I}_{ab}$ is the value of $\mathbf{I}_{ab}[a, b]$ after top-down accumulating its columns k times (i.e., after applying k times the assignment $\mathbf{I}_{ab}[i+1, j] \leftarrow \mathbf{I}_{ab}[i+1, j] + \mathbf{I}_{ab}[i, j]$, for $i = 1$ to $a-1$, and for $j = 1$ to b), and accumulating the resulting last row from left to right l times (i.e., after applying l times the assignment $\mathbf{I}_{ab}[a, j+1] \leftarrow \mathbf{I}_{ab}[a, j+1] + \mathbf{I}_{ab}[a, j]$, for $j = 1$ to $b-1$). The direct accumulation moment matrix is defined so that $\mathbf{L}_{mn}[k, l]$ is the direct accumulation moment of order $(k-1, l-1)$.

This definition is better understood through an example.

Example 2.2.1. Consider the matrix

$$\begin{pmatrix} 0 & 2 & 3 \\ 1 & 0 & 8 \\ 1 & 1 & 1 \end{pmatrix}. \tag{2.9}$$

According to the definition, its direct accumulation moment of order $(1, 2)$ is computed by top-down accumulating its columns twice and then left-right accumulating the resulting last row three times. The first and second columnwise accumulations lead to

$$\begin{pmatrix} 0 & 2 & 3 \\ 1 & 2 & 11 \\ 2 & 3 & 12 \end{pmatrix} \text{ and } \begin{pmatrix} 0 & 2 & 3 \\ 1 & 4 & 14 \\ 3 & 7 & 26 \end{pmatrix},$$

respectively, and the three accumulations of the last row to

$$\begin{pmatrix} 3 & 10 & 36 \end{pmatrix}, \begin{pmatrix} 3 & 13 & 49 \end{pmatrix} \text{ and } \begin{pmatrix} 3 & 16 & 65 \end{pmatrix}.$$

Then, it is said that the direct accumulation moment of order $(1, 2)$ of matrix (2.9) is 65.

Obviously, the same result would be obtained if the rows were accumulated from left to right three times and the resulting last column, top-down accumulated twice.

Any set of coefficients obtained by projecting an image onto a 2D discrete polynomial basis has generally been accepted as moments. Although it does not seem to be the case for the set of values just introduced, this polynomial relationship will be proved in chapter 9. Here, we prove that any complete set of accumulation moments up to a given order can be obtained from a set of geometric moments up to the same order. Actually, this property is satisfied by any set of moments.

It can be easily shown that the direct accumulation moment of order $(k-1, l-1)$ can be expressed, in terms of the image, as

$$\mathbf{L}_{mn}[k,l] = \sum_{r=1}^{a} \sum_{s=1}^{b} \binom{a-r+k-1}{a-r} \mathbf{I}_{ab}[r,s] \binom{b-s+l-1}{b-s}. \tag{2.10}$$

Then, we can write

$$\mathbf{L}_{mn} = (\mathbf{Q}_{am})^t \, \mathbf{I}_{ab} \, \mathbf{Q}_{bn}, \tag{2.11}$$

where $\mathbf{Q}_{pq}$ is an up-down-flipped non-square Pascal matrix of general term

$$\mathbf{Q}_{pq}[k,l] = \binom{p-k+l-1}{p-k}. \tag{2.12}$$

Theorem 2.2.1. *Matrix $\mathbf{Q}_{pq}$ can be factored as follows:*

$$\mathbf{Q}_{pq} = \mathbf{V}_{pq} \, \mathbf{G}_q^p, \tag{2.13}$$

where $\mathbf{V}_{pq}$ is a Vandermonde matrix and $\mathbf{G}_q^p$ an upper triangular matrix.

Proof. The combinatorial number in (2.12) can be decomposed into its multiplicative terms as follows:

$$\binom{p-k+l-1}{p-k} = \frac{(p-k+l-1)!}{(p-k)!(l-1)!} = \frac{(-1)^{l-1}}{(l-1)!} (k+\beta_{l-1}^p)(k+\beta_{l-2}^p) \cdots (k+\beta_1^p); \tag{2.14}$$

where $\beta_i^p = -p-i$, with $i = 1, \ldots, (l-1)$.

If this expression is considered as a polynomial in k, it can be directly expressed in terms of its coefficients instead of its roots (see [7] for details) leading to:

$$(k+\beta_{l-1}^p)(k+\beta_{l-2}^p)\cdots(k+\beta_1^p) = k^{l-1} + B_{1,l-1}^p k^{l-2} + \cdots + B_{l-1,l-1}^p,$$

where

$$\begin{aligned}
B_{1,l-1}^p &= \sum_{i_1=1}^{l-1} \beta_{i_1}^p \\
B_{2,l-1}^p &= \sum_{\substack{i_1,i_2=1 \\ i_1<i_2}}^{l-1} \beta_{i_1}^p \beta_{i_2}^p \\
B_{3,l-1}^p &= \sum_{\substack{i_1,i_2,i_3=1 \\ i_1<i_2<i_3}}^{l-1} \beta_{i_1}^p \beta_{i_2}^p \beta_{i_3}^p \\
&\vdots \\
B_{l-1,l-1}^p &= \beta_{i_1}^p \beta_{i_2}^p \cdots \beta_{i_{l-1}}^p,
\end{aligned} \tag{2.15}$$

and $B_{r,s}^p = 1$, either if $r = 0$ or $s = 0$.

Then, in vector form,

$$\mathbf{Q}_{pq}[k,l] = \frac{(-1)^{l-1}}{(l-1)!} \begin{pmatrix} 1 & k & \ldots & k^{l-1} \end{pmatrix} \begin{pmatrix} B_{l-1,l-1}^p \\ B_{l-2,l-1}^p \\ \vdots \\ B_{1,l-1}^p \\ 1 \end{pmatrix}.$$

Considering all the elements of matrix $\mathbf{Q}_{pq}$, the above vector product turns into the matrix product stated in equation (2.13), where

$$\mathbf{G}_q^p[k,l] = \begin{cases} \frac{(-1)^{l-1}}{(l-1)!} B_{l-k,l-1}^p, & \text{if } l \geq k, \\ 0, & \text{otherwise,} \end{cases} \tag{2.16}$$

is a square upper triangular non-singular matrix.

□

Using theorem 2.2.1 and corollary 2.1.1, the following result is obtained.

Corollary 2.2.1. *Direct accumulation moments can be expressed in terms of geometric moments and vice versa as:*

$$\mathbf{L}_{mn} = (\mathbf{G}_m^a)^t \, \mathbf{M}_{mn} \, \mathbf{G}_n^b, \tag{2.17}$$

and

$$\mathbf{M}_{mn} = \left((\mathbf{G}_m^a)^{-1}\right)^t \mathbf{L}_{mn} \left(\mathbf{G}_n^b\right)^{-1}, \tag{2.18}$$

respectively.

Corollary 2.2.2. *Since $\mathbf{G}_m^a$ and $\mathbf{G}_n^b$ are upper triangular matrices, the geometric moment of order (m, n) of an image can be obtained from the accumulation moments up to order (m, n) and vice versa.*

Values for $(\mathbf{G}_n^a)^{-1}$ and $\left(\mathbf{G}_m^b\right)^{-1}$ can be obtained by numerically inverting $\mathbf{G}_n^a$ and $\mathbf{G}_m^b$, respectively.

Example 2.2.2.

$$\left(\mathbf{G}_4^{16}\right)^{-1} = \begin{pmatrix} 1 & 17 & 289 & 4913 \\ 0 & -1 & -35 & -919 \\ 0 & 0 & 2 & 108 \\ 0 & 0 & 0 & -6 \end{pmatrix},$$

$$\left(\mathbf{G}_5^{16}\right)^{-1} = \begin{pmatrix} 1 & 17 & 289 & 4913 & 83521 \\ 0 & -1 & -35 & -919 & -21455 \\ 0 & 0 & 2 & 108 & 3890 \\ 0 & 0 & 0 & -6 & -444 \\ 0 & 0 & 0 & 0 & 24 \end{pmatrix},$$

and

$$\left(\mathbf{G}_4^{17}\right)^{-1} = \begin{pmatrix} 1 & 18 & 324 & 5832 \\ 0 & -1 & -370 & -1027 \\ 0 & 0 & 2 & 114 \\ 0 & 0 & 0 & -6 \end{pmatrix}$$

Note the increasing dispersion in the elements of $\left(\mathbf{G}_q^p\right)^{-1}$ as p and q increase. This suggests an underlying numerical ill-conditioning due to roundoff errors as the order increases, as it will be explained in chapter 9. A measure of the ill-conditioning in the inversion of $\mathbf{G}_q^p$ is given by its condition number, that is the ratio between its largest and its smallest eigenvalue, for different values of p and q. The results are plotted in figure 2.1a and 2.1b, for increasing values of q and p, respectively. It shows that, although $\mathbf{G}_q^p$ is non-singular, its inverse for high order moments or large images cannot be accurately computed.

Next, it is explored the possibility of accumulating image values in the opposite directions for a better conditioned relationship with the geometric moments. This is encouraged by the fact that, while direct accumulation moments are more sensitive to variations of pixel values that are close to the origin, geometric moments are more influenced by those far from it.

2.3 Reverse accumulation moments

Definition 2.3.1 (Reverse accumulation moment matrix). The reverse accumulation moment of order $(k-1, l-1)$ of matrix $\mathbf{I}_{ab}$ is the value of $\mathbf{I}_{ab}[1, 1]$ after bottom-up

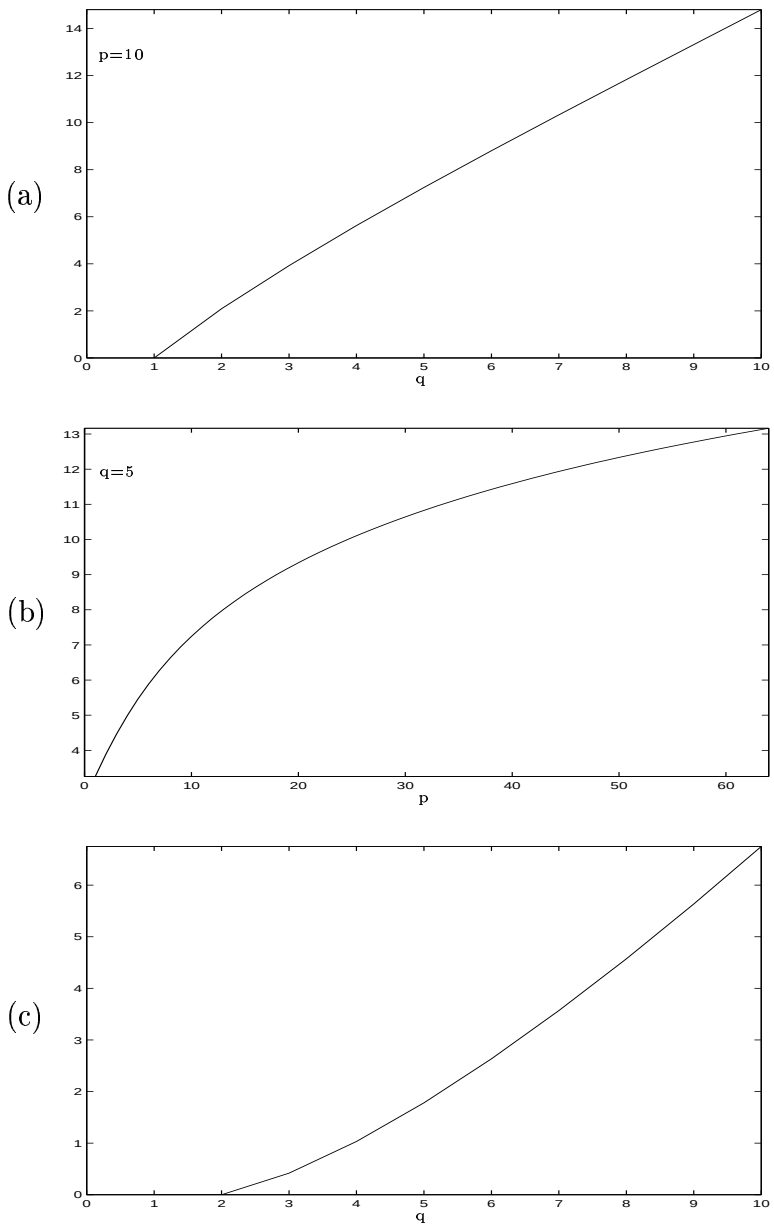

Figure 2.1: *(a) Condition number of* $\mathbf{G}_q^p$ *as a function of* q *and (b) as a function of* p*. (c) Condition number of* $\mathbf{H}_q$ *as a function of* q*. The vertical scale is given in powers of ten.*

accumulating its columns k times (i.e., after applying k times the assignment $\mathbf{I}_{ab}[a-i,j] \leftarrow \mathbf{I}_{ab}[a-i,j]+\mathbf{I}_{ab}[a-i+1,j]$, for $i=1$ to $a-1$, and for $j=1$ to b), and accumulating the resulting first row from right to left l times (i.e., after applying l times the assignment $\mathbf{I}_{ab}[1,b-j] \leftarrow \mathbf{I}_{ab}[1,b-j]+\mathbf{I}_{ab}[1,b-j+1]$, for $j=1$ to $b-1$). The reverse accumulation moment matrix is defined so that $\mathbf{R}_{mn}[k,l]$ is the reverse accumulation moment of order $(k-1,l-1)$.

Example 2.3.1. Using the same matrix as in example 2.2.1, the reverse accumulation moment of order $(1,2)$ requires two columnwise accumulations, which leads to

$$\begin{pmatrix} 2 & 3 & 12 \\ 2 & 1 & 9 \\ 1 & 1 & 1 \end{pmatrix} \text{ and } \begin{pmatrix} 5 & 5 & 22 \\ 3 & 2 & 10 \\ 1 & 1 & 1 \end{pmatrix}$$

respectively, and the three right-to-left accumulations of the first row to

$$\begin{pmatrix} 32 & 27 & 22 \end{pmatrix}, \begin{pmatrix} 81 & 49 & 22 \end{pmatrix} \text{ and } \begin{pmatrix} 152 & 71 & 22 \end{pmatrix}.$$

Then, it is said that the reverse accumulation moment of order $(1,2)$ of matrix (2.9) is 152.

It can be easily shown that the reverse accumulation moment of order $(k-1,l-1)$ can be expressed, in terms of the image, as:

$$\mathbf{R}_{mn}[k,l] = \sum_{r=1}^{a}\sum_{s=1}^{b} \binom{r+k-2}{r-1} \mathbf{I}_{ab}[r,s] \binom{s+l-2}{s-1}. \tag{2.19}$$

Then, we can write

$$\mathbf{R}_{mn} = (\mathbf{P}_{am})^t \, \mathbf{I}_{ab} \, \mathbf{P}_{bn}, \tag{2.20}$$

where $\mathbf{P}_{pq}$ is a non-square Pascal matrix of general term:

$$\mathbf{P}_{pq}[k,l] = \binom{k+l-2}{k-1}. \tag{2.21}$$

Theorem 2.3.1. *Matrix $\mathbf{P}_{pq}$ can be factored as follows:*

$$\mathbf{P}_{pq} = \mathbf{V}_{pq} \, \mathbf{H}_q, \tag{2.22}$$

where $\mathbf{H}_q$ is an upper triangular matrix.

Proof. The development of the combinatorial number in (2.21), as in the proof of theorem 2.2.1, leads to:

$$\mathbf{P}_{pq}[k,l] = \frac{1}{(l-1)!} \begin{pmatrix} 1 & k & \dots & k^{l-1} \end{pmatrix} \begin{pmatrix} (-1)^{l-1} B^{-1}_{l-1,l-1} \\ (-1)^{l-2} B^{-1}_{l-2,l-1} \\ \vdots \\ (-1) B^{-1}_{1,l-1} \\ 1 \end{pmatrix}.$$

Considering all the elements of matrix $\mathbf{P}_{pq}$, the vector product turns into the matrix product stated in equation (2.22), where

$$\mathbf{H}_q[k,l] = \begin{cases} \frac{(-1)^{l-k}}{(l-1)!}\, B^{-1}_{l-k,l-1}, & \text{if } \; l \geq k \\ 0, & \text{otherwise,} \end{cases} \tag{2.23}$$

is a square upper triangular non-singular matrix and

$$B^r_{p,q} = \sum_{\substack{i_1,i_2,\ldots,i_p=1 \\ i_1<i_2<\cdots<i_p}}^{q} (-r-i_1)(-r-i_2)\ldots(-r-i_p).$$

□

Using theorem 2.3.1 and corollary 2.1.1, the following result is obtained.

Corollary 2.3.1. *Reverse accumulation moments can be expressed in terms of geometric moments and vice versa as:*

$$\mathbf{R}_{mn} = (\mathbf{H}_m)^t\, \mathbf{M}_{mn}\, \mathbf{H}_n \tag{2.24}$$

and

$$\mathbf{M}_{mn} = \left((\mathbf{H}_m)^{-1}\right)^t\, \mathbf{R}_{mn}\, (\mathbf{H}_n)^{-1}, \tag{2.25}$$

respectively.

The condition number of $\mathbf{H}_p$ as a function of p is shown in figure 2.1c. Clearly, the relationship between reverse accumulation moments and geometric moments, besides being independent from the size of the image, is better conditioned as suspected, so that it is more interesting for reliable computations.

Now, it is possible to directly relate direct and reverse accumulation moments.

Theorem 2.3.2.

$$\mathbf{G}^q_p = \mathbf{D}_p\, \mathbf{T}^{-(q+1)}_p\, \mathbf{H}_p, \tag{2.26}$$

where $\mathbf{D}_p$ *is a diagonal matrix of the form* $\mathbf{D}_p[k,k] = (-1)^{k-1}$.

Proof. From definitions 2.2.1 and 2.3.1, it is obvious that the direct accumulation moments of an image $\mathbf{I}_{ab}[k,l]$ and the reverse accumulation moments of the reflected and displaced image $\mathbf{I}_{ab}[(a+1)-k,(b+1)-l]$ are equal. Let us distinguish the moment matrices associated with each image by numbering them 1 and 2, respectively. Then, it can be proved that the relationship between the geometric moments of both images is

$$\mathbf{M2}_{mn} = \left(\mathbf{T}^{-(a+1)}_m\right)^t\, \mathbf{D}_m\, \mathbf{M1}_{mn}\, \mathbf{D}_n\, \mathbf{T}^{-(b+1)}_n,$$

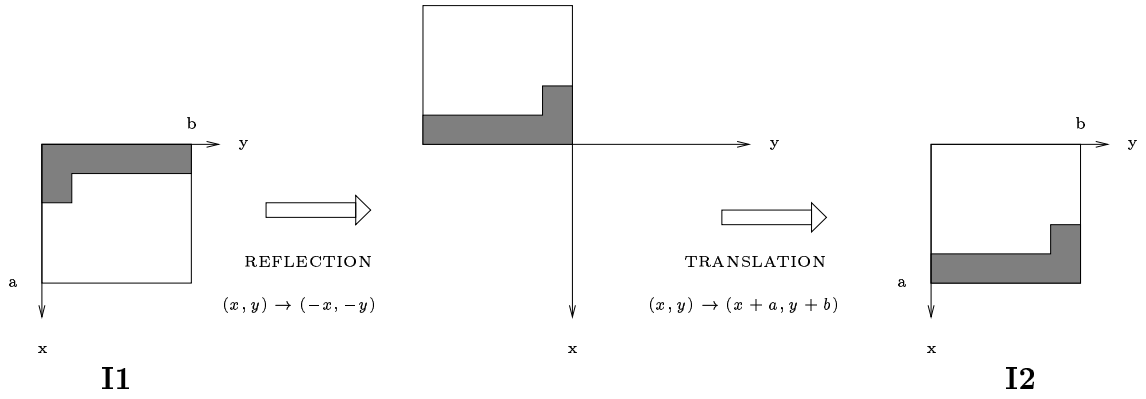

Figure 2.2: *Reflected and translated image.*

where $\mathbf{D}_p$ are diagonal matrices that account for the reflection of the image, and $\mathbf{T}_p^q$ are obtained according to corollary 2.1.2 (see figure 2.2).

Using corollary 2.3.1,

$$\mathbf{R2}_{mn} = (\mathbf{H}_m)^t \left(\mathbf{T}_m^{-(a+1)}\right)^t \mathbf{D}_m \, \mathbf{M1}_{mn} \, \mathbf{D}_n \, \mathbf{T}_n^{-(b+1)} \, \mathbf{H}_n.$$

Since $\mathbf{R2}_{mn} = \mathbf{L1}_{mn}$, corollary 2.2.1 finally permits to obtain equation (2.26).

□

Corollary 2.3.2.

$$\left(\mathbf{G}_p^q\right)^{-1} = (\mathbf{H}_p)^{-1} \, \mathbf{T}_p^{(q+1)} \, \mathbf{D}_p. \tag{2.27}$$

Using this corollary and corollaries 2.2.1 and 2.3.1, the following result, that finally relates direct and reverse accumulation moments, is obtained.

Corollary 2.3.3. *The direct* $(\mathbf{L}_{mn})$ *and reverse* $(\mathbf{R}_{mn})$ *accumulation moment matrices of an image are related as follows:*

$$\mathbf{R}_{mn} = (\mathbf{W}_m^a)^t \, \mathbf{L}_{mn} \, \mathbf{W}_n^b, \tag{2.28}$$

and

$$\mathbf{L}_{mn} = (\mathbf{W}_m^a)^t \, \mathbf{R}_{mn} \, \mathbf{W}_n^b, \tag{2.29}$$

where

$$\mathbf{W}_p^q[k,l] = \begin{cases} \frac{(-1)^{k+1}}{(l-1)!} \, B_{l-1,l-1}^{q+k-1}, & \text{if} \quad l \geq k, \\ 0, & \text{otherwise;} \end{cases} \tag{2.30}$$

and

$$B^r_{p,q} = \sum_{\substack{i_1,i_2,\ldots,i_p=1 \\ i_1<i_2<\cdots<i_p}}^{q} (-r-i_1)(-r-i_2)\ldots(-r-i_p).$$

Note that $\left(\mathbf{W}^q_p\right)^{-1} = \mathbf{W}^q_p$.

Example 2.3.2. Consider the matrix $\mathbf{I}_2 = \begin{pmatrix} 1 & 0 \\ 0 & 0 \end{pmatrix}$. Then,

$$\mathbf{L}_2 = \begin{pmatrix} 1 & 2 \\ 2 & 4 \end{pmatrix}, \quad \mathbf{R}_2 = \begin{pmatrix} 1 & 1 \\ 1 & 1 \end{pmatrix}, \quad \text{and} \quad \mathbf{W}^2_2 = \begin{pmatrix} 1 & 3 \\ 0 & -1 \end{pmatrix}.$$

It can be easily checked that $\mathbf{L}_2 = (\mathbf{W}^2_2)^t\,\mathbf{R}_2\,\mathbf{W}^2_2$ and $\mathbf{R}_2 = (\mathbf{W}^2_2)^t\,\mathbf{L}_2\,\mathbf{W}^2_2$.

The mathematical development presented up to this point provide practical connections between geometric moments and direct and reverse accumulation moments by means of the one-to-one linear transformations graphically summarized in figure 2.3. All the involved constant matrices are compiled in table 2.1.

$\mathbf{V}_{pq}[k,l] = k^{l-1}$
$\mathbf{Q}_{pq}[k,l] = \binom{p-k+l-1}{p-k}$
$\mathbf{P}_{pq}[k,l] = \binom{k+l-2}{k-1}$
$\mathbf{T}^q_p[k,l] = \begin{cases} \binom{l-1}{k-1}(-q)^{l-k}, & l \geq k, \\ 0, & \text{otherwise.} \end{cases}$
$\mathbf{G}^p_q[k,l] = \begin{cases} \frac{(-1)^{l-1}}{(l-1)!} B^p_{l-k,l-1}, & l \geq k, \\ 0, & \text{otherwise.} \end{cases}$
$\mathbf{H}_p[k,l] = \begin{cases} \frac{(-1)^{l-1}}{(l-1)!} B^{-1}_{l-k,l-1}, & l \geq k, \\ 0, & \text{otherwise.} \end{cases}$
$\mathbf{W}^q_p[k,l] = \begin{cases} \frac{(-1)^{k+1}}{(l-1)!} B^{q+k-1}_{l-1,l-1}, & l \geq k, \\ 0, & \text{otherwise.} \end{cases}$
$B^r_{p,q} = \sum^{q}_{\substack{i_1,i_2,\ldots,i_p=1 \\ i_1<i_2<\cdots<i_p}} (-r-i_1)(-r-i_2)\ldots(-r-i_p)$

Table 2.1: *Defined constant matrices connecting geometric, direct and reverse accumulation moments.*

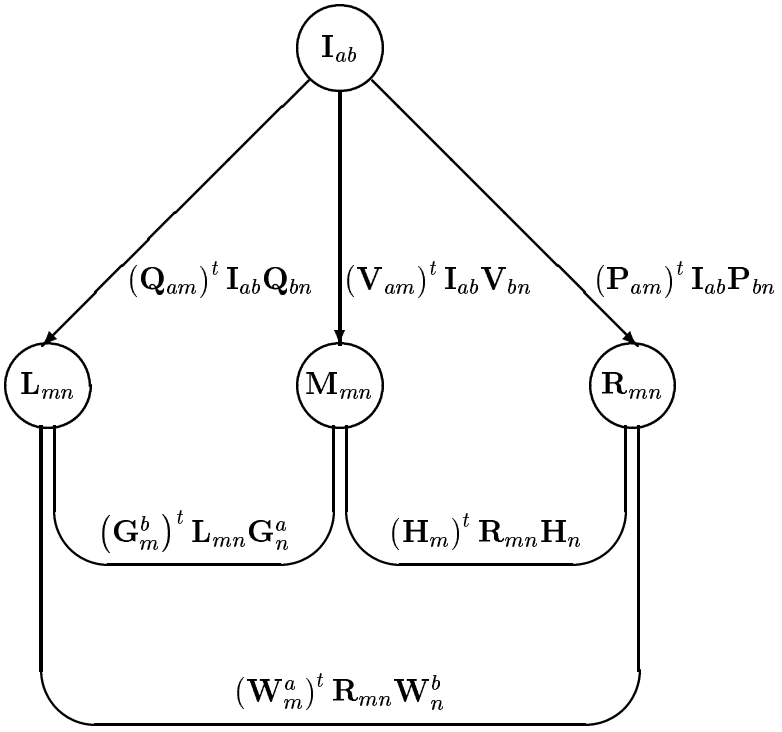

Figure 2.3: *The linear transformations relating the three moment matrices defined here.*

Notice that it is not possible to obtain any set of moments up to order $N = m + n$ – using the traditional definition of order – from another set of moments up to order (m, n) – using our definition. In this case, a set of moments up to order $(m + n + 1, m + n + 1)$ would be necessary. Nevertheless, the set of moments up to order (m, n) – as defined here – can be obtained from another set of moments up to order $N = m + n + 1$ – as traditionally defined.

In chapters 4 and 5, it is shown that all the applications that traditionally required geometric moments can benefit from the use of accumulation moments.

Chapter 3

Computational considerations

The main advantage of using accumulation moments instead of other well-known moments is that their computation only requires additions. In this sense, a hardware implementation much simpler than those proposed for the computation of geometric moments up to third order in [33] and [119] can be developed for accumulation moments.

The use of moments in real-time applications requires specialized hardware. Implemented structures include optical [12, 107], VLSI [33, 119] and parallel ones [16]. However, the accumulation moment implementation basically requires bit-serial adders and shift registers.

The general idea of the implementation scheme is shown in figure 3.2. The basic structure, shown in figure 3.1, is formed by a bit-serial adder and a feedback loop that includes shift registers.

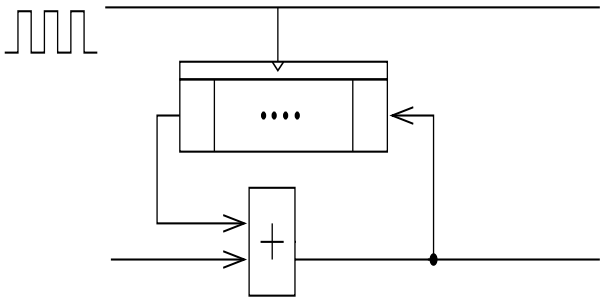

Figure 3.1: *Basic structure of the implementation scheme.*

Given as input the bit 0 of pixel i, the register of the first basic structure contains all the bits of data $i-1$, such that at each clock tick one bit is shifted and a new bit of the input data i is introduced. Clock frequency is determined by the delay of the bit-adders and video rate. Each basic structure increases one order the number of accumulations. The same basic structure is repeated m times in the horizontal direction in order to

accumulate m times the value of every pixel of each image row. On the other hand, each vertical series of n basic structures are activated when the bits associated with the accumulated values of the last pixel of each image row are available at their inputs. Notice that in the serial combination of basic structures each module is delayed one tick with respect to the previous one. Finally, the outputs of the basic structures in the vertical direction allow to obtain the accumulation moments.

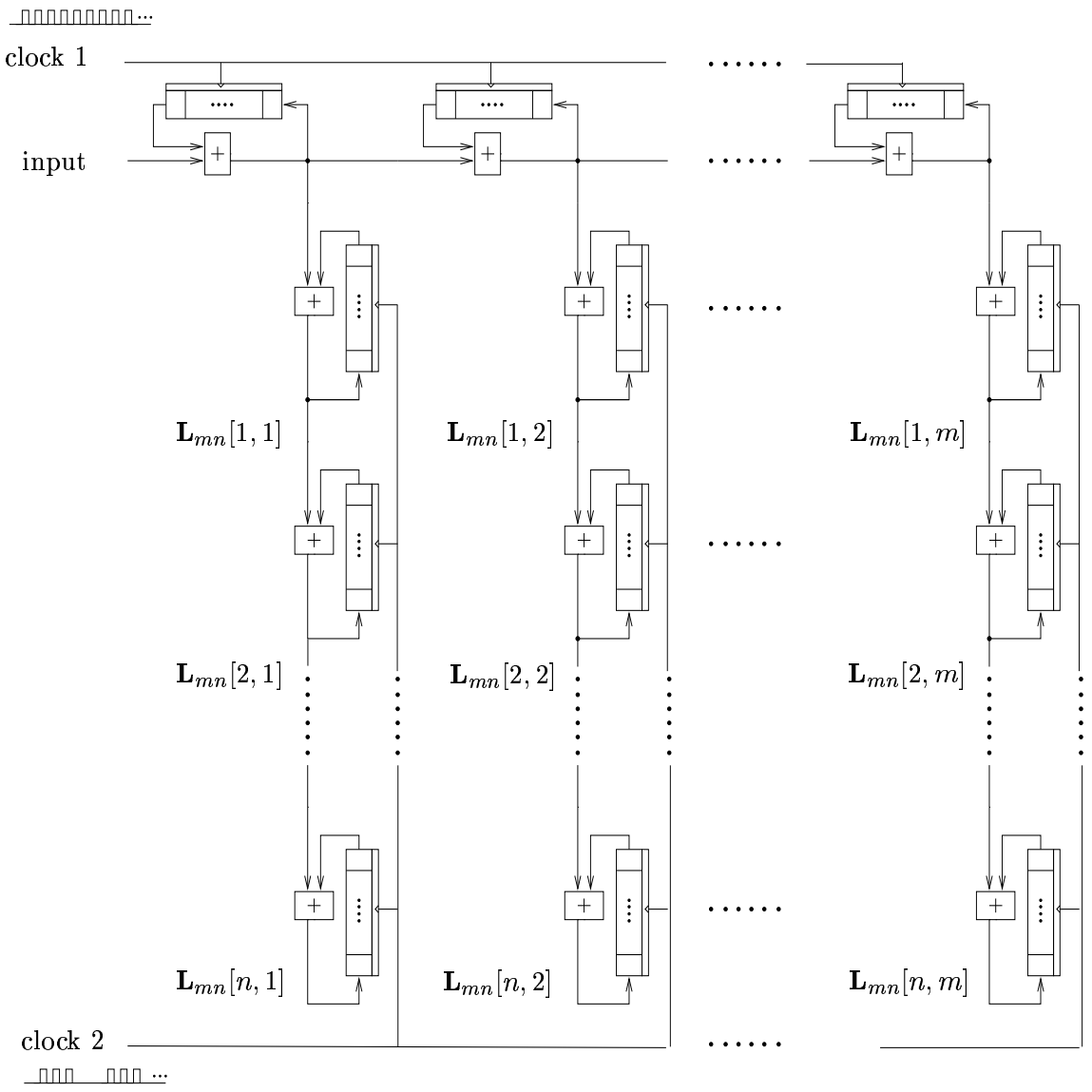

Figure 3.2: *Implementation scheme for accumulation moment computation.*

Notice that higher order accumulation moments require increasing number of bits because its numerical value increases with order. Assuming a uniform square image of size a and 8 bits per pixel, the maximum value of its direct or reverse accumulation

moment is

$$\max(\mathbf{L}_m[m,m]) = \max(\mathbf{R}_m[m,m]) = 255 * (\mathbf{P}_{a+1,m}[a+1,m])^2 = 255 * (\mathbf{Q}_{a+1,m}[1,m])^2,$$

as it can be obtained from equations (2.10) or (2.19). Figure 3.3a plots this value for a fixed image of size $a = 512$ and increasing values of m, and figure 3.3b shows the required number of bits.

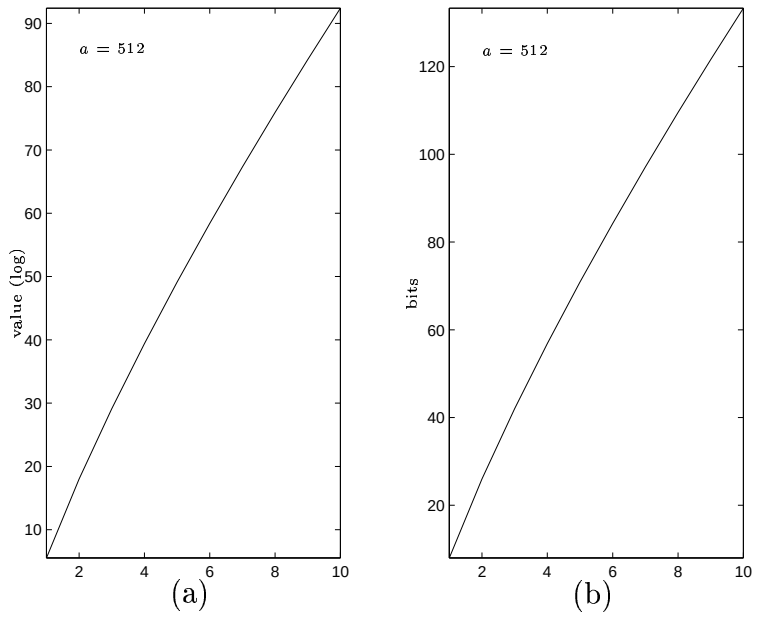

Figure 3.3: *(a) Maximum numerical value of the accumulation moments as order increases; and (b) required number of bits for these numerical values.*

Real-time applications imply computing the accumulation moments of an image typically at TV rates, that is $\frac{1}{30}\,sec.$ Given a 512×512 image, the pixel time is $127\,nsec.$ Assuming that the delay of a bit-adder is less than $5\,ns$, it is impossible to perform more than 25 bit-serial additions. In case the input data contains more bits, it can be multiplexed into k parallel structures equal to the one in figure 3.2, where separate bit-adders are used for different groups of bits of any input data. In [119], separate bit-adders are proposed for high and low bits of an input, to perform cumulated summations in parallel. Then, including this considerations in the diagram of figure 3.2, with a careful control of synchronization, it is possible to obtain high order accumulation moments in spite of the increasing amount of required bits.

Chapter 4

Application to the fast computation of geometric moments and its associated invariants

4.1 Computing geometric moments

Taking into account the relevance of moments in such a broad field of applications as pattern recognition [9, 83, 97], feature extraction [27, 28], motion estimation [8, 84], medical imaging [32, 41], 3D modeling [6, 90, 59], subband analysis [116], texture segmentation [104, 109] and reconstruction [77, 72, 71, 79, 81], any effort in order to attain low complexity algorithms for their computation is justified.

Software implementation of geometric moment computation using its direct formulation, i.e. equation (2.6) in corollary 2.1.1, leads to very long processing time. It is easy to verify that, given a square image of size a, the computation of $\mathbf{M}_m$ requires $a^2m + am^2$ multiplications and $a(a-1)m + (a-1)m^2$ additions. Assuming $a = 512$ and $m = 3$, over 1.5 Mflops are required. Obviously, this has to be reduced, specially in real-time applications, where a new image frame is obtained every $\frac{1}{30}$ sec.

Most of the efforts for the efficient computation of geometric moments have focused on the binary domain. Two different approaches have been considered: (1) reducing the number of involved pixels and (2) using recursivity. The first approach is carried out either by decomposing the image into simpler areas such as one-line-thick rectangles (run-lengths) [18, 54, 117] or triangles [52] or by transforming the summation over an area to the summation along its contour using the discrete version of the Green's theorem [85]. The second approach uses geometric moments of lower order to compute higher order geometric moments [75, 100]. Obviously, both approaches have also been jointly considered [42, 57, 113, 114] and extended to the 3D case [58, 53, 56, 115].

In the gray-level domain, the first approach that avoided the direct evaluation of (2.6) was presented in [33], where the idea that a 2-D filter with separable impulse response $x^m u(x) y^n u(y)$ could be used to generate the (m,n)th order moment of a digital image

was exploited. The result was limited to third order moments. A generalization to higher order moments was provided in [55]. Hardware implementation structures have also been explored including optical, VLSI and parallel ones as mentioned in chapter 3.

Using accumulation moments and corollary 2.3.1, the complexity of computing the geometric moments of an image, in terms of the number of products and additions, is reduced [68]. Given a square image of size a, the number of multiplications and additions required to compute $\mathbf{M}_m$ using (2.25) in corollary 2.3.1 is $m^2(m+1)$ and $m(m-1)^2$, respectively, because $\mathbf{H}_m$ are triangular matrices. Taking into account that the computation of $\mathbf{R}_m$ involves $a(a-1)m + m^2(a-1)$ additions, the total number of additions is $a(a-1)m + m^2(a-1) + m(m-1)^2$.

Table 4.1 compiles these results. Note that, when accumulation moments are used, the number of multiplications is independent from the size of the image.

	Additions	*Multiplications*
Evaluation of (2.6)	$a(a-1)m + (a-1)m^2$	$a^2m + am^2$
Evaluation of (2.25)	$a(a-1)m + (a-1)m^2 + m(m-1)^2$	$m^2(m+1)$

Table 4.1: *Number of operations required to compute geometric moments either directly or through accumulation moments.*

Figure 4.1 shows the theoretical time comparison between the evaluation of (2.6) and (2.25). The comparison is done for different values of the maximum order of the required moments (figure 4.1a), and for different image sizes (figure 4.1b). Here, multiplication and addition operations are assumed to require the same time, as it is the case in modern RISC processors.

Thus, the advantage of using (2.25) for computing geometric moments has been clearly established. Moreover, the hardware computation of the accumulation moments introduced in chapter 3, makes the geometric moment computation independent from the image size.

4.2 Computing moment invariants

Feature-based recognition of objects or patterns independently of their position, size, orientation and other variations has been an active research field (see [112] for a review).

Two different approaches concerning invariant features have been proposed in the literature. The first one is based on invariant properties of the projection basis associated with the obtained linear features. For instance, the modulus of the Fourier transform is invariant with respect to translation and the modulus of some Mellin-like transforms is invariant with respect to scale and rotation. Hence, values from these modulus can be used as invariant features [101, 102, 110].

The second approach is based on moments. Geometric moments up to third order

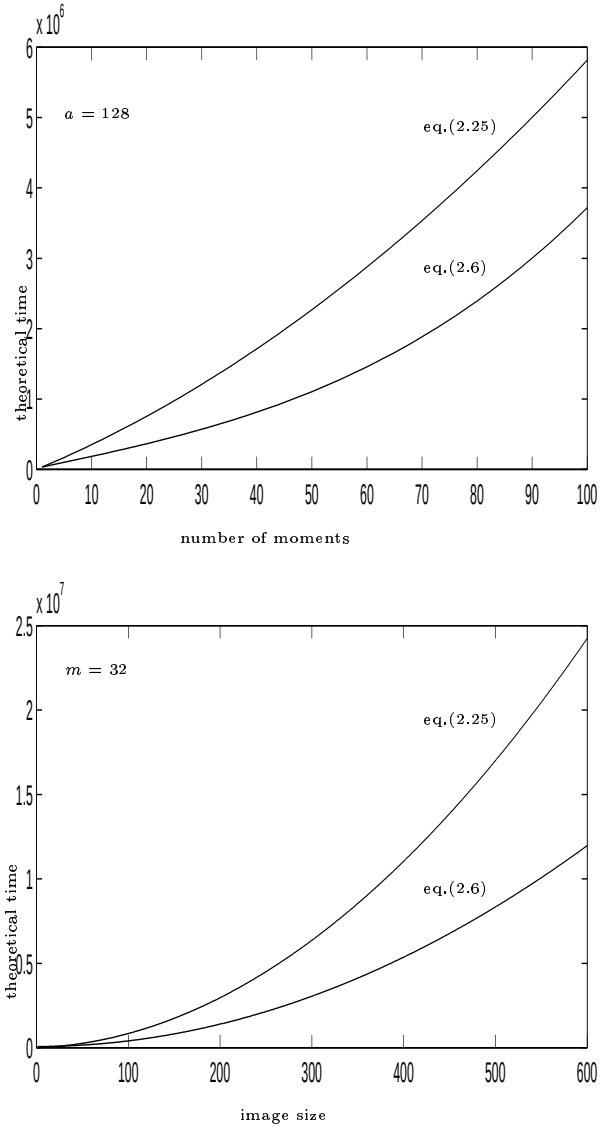

Figure 4.1: *Time comparison between the evaluation of equations (2.6) and (2.25), assuming that multiplication and addition operations require the same time.*

have been widely used because of their geometric and physical interpretation; parameters such as the area, the center of mass and the principal axes of inertia are derived from these moments [25, 89]. Then, different strategies use these physical parameters to normalize the image under scale, position and rotation transformations prior to compute discriminant features. Since image symmetries generate ambiguities in the principal axes definition, many ad doc methods that depend on the particular application have been developed [14, 25, 31, 98, 101].

A more general approach to obtain moment invariants is based on algebraic invariants [2, 21, 40, 63, 91, 96]. An algebraic invariant of weight w and order p is defined as a homogeneous polynomial $\rho(a_{0p}, \ldots, a_{p0})$ obtained from the coefficients of a binary form of order p, i.e.

$$(Ax_1 + Bx_2)^p = \sum_{k=0}^{p} a_{k\,p-k} \binom{p}{k} x_1^{p-k} x_2^k,$$

that verifies

$$\rho(a'_{0p}, \ldots, a'_{p0}) = \triangle^w \rho(a_{0p}, \ldots, a_{p0}),$$

where $a'_{0p}, \ldots, a'_{p0}$ are the coefficients obtained from substituing the following general linear transformation into the original form:

$$x_1 = b_{11}x'_1 + b_{12}x'_2$$
$$x_2 = b_{21}x'_1 + b_{22}x'_2$$

and

$$\triangle = \begin{vmatrix} b_{11} & b_{12} \\ b_{21} & b_{22} \end{vmatrix}.$$

If $w = 0$, the invariant is called an absolute invariant; if $w \neq 0$ it is called a relative invariant. By eliminating $\triangle$ between two relative invariants, an absolute invariant can always be obtained.

This approach was formalized by Hu [40] as *the fundamental theorem of moment invariants* which states as follows: If the algebraic form of order p has an algebraic invariant,

$$\rho(a_{0p}, \ldots, a_{p0}) = \triangle^w \rho(a_{0p}, \ldots, a_{p0}),$$

then the moments μ_{kl} such that $k+l = p$ have the same invariants but with the additional factor $|J|$, which is the Jacobian of the transformation, i.e.

$$\rho(\mu_{0p}, \ldots, \mu_{p0}) = |J| \ \triangle^w \rho(\mu_{0p}, \ldots, \mu_{p0}).$$

This theorem was later revised by Reiss [91] who stated that the additional factor was $|J|^k$ for affine transformations instead of $|J|$. The same invariants were obtained by Flusser in [21] using a different derivation. This revised theorem also holds for algebraic invariants

containing coefficients from two or more forms of different orders and moment invariants containing moments of the corresponding orders.

The most widely used moment invariants are derived from central moments up to trird order. Central moments are related to geometric moments through corollary 2.1.2, when v and w refer to the coordinates of the center of mass. However, using corollary 2.3.1, these particular central moments can be directly obtained from the reverse accumulation moments as follows:

$$\mathbf{M}_4^{v_c w_c}[1,1] = \mathbf{R}_4[1,1], \tag{4.1}$$

$$\mathbf{M}_4^{v_c w_c}[1,2] = 0, \tag{4.2}$$

$$\mathbf{M}_4^{v_c w_c}[2,1] = 0, \tag{4.3}$$

$$\mathbf{M}_4^{v_c w_c}[2,2] = -\frac{\mathbf{R}_4[2,1]\mathbf{R}_4[1,2]}{\mathbf{R}_4[1,1]} + \mathbf{R}_4[2,2], \tag{4.4}$$

$$\mathbf{M}_4^{v_c w_c}[1,3] = -\frac{(\mathbf{R}_4[1,2])^2}{\mathbf{R}_4[1,1]} - \mathbf{R}_4[1,2] + 2\,\mathbf{R}_4[1,3], \tag{4.5}$$

$$\mathbf{M}_4^{v_c w_c}[3,1] = -\frac{(\mathbf{R}_4[2,1])^2}{\mathbf{R}_4[1,1]} - \mathbf{R}_4[2,1] + 2\,\mathbf{R}_4[3,1], \tag{4.6}$$

$$\begin{aligned}\mathbf{M}_4^{v_c w_c}[2,3] = &-\frac{\mathbf{R}_4[1,2]}{\mathbf{R}_4[1,1]}\,\mathbf{M}_4^{v_c w_c}[2,2] - \frac{\mathbf{R}_4[2,1]}{\mathbf{R}_4[1,1]}\,\mathbf{M}_4^{v_c w_c}[1,3] - \mathbf{R}_4[2,2]\left(\frac{\mathbf{R}_4[1,2]}{\mathbf{R}_4[1,1]} + 1\right)\\ &+ 2\,\mathbf{R}_4[2,3],\end{aligned} \tag{4.7}$$

$$\begin{aligned}\mathbf{M}_4^{v_c w_c}[3,2] = &-\frac{\mathbf{R}_4[2,1]}{\mathbf{R}_4[1,1]}\,\mathbf{M}_4^{v_c w_c}[2,2] - \frac{\mathbf{R}_4[1,2]}{\mathbf{R}_4[1,1]}\,\mathbf{M}_4^{v_c w_c}[3,1] - \mathbf{R}_4[2,2]\left(\frac{\mathbf{R}_4[2,1]}{\mathbf{R}_4[1,1]} + 1\right)\\ &+ 2\,\mathbf{R}_4[3,2],\end{aligned} \tag{4.8}$$

$$\mathbf{M}_4^{v_c w_c}[1,4] = -3\left(\frac{\mathbf{R}_4[1,2]}{\mathbf{R}_4[1,1]} + 1\right)\mathbf{M}_4^{v_c w_c}[1,3] - 3\,\frac{(\mathbf{R}_4[1,2])^2}{\mathbf{R}_4[1,1]} - 2\,\mathbf{R}_4[1,2] + 6\,\mathbf{R}_4[1,4], \tag{4.9}$$

$$\mathbf{M}_4^{v_c w_c}[4,1] = -3\left(\frac{\mathbf{R}_4[2,1]}{\mathbf{R}_4[1,1]} + 1\right)\mathbf{M}_4^{v_c w_c}[3,1] - 3\,\frac{(\mathbf{R}_4[2,1])^2}{\mathbf{R}_4[1,1]} - 2\,\mathbf{R}_4[2,1] + 6\,\mathbf{R}_4[4,1], \tag{4.10}$$

where v_c and w_c denote the coordinates of the center of mass, which can also be obtained from corollary 2.3.1 as

$$v_c = \frac{\mathbf{R}[2,1]}{\mathbf{R}[1,1]} \quad \text{and} \quad w_c = \frac{\mathbf{R}[1,2]}{\mathbf{R}[1,1]}.$$

Let denote $\mathbf{R}[1,1]$ as a and expressions (4.4) to (4.10) as b, c, d, e, f, g and h, respec-

tively. Then, the invariants from second and third order moments are [21, 91]:

$$\rho_1 = \frac{cd - b^2}{a^4} \tag{4.11}$$

$$\rho_2 = \frac{g^2h^2 - 6efgh + 4e^3h + 4gf^3 - 3e^2f^2}{a^{10}} \tag{4.12}$$

$$\rho_3 = \frac{d(fg - e^2) - b(gh - ef) + c(eh - f^2)}{a^7} \tag{4.13}$$

$$\rho_4 = \frac{d^3g^2 - 6bd^2eg - 6cd^2fg + 9cd^2e^2 + 12b^2dfg + 6bcdgh - 18bcdef}{a^{11}} + \frac{9c^2df^2 - 8b^3gh - 6c^2deh + 12b^2ceh - 6bc^2fh + c^3h^2}{a^{11}} \tag{4.14}$$

Invariants involving higher order moments can also be derived from central moments [60, 111].

Non-linear combination of Zernique, complex and rotational moments also generate some other moment invariants [5, 99]; they are obtained by combining moments so that their individual dependence on the transformations is eliminated.

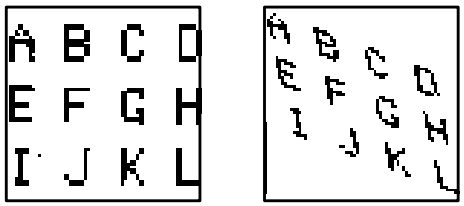

(a) (b)

Figure 4.2: *Templates from which the affine moment invariants are obtained: (a) capital letters and (b) affine transformed capital letters.*

In table 4.2, the four absolute affine invariants derived by Flusser [21] and Reiss [91] are obtained for the capital letters shown in figure 4.2a and their affine transformation in figure 4.2b. A simple measure of their discriminality is provided by the parameter $\mathbf{d}[j]$, for $j = 1, 2, \ldots, 12$, defined as

$$\mathbf{d}[j] = \sqrt{(\tilde{\rho}_1[j])^2 + (\tilde{\rho}_2[j])^2 + (\tilde{\rho}_3[j])^2 + (\tilde{\rho}_4[j])^2},$$

where $\tilde{\rho}_i$ are the absolute affine invariants normalized in the range [0,1], that is,

$$\tilde{\rho}_i[j] = \frac{\rho_i[j] - min(\rho_i[1], \ldots, \rho_i[12])}{max(\rho_i[1], \ldots, \rho_i[12]) - min(\rho_i[1], \ldots, \rho_i[12])}.$$

Invariant pattern recognition systems require discriminality and reduced computational complexity. Since the use of the affine invariants has been proved to be useful in many applications [21, 51, 99, 111, 118], their efficient computation is a relevant problem.

j		$\rho_1 \times 10^{-3}$	$\rho_2 \times 10^{-8}$	$\rho_3 \times 10^{-6}$	$\rho_4 \times 10^{-6}$	**d**
1	**A**	29.29	29.07	96.10	27.45	0.68
		29.19	0.54	88.17	23.34	0.68
2	**B**	23.91	-0.45	-11.44	2.35	0.71
		25.27	-0.58	-7.42	2.13	0.72
3	**C**	63.94	313.85	96.71	24.82	1.27
		63.71	525.07	99.07	40.20	1.27
4	**D**	37.06	-2.31	-31.04	9.57	0.80
		41.00	-1.30	-28.64	10.78	0.85
5	**E**	32.50	54.26	42.31	2.06	0.80
		33.33	151.07	53.43	6.77	0.82
6	**F**	32.71	150.25	-98.12	41.60	0.71
		28.45	192.31	-264.45	64.34	0.57
7	**G**	41.92	-8.40	-65.00	23.31	0.84
		43.00	-10.9	-80.20	31.52	0.84
8	**H**	35.68	0.00	0.10	0.07	0.80
		36.14	0.00	0.03	0.10	0.80
9	**I**	18.35	0.04	1.74	0.01	0.71
		21.33	0.00	1.87	1.29	0.71
10	**J**	52.64	3051.04	-972.17	538.68	1.23
		50.30	2014.31	-850.46	449.92	1.07
11	**K**	41.05	226.54	99.40	5.52	0.92
		41.88	255.55	93.60	7.96	0.93
12	**L**	56.46	8155.98	758.58	560.01	1.37
		53.32	20169.53	397.95	260.49	1.67

Table 4.2: *Affine invariants:* ρ_1, ρ_2, ρ_3 *and* ρ_4*; and discriminant value* **d** *for the capital letters of figure 4.2.*

Given the relationship between central and accumulation moments, moment invariants can be directly obtained from accumulation moments. The computational cost is reduced since computing accumulation moments up to third order requires only $4a^2 + 12a - 4$ additions and 80 multiplications while computing geometric moments up to the same order requires $4a^2 + 16a - 16$ additions and $4a^2 + 16a$ multiplications, as it can be easily deduced from table 4.1.

Chapter 5

Application to the fast actualization of moments in a sliding window

Many image analysis techniques place a window at different locations of the image to derive a local description vector. This technique can be found within some texture segmentation [15, 104] and optic flow computation algorithms [28] which are described in terms of a sliding window that displaces all over the image. In general, description vectors obtained in a particular window location can be related to those in previous locations of the window if overlapping occurs.

This chapter describes a fast actualization rule of the accumulation moments in a sliding window moving all over an image. When accumulation moments are used instead of geometric moments as description parameters in sliding window applications, it is shown how the actualization cost drops from $O(m^3)$ to $O(m^2)$, where m refers to the amount of moments. Therefore, any application of this kind that traditionally required geometric moments can benefit from the use of accumulation moments since, as we have already seen, geometric and accumulation moments are related through a one-to-one linear transformation: any set of geometric moments up to a given order is uniquely related to a set of accumulation moments up to the same order.

5.1 Actualization of moments

Consider that image $\mathbf{I}_{ab}$ is split into non-overlapping regions $\mathbf{Ik}_{a_k b_k}$, for $k = 1, 2, \cdots$, displaced (x_k, y_k) from the origin, as shown in figure 5.1.

Since geometric moment computation only involves linear operations, the geometric moments $\mathbf{M}_{mn}$ of $\mathbf{I}_{ab}$ can be obtained as a linear combination of the geometric moments $\mathbf{Mk}_{mn}$ of each region with respect to their displacement from the origin. Then, using corollary 2.1.2,

$$\mathbf{M}_{mn} = \sum_{\mathbf{k}} \mathbf{Mk}_{mn}^{-x_k,-y_k} = \sum_{\mathbf{k}} (\mathbf{T}_m^{-x_k})^t \, \mathbf{Mk}_{mn} \, \mathbf{T}_n^{-y_k}. \tag{5.1}$$

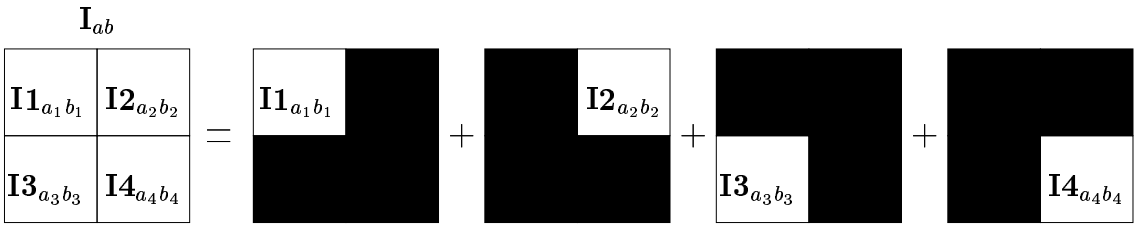

Figure 5.1: *A partition of an image into four non-overlapping regions.*

That is, for the particular case of figure 5.1,

$$\mathbf{M}_{mn} = \mathbf{M1}_{mn} + \mathbf{M2}_{mn}\,\mathbf{T}_n^{-b_1} + \mathbf{T}_m^{-a_1}\,\mathbf{M3}_{mn} + \mathbf{T}_m^{-a_1}\,\mathbf{M4}_{mn}\,\mathbf{T}_n^{-b_1}. \tag{5.2}$$

Lemma 5.1.1. *Consider the three regions induced by a $w \times w$ sliding window in two consecutive locations (see figure 5.2). Let $\mathbf{M12}_{mn}$ and $\mathbf{M23}_{mn}$ denote the geometric moments of the window encompassing regions 1 and 2, and 2 and 3, respectively. Then, if the window slides from left to right,*

$$\mathbf{M23}_{mn}^{x(y+h)} = \left(\mathbf{M12}_{mn}^{xy} - \mathbf{M1}_{mn}^{xy}\right)\mathbf{T}_n^{h} + \mathbf{M3}_{mn}^{x(y+w)}\,\mathbf{T}_n^{h-w}; \tag{5.3}$$

otherwise, if the window slides from top to bottom,

$$\mathbf{M23}_{mn}^{(x+v)y} = \left(\mathbf{T}_m^{v}\right)^t\left(\mathbf{M12}_{mn}^{xy} - \mathbf{M1}_{mn}^{xy}\right) + \left(\mathbf{T}_m^{v-w}\right)^t\mathbf{M3}_{mn}^{(x+w)y}. \tag{5.4}$$

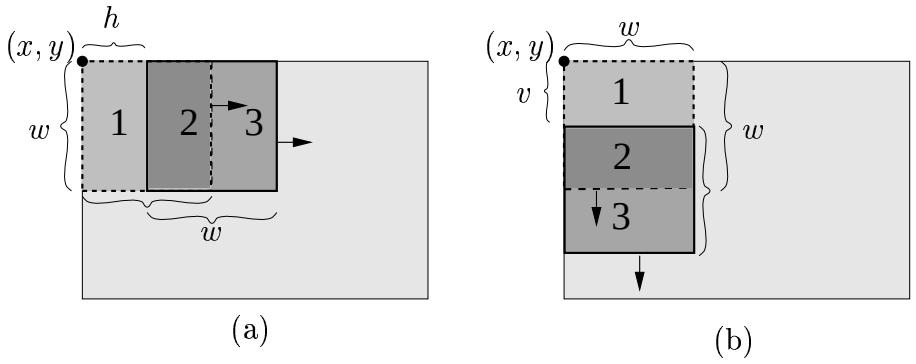

Figure 5.2: *A sliding window in two consecutive (a) horizontal and (b) vertical locations.*

Proof. Consider the horizontal sliding window of figure 5.2a. Then,

$$\begin{aligned}\mathbf{M12}_{mn}^{xy} &= \mathbf{M1}_{mn}^{xy} + \mathbf{M2}_{mn}^{x(y+h)}\,\mathbf{T}_n^{-h}\\ \mathbf{M23}_{mn}^{x(y+h)} &= \mathbf{M2}_{mn}^{x(y+h)} + \mathbf{M3}_{mn}^{x(y+h)}\,\mathbf{T}_n^{h-w}.\end{aligned}$$

Substituing one equation into the other and given that, from property 2.1.1,

$$(\mathbf{T}_p^q)^{-1} = \mathbf{T}_p^{-q},$$

equation (5.3) is straightforwardly obtained. Likewise, considering the vertical sliding window of figure 5.2b,

$$\begin{aligned}\mathbf{M12}_{mn}^{xy} &= \mathbf{M1}_{mn}^{xy} + \mathbf{T}_m^{-v}\,\mathbf{M2}_{mn}^{xy}\\ \mathbf{M23}_{mn}^{(x+v)y} &= \mathbf{M2}_{mn}^{(x+v)y} + \mathbf{T}_m^{v-w}\,\mathbf{M3}_{mn}^{(x+v)y},\end{aligned}$$

from which equation (5.4) is obtained. □

Theorem 5.1.2. *Consider the three regions induced by a $w \times w$ sliding window in two consecutive locations (see figure 5.2). Let $\mathbf{R12}_{mn}$ and $\mathbf{R23}_{mn}$ denote the reverse accumulation moments of the window encompassing regions 1 and 2, and 2 and 3, respectively. Then, if the window slides from left to right,*

$$\mathbf{R23}_{mn}^{x(y+h)} = \left(\mathbf{R12}_{mn}^{xy} - \mathbf{R1}_{mn}^{xy}\right)(\mathbf{U}_n)^{-h} + \mathbf{R3}_{mn}^{x(y+w)}\,(\mathbf{U}_n)^{w-h}; \tag{5.5}$$

otherwise, if the window slides from top to bottom,

$$\mathbf{R23}_{mn}^{(x+v)y} = \left((\mathbf{U}_m)^t\right)^v\left(\mathbf{R12}_{mn}^{xy} - \mathbf{R1}_{mn}^{xy}\right) + \left((\mathbf{U}_m)^t\right)^{w-v}\mathbf{R3}_{mn}^{(x+w)y}; \tag{5.6}$$

where $\mathbf{U}_p$ are triangular matrices of the form

$$\mathbf{U}_p[k,l] = \begin{cases}1, & \text{if } \ l \geq k,\\ 0, & \text{otherwise.}\end{cases} \tag{5.7}$$

Proof. Taking into account that

$$\left(\mathbf{H}_p\right)^{-1}\mathbf{T}_p^q\,\mathbf{H}_p = \left(\mathbf{U}_p\right)^{-q} \tag{5.8}$$

and using the relationship between geometric and accumulation moments stated in corollary 2.3.1, it is easy to derive equations (5.5) and (5.6) from the ones in lemma 5.1.1. □

In order to obtain a description vector for each pixel of the image, two consecutive locations of the sliding window should differ in just one pixel. In this case, referring to figure 5.2, region 1 will be called the *outgoing vector;* region 2, the *overlapped region;* and region 3, the *incoming vector.*

Property 5.1.1. *The moment matrices of a columnwise vector has equal values for all their columns. Then, it can be expressed as:*

$$\begin{aligned}\mathbf{M}_{pq} &= \mathbf{M}_{pq}[:,1]\,\left(\mathbf{s}_q\right)^t,\\ \mathbf{R}_{pq} &= \mathbf{R}_{pq}[:,1]\,\left(\mathbf{s}_q\right)^t,\end{aligned}$$

where

$$\mathbf{s}_q = \begin{pmatrix} 1 & \cdots & 1 \end{pmatrix}^t.$$

Likewise, the moment matrices of a rowwise vector has equal values for all their rows. Then, in these cases,

$$\mathbf{M}_{pq} = \mathbf{s}_p \left(\mathbf{M}_{pq}[1,:]\right)^t,$$
$$\mathbf{R}_{pq} = \mathbf{s}_p \left(\mathbf{R}_{pq}[1,:]\right)^t.$$

Corollary 5.1.1. *By lemma 5.1.1,*

$$\mathbf{M23}_{mn}^{x(y+1)} = \mathbf{M12}_{mn}^{xy}\, \mathbf{T}_n^1 - \mathbf{M1}_{mn}^{xy}[:,1]\, (\mathbf{u}_n)^t + \mathbf{M3}_{mn}^{x(y+w)}[:,1]\, (\mathbf{v}_n^w)^t \tag{5.9}$$

and

$$\mathbf{M23}_{mn}^{(x+1)y} = \left(\mathbf{T}_m^1\right)^t \mathbf{M12}_{mn}^{xy} - \mathbf{u}_m \left(\mathbf{M1}_{mn}^{xy}[1,:]\right)^t + \mathbf{v}_m^w \left(\mathbf{M3}_{mn}[1,:]^{(x+w)y}\right)^t, \tag{5.10}$$

are obtained for unitary horizontal and vertical displacements of the sliding window, respectively; where

$$\mathbf{u}_p = \begin{pmatrix} 1 & 0 & 0 & \ldots & 0 \end{pmatrix}$$

and

$$\mathbf{v}_p^q[k] = (q+1)^{k-1}.$$

Corollary 5.1.2. *By theorem 5.1.2,*

$$\mathbf{R23}_{mn}^{x(y+1)} = \mathbf{R12}_{mn}^{xy}\, (\mathbf{U}_n)^{-1} - \mathbf{R1}_{mn}^{xy}[:,1]\, (\mathbf{u}_n)^t + \mathbf{R3}_{mn}^{x(y+w)}[:,1]\, (\mathbf{b}_n^{w-1})^t \tag{5.11}$$

and

$$\mathbf{R23}_{mn}^{(x+1)y} = \left((\mathbf{U}_m)^{-1}\right)^t \mathbf{R12}_{mn}^{xy} - \mathbf{u}_m \left(\mathbf{R1}_{mn}^{xy}[1,:]\right)^t + \mathbf{b}_m^{w-1} \left(\mathbf{R3}_{mn}^{(x+w)y}[1,:]\right)^t \tag{5.12}$$

are obtained for unitary horizontal and vertical displacements of the sliding window, respectively; where

$$\mathbf{u}_p = \begin{pmatrix} 1 & 0 & 0 & \ldots & 0 \end{pmatrix},$$

and

$$\mathbf{b}_p^q[k] = \binom{q+k-1}{k-1}.$$

5.2 Computational complexity

Although equations in lemma 5.1.1 and theorem 5.1.2 provide an efficient way to update geometric and accumulation moments in sliding window applications, the overall computational cost is much lower for the latter.

Let us consider a unitary displacement and square moment matrices of size m; then, evaluating equations in corollary 5.1.1 involves:

- computing the geometric moments of both the incoming and outgoing vectors, which requires $2m(w-1)$ additions and $2mw$ multiplications; and
- multiplying matrices and vectors and summing up the result, which requires $\frac{3}{2}m^3 + \frac{3}{2}m^2$ additions and $\frac{1}{2}m^3 + \frac{1}{2}m^2$ multiplications.

On the other hand, evaluating equations in corollary 5.1.2 involves:

- computing the accumulation moments of both the incoming and outgoing vector, which requires $2m(w-1)$ additions; and
- multiplying matrices and vectors and summing up the result, which involves $5m^2 - m$ additions and m^2 multiplications, taking into account the particularities of the involved vector and matrices.

	Actualization of $\mathbf{M}$
Additions	$2m(w-1) + \frac{3}{2}m^3 + \frac{3}{2}m^2$
Multiplications	$2mw + \frac{1}{2}m^3 + \frac{1}{2}m^2$
	Actualization of $\mathbf{R}$
Additions	$2m(w-1) + 5m^2 - m$
Multiplications	m^2

Table 5.1: *Number of operations required to update geometric and accumulation moments in two consecutive locations of a unitary displaced sliding window.*

Table 5.1 compiles these results, where it is easy to see that the complexity of the actualization drops from $O(m^3)$ to $O(m^2)$ when accumulation moments are used instead of geometric moments. Not only asymptotical complexity is better but for any value of m. Figure 5.3 shows the theoretical time comparison between both actualization costs assuming that multiplication and addition operations require the same time.

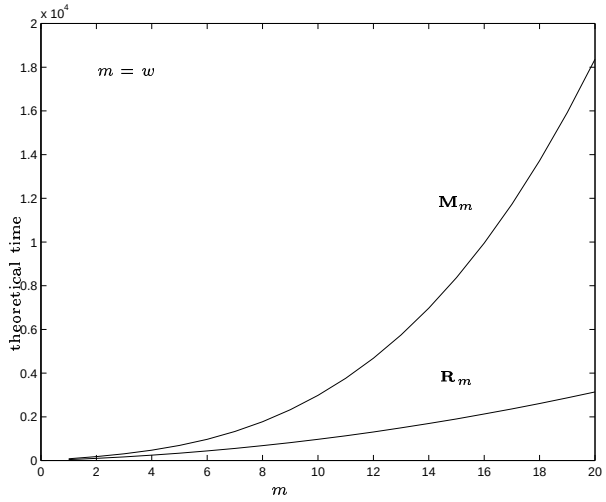

Figure 5.3: *Comparison between the time required to update geometric and accumulation moments assuming that multiplication and addition operations require the same time.*

Chapter 6

Generalization to higher dimensions

In this chapter, we provide a generalization of concepts and results introduced in previous chapters to higher dimensions. We focus ourselves in the 3D case; however, the method we follow to develop this generalization is straightforwardly applicable to higher dimensions.

The interest in analyzing moments of 3D data is motivated by their relevance in physical based modeling and dynamic simulation [22]. The location of a body's center of mass, and its moments and products of inertia about various axes are important physical quantities for this type of applications: they allow to obtain the body's linear and angular momentum if the linear and angular velocities of its center of mass are known. Therefore, moments up to second order are essential in these applications. In related literature, it is assumed that rigid bodies are composed of uniform density polyhedra. Then, the basic idea is to use the divergence theorem to reduce each volume integral to a sum of surface integrals over the individual faces of the polyhedron. Each of these surface integrals are evaluated in terms of integrals over a planar projection of the surface. Once the problem is translated into the one of obtaining moments of polygons in a plane, any method described in chapter 4 for computing moments of binary images can be used [74, 115, 58, 53, 56].

However, modeling a body as composed of uniform density polyhedra requires a 3D segmentation. Segmentation is a hard task, specially in those applications related to tomographic data [32, 1, 11, 19, 43]. In this case, volume data is obtained by stacking 2D cross sections and assuming constant values within planes. This is known as a voxel based model. Since common applications require the highest possible resolution, a great amount of voxels are involved. Then, it is important to provide algorithms that are able to obtain global features from this set of voxels avoiding a previous segmentation. In this sense, the efficient computation of moments from gray-level 3D data is of great relevance.

6.1 Preliminaries

Definition 6.1.1 (Kronecker product). Given any pair of matrices $\mathbf{A}_{pq}$ and $\mathbf{B}_{rs}$, their Kronecker product is defined as

$$\mathbf{A}_{pq} \otimes \mathbf{B}_{rs} = \begin{pmatrix} \mathbf{A}_{pq}[1,1]\mathbf{B}_{rs} & \dots & \mathbf{A}_{pq}[1,q]\mathbf{B}_{rs} \\ \vdots & & \vdots \\ \mathbf{A}_{pq}[p,1]\mathbf{B}_{rs} & \dots & \mathbf{A}_{pq}[p,q]\mathbf{B}_{rs} \end{pmatrix}.$$

Definition 6.1.2 (Columnwise form of a matrix). Given a 2D matrix $\mathbf{A}_{pq}$, its associated columnwise form $\mathbf{a}_{pq}$ is obtained by sequentially reading each row, that is,

$$\mathbf{a}_{pq} = \begin{pmatrix} \mathbf{A}_{pq}[1,1] & \dots & \mathbf{A}_{pq}[1,q] & \mathbf{A}_{pq}[2,1] & \dots & \mathbf{A}_{pq}[p,q] \end{pmatrix}^t.$$

Likewise, given a 3D matrix $\mathbf{A}_{pqr}$, its associated columnwise form $\mathbf{a}_{pqr}$ is obtained by sequentially reading each row of each depth plane; were rows range for $k = 1, \dots, p$; columns for $l = 1, \dots, q$; and depth planes for $j = 1, \dots, r$. That is,

$$\mathbf{a}_{pqr} = \begin{pmatrix} \mathbf{A}_{pqr}[1,1,1] & \mathbf{A}_{pqr}[1,2,1] & \dots & \mathbf{A}_{pqr}[1,q,1] & \mathbf{A}_{pqr}[2,1,1] & \mathbf{A}_{pqr}[2,2,1] & \dots \\ \dots & \mathbf{A}_{pqr}[p,q,1] & \mathbf{A}_{pqr}[1,1,2] & \mathbf{A}_{pqr}[1,2,2] & \dots & \mathbf{A}_{pqr}[p,q,r] \end{pmatrix}^t.$$

Property 6.1.1 (Columnwise transformation). *Given*

$$\mathbf{Y}_{ps} = (\mathbf{A}_{qp})^t \, \mathbf{X}_{qr} \, \mathbf{B}_{rs},$$

its associated columnwise form $\mathbf{y}_{ps}$ *is obtained from*

$$\mathbf{y}_{ps} = \left((\mathbf{A}_{qp})^t \otimes (\mathbf{B}_{rs})^t \right) \mathbf{x}_{qr},$$

where $\mathbf{x}_{qr}$ *is the columnwise form of the matrix* $\mathbf{X}_{qr}$.

6.2 3D geometric moments

A 3D discrete image can be represented by a stack of 2D discrete images, as shown in figure 6.1. Their values are stored in 3D matrices $\mathbf{I}_{abc}$ of size $a \times b \times c$.

Definition 6.2.1 (3D geometric moments). The geometric moment of order (k, l, j) of a 3D image $\mathbf{I}_{abc}$ is defined as

$$\mu_{pqr} = \sum_{x=1}^{a} \sum_{y=1}^{b} \sum_{z=1}^{c} x^k y^l z^j \, \mathbf{I}_{abc}[x,y,z].$$

Then, the 3D geometric moment matrix $\mathbf{M}_{pqr}$ is defined as

$$\mathbf{M}_{pqr}[k,l,j] = \mu_{p-1,q-1,r-1}.$$

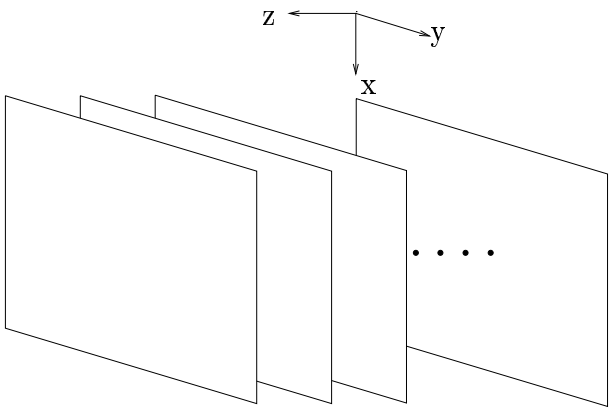

Figure 6.1: *3D image as a stack of 2D images.*

Lemma 6.2.1.

$$\mathbf{m}_{pqr} = \left((\mathbf{V}_{ap})^t \otimes (\mathbf{V}_{bq})^t \otimes (\mathbf{V}_{cr})^t \right) \mathbf{i}_{abc}; \tag{6.1}$$

where $\mathbf{m}_{pqr}$ *and* $\mathbf{i}_{abc}$ *are the associated columnwise forms of the 3D matrices* $\mathbf{M}_{pqr}$ *and* $\mathbf{I}_{abc}$*, respectively; and* $\mathbf{V}_{pq}$ *are the Vandermonde matrices defined in equation (2.5).*

Proof. Definition 6.2.1 can be rearranged so that it refers to the geometric moment of a 1D function in the z variable, i.e.

$$\mathbf{M}_{pqr}[k,l,j] = \sum_{z=1}^{c} z^{j-1}\, \mathbf{m}^z_{pq}[k,l]; \tag{6.2}$$

where

$$\mathbf{m}^z_{pq}[k,l] = \sum_{x=1}^{a}\sum_{y=1}^{b} x^{k-1} y^{l-1} \mathbf{I}_{abc}[x,y,z]. \tag{6.3}$$

Let $\mathbf{M}_{pqr}[k,l,:]$ be the rowwise vector containing the geometric moments up to order $(r-1)$ of the vector $\mathbf{m}^z_{pq}[k,l]$. Then, from corollary 2.1.1,

$$\mathbf{M}_{pqr}[k,l,:] = \begin{pmatrix} \mathbf{m}^1_{pq}[k,l] & \dots & \mathbf{m}^c_{pq}[k,l] \end{pmatrix} \mathbf{V}_{cr}; \tag{6.4}$$

where $\mathbf{V}_{cr}$ is a Vandermonde matrix.

On the other hand, it is easy to prove that expanding equation (6.3), for $z = 1, \dots, c$, one obtains

$$\begin{pmatrix} \mathbf{m}^1_{pq}[k,l] & \dots & \mathbf{m}^c_{pq}[k,l] \end{pmatrix} = \left(\begin{pmatrix} 1 & \cdots & a^p \end{pmatrix} \otimes \begin{pmatrix} 1 & \cdots & b^q \end{pmatrix} \right) \begin{pmatrix} \mathbf{I}_{abc}[1,1,:] \\ \mathbf{I}_{abc}[1,2,:] \\ \vdots \\ \mathbf{I}_{abc}[a,b,:] \end{pmatrix},$$

where $\mathbf{I}_{abc}[x, y, :]$ is a rowwise vector containing the image in the z direction.

Including this expression in equation (6.4) and considering geometric moments up to order $(p-1, q-1, r-1)$, the following geometric moment matrix of size $pq \times r$ is obtained,

$$\begin{pmatrix} \mathbf{M}_{pqr}[1,1,:] \\ \mathbf{M}_{pqr}[1,2,:] \\ \vdots \\ \mathbf{M}_{pqr}[p,q,:] \end{pmatrix} = \left((\mathbf{V}_{ap})^t \otimes (\mathbf{V}_{bq})^t \right) \begin{pmatrix} \mathbf{I}_{abc}[1,1,:] \\ \mathbf{I}_{abc}[1,2,:] \\ \vdots \\ \mathbf{I}_{abc}[a,b,:] \end{pmatrix} \mathbf{V}_{cr}. \tag{6.5}$$

Then, applying the columnwise transformation of property 6.1.1, lemma 6.2.1 is finally obtained.

□

6.3 3D accumulation moments

Definition 6.3.1 (3D direct and reverse accumulation moments). The 3D accumulation moments are defined as cumulative additions in three orthogonal directions of a volume. The 3D direct accumulation moments extend the definition 2.2.1 by accumulating the result of the 2D direct accumulation moments of each 2D image plane of the stack along the positive direction of the third coordinate. In the same way, the 3D reverse accumulation moments extend the definition 2.3.1 by accumulating the result of the 2D reverse accumulation moments of each 2D image plane of the stack along the negative direction of the third coordinate.

The direct and reverse accumulation moments up to order $(p-1, q-1, r-1)$ are stored in the 3D matrices $\mathbf{L}_{pqr}$ and $\mathbf{R}_{pqr}$, respectively, of size $p \times q \times r$.

Lemma 6.3.1. *Given the columnwise form of the 3D direct and reverse accumulation moments, $\mathbf{l}_{pqr}$ and $\mathbf{r}_{pqr}$, respectively; they are related to the columnwise form of the 3D image $\mathbf{i}_{abc}$ as follows:*

$$\mathbf{l}_{pqr} = \left((\mathbf{Q}_{ap})^t \otimes (\mathbf{Q}_{bq})^t \otimes (\mathbf{Q}_{cr})^t \right) \mathbf{i}_{abc}; \tag{6.6}$$

and

$$\mathbf{r}_{pqr} = \left((\mathbf{P}_{ap})^t \otimes (\mathbf{P}_{bq})^t \otimes (\mathbf{P}_{cr})^t \right) \mathbf{i}_{abc}, \tag{6.7}$$

respectively; where $\mathbf{Q}_{pq}$ and $\mathbf{P}_{pq}$ are the Pascal-like matrices defined in equations (2.12) and (2.21), respectively.

Proof. An extension of the equations (2.10) and (2.19) to the 3D case leads to

$$\mathbf{L}_{pqr}[k,l,j] = \sum_{x=1}^{a} \sum_{y=1}^{b} \sum_{z=1}^{c} \binom{a-x+k-1}{a-x} \binom{b-y+l-1}{b-y} \binom{c-z+j-1}{c-z} \mathbf{I}_{abc}[x,y,z] \tag{6.8}$$

and

$$\mathbf{R}_{pqr}[k,l,j] = \sum_{x=1}^{a}\sum_{y=1}^{b}\sum_{z=1}^{c}\binom{x+k-2}{x-1}\binom{y+l-2}{y-1}\binom{z+j-1}{c-z}\mathbf{I}_{abc}[x,y,z], \tag{6.9}$$

respectively.

Then, for both equations, it is easy to see that using a similar development to the one in the proof of lemma 6.2.1, this lemma is obtained.

□

Corollary 6.3.1. *Given*

$$\mathbf{i}_{ab}^{z} = \begin{pmatrix}\mathbf{I}_{abc}[1,1,z] & \mathbf{I}_{abc}[1,2,z] & \dots & \mathbf{I}_{abc}[a,b,z]\end{pmatrix}^{t}, \tag{6.10}$$

$$\mathbf{l}_{pq}^{z} = \begin{pmatrix}\mathbf{L}_{pqr}[1,1,z] & \mathbf{L}_{pqr}[1,2,z] & \dots & \mathbf{L}_{pqr}[p,q,z]\end{pmatrix}^{t}, \tag{6.11}$$

$$\mathbf{r}_{pq}^{z} = \begin{pmatrix}\mathbf{R}_{pqr}[1,1,z] & \mathbf{R}_{pqr}[1,2,z] & \dots & \mathbf{R}_{pqr}[p,q,z]\end{pmatrix}^{t}; \tag{6.12}$$

then,

$$\mathbf{l}_{pqr} = \begin{pmatrix}\mathbf{l}_{pq}^{1} & \dots & \mathbf{l}_{pq}^{c}\end{pmatrix}\mathbf{Q}_{cr}; \tag{6.13}$$

and

$$\mathbf{r}_{pqr} = \begin{pmatrix}\mathbf{r}_{pq}^{1} & \dots & \mathbf{r}_{pq}^{c}\end{pmatrix}\mathbf{P}_{cr}. \tag{6.14}$$

Lemma 6.3.2.

$$\mathbf{m}_{pqr} = \left(((\mathbf{G}_{p}^{a})^{t})^{-1} \otimes ((\mathbf{G}_{q}^{b})^{t})^{-1} \otimes ((\mathbf{G}_{r}^{c})^{t})^{-1}\right)\mathbf{l}_{pqr}. \tag{6.15}$$

$$\mathbf{m}_{pqr} = \left(((\mathbf{H}_{p})^{t})^{-1} \otimes ((\mathbf{H}_{q})^{t})^{-1} \otimes ((\mathbf{H}_{r})^{t})^{-1}\right)\mathbf{r}_{pqr}. \tag{6.16}$$

Proof. From equation(6.4),

$$\mathbf{M}_{pqr}[k,l,:] = \begin{pmatrix}\mathbf{m}_{pq}^{1}[k,l] & \dots & \mathbf{m}_{pq}^{c}[k,l]\end{pmatrix}\mathbf{V}_{cr}, \tag{6.17}$$

where $\mathbf{m}_{pq}^{i}[k,l]$ is the geometric moment of order $(k-1, l-1)$ of the image plane at position i in the z coordinate of the 3D image.

By corollary 2.2.1, the geometric moments can be expressed in terms of the direct accumulation moments; that is,

$$\mathbf{M}_{pqr}[k,l,:] = \begin{pmatrix}\mathbf{L}_{pqr}[k,l,1] & \dots & \mathbf{L}_{pqr}[k,l,r]\end{pmatrix}(\mathbf{G}_{r}^{c})^{-1}; \tag{6.18}$$

where $\mathbf{L}_{pqr}[k,l,j]$ refers to the direct accumulation moment of order $(j-1)$ obtained from the unidimensional function $\mathbf{m}_{pq}^{i}[k,l]$ in the z variable.

From equation (2.11), the relationship between the direct accumulation moments and the function from which they are obtained is established through the up-down-flipped Pascal matrix $\mathbf{Q}_{cr}$. Then,

$$\begin{pmatrix}\mathbf{L}_{pq}[k,l,1] & \dots & \mathbf{L}_{pq}[k,l,r]\end{pmatrix} = \begin{pmatrix}\mathbf{m}^1_{pq}[k,l] & \dots & \mathbf{m}^c_{pq}[k,l]\end{pmatrix}\ \mathbf{Q}_{cr}.$$

Including this expression in equation (6.18) and ranging for $k = 1,\dots,p$ and $l = 1,\dots,q$,

$$\begin{pmatrix}\mathbf{M}_{pqr}[1,1,:]\\ \mathbf{M}_{pqr}[1,2,:]\\ \vdots\\ \mathbf{M}_{pqr}[p,q,:]\end{pmatrix} = \begin{pmatrix}\mathbf{m}^1_{pq} & \dots & \mathbf{m}^c_{pq}\end{pmatrix}\ \mathbf{Q}_{cr}\ (\mathbf{G}^c_r)^{-1};$$

where

$$\mathbf{m}^i_{pq} = \begin{pmatrix}\mathbf{m}^i_{pq}[1,1] & \mathbf{m}^i_{pq}[1,2] & \dots & \mathbf{m}^i_{pq}[p,q]\end{pmatrix}^t$$

Since $\mathbf{m}^i_{pq}$ is the columnwise form of the geometric moments of the image in the i plane, they can be related to the columnwise form of its accumulation moments. Using corollary 2.2.1 and property 6.1.1,

$$\begin{pmatrix}\mathbf{M}_{pqr}[1,1,:]\\ \mathbf{M}_{pqr}[1,2,:]\\ \vdots\\ \mathbf{M}_{pqr}[p,q,:]\end{pmatrix} = \left(((\mathbf{G}^a_p)^t)^{-1} \otimes ((\mathbf{G}^b_q)^t)^{-1}\right)\ \begin{pmatrix}\mathbf{l}^1_{pq} & \dots & \mathbf{l}^c_{pq}\end{pmatrix}\ \mathbf{Q}_{cr}\ (\mathbf{G}^c_r)^{-1},$$

where $\mathbf{l}^z_{pq}$ is defined as in equation (6.11).

Then, by corollary 6.3.1 and the application of the columnwise transformation of property 6.1.1, equation (6.15) is obtained. An analogous development for the case of reverse accumulation moments proves equation (6.16).

□

Example 6.3.1. Assume a 3D image of size $3 \times 4 \times 2$ so that the 2D images planes are

$$\mathbf{I}_{342}[:,:,1] = \begin{pmatrix}1 & 2 & 3 & 1\\ 1 & 0 & 2 & 0\\ 4 & 2 & 3 & 1\end{pmatrix} \qquad \text{and} \qquad \mathbf{I}_{342}[:,:,2] = \begin{pmatrix}1 & 0 & 1 & 0\\ 0 & 2 & 1 & 0\\ 1 & 0 & 0 & 1\end{pmatrix}.$$

Then, its associated columnwise form is

$$\mathbf{i}_{342} = \begin{pmatrix}1\ 2\ 3\ 1\ 1\ 0\ 2\ 0\ 4\ 2\ 3\ 1\ 1\ 2\ 3\ 1\ 1\ 0\ 2\ 0\ 4\ 2\ 3\ 1\end{pmatrix}.$$

Using the following Vandermonde matrices – as defined in (2.1.1) –

$$\mathbf{V}_{34} = \begin{pmatrix} 1 & 1 & 1 & 1 \\ 1 & 2 & 4 & 8 \\ 1 & 3 & 9 & 27 \end{pmatrix}, \qquad \mathbf{V}_{43} = \begin{pmatrix} 1 & 1 & 1 \\ 1 & 2 & 4 \\ 1 & 3 & 9 \\ 1 & 4 & 16 \end{pmatrix} \quad \text{and} \quad \mathbf{V}_{22} = \begin{pmatrix} 1 & 1 \\ 1 & 2 \end{pmatrix}$$

and according to lemma 6.2.1, the columnwise form of the geometric moments is

$$\mathbf{m}_{432} = \big(40 \quad 52 \quad 100 \quad 128 \quad 300 \quad 380 \quad 83 \quad 107 \quad 217 \quad 279 \quad 667 \quad 855 \\ 195 \quad 249 \quad 529 \quad 679 \quad 1655 \quad 2127 \quad 497 \quad 629 \quad 1387 \quad 1773 \quad 4393 \quad 5637\big)$$

On the other hand, using the following Pascal matrices – as defined in (2.21) –

$$\mathbf{P}_{34} = \begin{pmatrix} 1 & 1 & 1 & 1 \\ 1 & 2 & 3 & 4 \\ 1 & 3 & 6 & 10 \end{pmatrix}, \qquad \mathbf{P}_{43} = \begin{pmatrix} 1 & 1 & 1 \\ 1 & 2 & 3 \\ 1 & 3 & 6 \\ 1 & 4 & 10 \end{pmatrix} \quad \text{and} \quad \mathbf{P}_{22} = \begin{pmatrix} 1 & 1 \\ 1 & 2 \end{pmatrix}$$

and according to lemma 6.3.1, the columnwise form of the reverse accumulation moments is

$$\mathbf{r}_{432} = \big(40 \quad 52 \quad 100 \quad 128 \quad 200 \quad 254 \quad 83 \quad 107 \quad 217 \quad 279 \quad 442 \quad 567 \\ 139 \quad 178 \quad 373 \quad 479 \quad 767 \quad 985 \quad 208 \quad 265 \quad 568 \quad 728 \quad 1175 \quad 1508\big).$$

Then, it is not difficult to verify that, using the following matrices – as defined in (2.23) –

$$\mathbf{H}_4 = \begin{pmatrix} 1 & 0 & 0 & 0 \\ 0 & 1 & \frac{1}{2} & \frac{1}{3} \\ 0 & 0 & \frac{1}{2} & \frac{1}{2} \\ 0 & 0 & 0 & \frac{1}{6} \end{pmatrix} \qquad \mathbf{H}_3 = \begin{pmatrix} 1 & 0 & 0 \\ 0 & 1 & \frac{1}{2} \\ 0 & 0 & \frac{1}{2} \end{pmatrix} \qquad \mathbf{H}_2 = \begin{pmatrix} 1 & 0 \\ 0 & 1 \end{pmatrix}$$

and according to lemma 6.3.2, the columnwise form of the geometric moments can be related to the columnwise form of the reverse accumulation moments.

Hence, we have just proved that all matrix relationships obtained in chapter 2 can be generalized to the nD case by simply using the Kronecker product and the columnwise form of the data matrix as defined in 6.1.1 and 6.1.2, respectively.

Part II

Reconstructing an image from a set of its accumulation moments

Chapter 7

Reconstructing by backprojecting

Since accumulation moments are obtained from accumulated additions over the image values, the inverse process, that is, the reconstruction of the image from a finite set of its accumulation moments can be done, as intuitively expected, by the inverse operation, i.e., by accumulated subtractions.

We have devised a method that proceeds in two steps. The first step starts by subtracting the accumulation moments of higher order from their immediate predecessor. Resulting values are subtracted following the same order. The algorithm iterates until only one number remains. The second step initiates with the values obtained from the last subtraction of each iteration in the first step. It proceeds by subtracting each number from the one obtained from the subtraction of the two numbers on its right side. The last value of this sequence of subtractions is already part of the solution. All the others are processed following the same algorithm until the solution is completed. This idea is formalized in algorithm 7.1.

The method is better understood through the following example.

Example 7.0.2. Let us assume

$$\mathbf{R}_{14} = \begin{pmatrix} 10 & 30 & 65 & 119 \end{pmatrix}.$$

Figure 7.1 shows the way in which the subtractions proceed to obtain the reconstructed image

$$\mathbf{I}_{14} = \begin{pmatrix} 1 & 2 & 3 & 4 \end{pmatrix}.$$

It is easy to prove that, assuming $m = n$, the total amount of operations is simply $m^2(m-1)$ subtractions.

If the number of accumulation moments is smaller than the image size, the reconstruction is an ill-posed problem, that is, the reconstructed image is not unique. Since additional constraints are required to solve this ill-posedness, two reasonable assumptions comes up:

Algorithm: backprojection
Input: $\mathbf{R}_{mn}$
Output: $\mathbf{I}_{mn}$

FOR every column *c*
$\mathbf{R}_{mn}[:, c]$ = step2 (step1 ($\mathbf{R}_{mn}[:, c]$))
ENDFOR

FOR every row *r*
$\mathbf{R}_{mn}[r, :]$ = step2 (step1 ($\mathbf{R}_{mn}[r, :]$))
ENDFOR

$\mathbf{I}_{mn} \leftarrow \mathbf{R}_{mn}$

Algorithm: step1
Input: $\mathbf{r}_p$
Output: $\mathbf{r}_p$

FOR i=1 TO p-1
FOR j=p-1 TO i

$$\mathbf{r}_p[j+1] \longleftarrow \mathbf{r}_p[j+1] - \mathbf{r}_p[j]$$

ENDFOR
ENDFOR

Algorithm: step2
Input: $\mathbf{r}_p$
Output: $\mathbf{r}_p$

FOR i=p-1 TO 1
FOR j=1 TO i

$$\mathbf{r}_p[p-j] \longleftarrow \mathbf{r}_p[p-j] - \mathbf{r}_p[p-j-1]$$

ENDFOR
ENDFOR

Algorithm 7.1: *Backprojection reconstruction.*

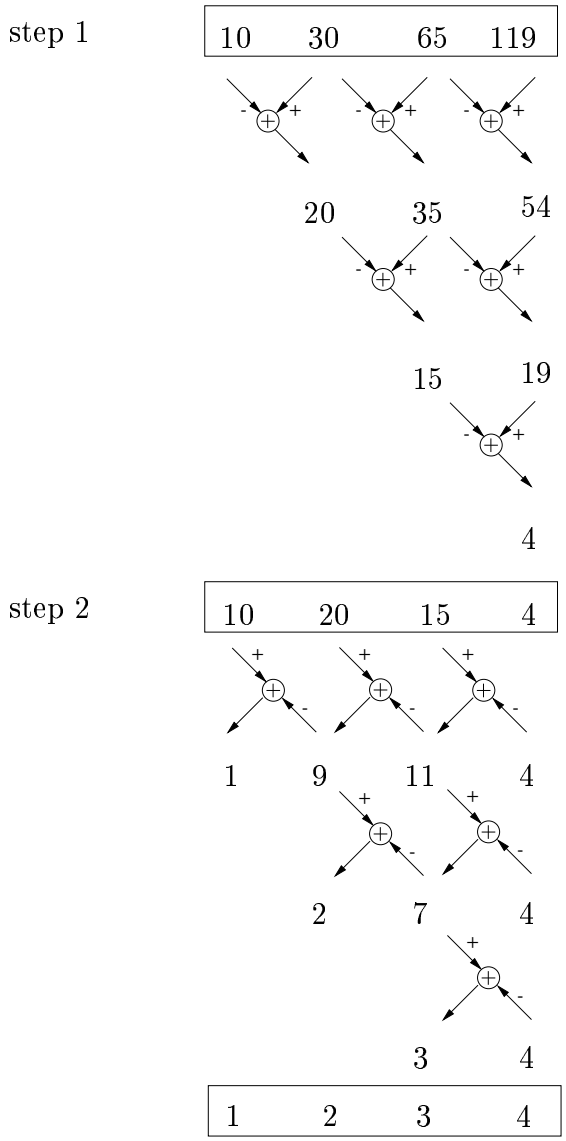

Figure 7.1: *The two steps of the backprojection reconstruction method.*

- reconstruct an image of the same size as the number of available moments and assume null values for the rest of the image; or
- assume null values for unknown moments and reconstruct an image of the desired size.

In the previous example, assuming that $\mathbf{R}_{14}$ is derived from a larger image, a possible solution would be

$$\tilde{\mathbf{I}}_{1\ n+4} = (1 \quad 2 \quad 3 \quad 4 \quad \underbrace{0 \quad \cdots \quad 0}_{n}).$$

However, this solution is probably not very much alike the original image from which the accumulation moments were obtained. This is clearly shown in the following example.

Example 7.0.3. Given $\mathbf{I}_{17} = (1 \quad 2 \quad 3 \quad 4 \quad 3 \quad 2 \quad 1)$, the reconstructed images $\tilde{\mathbf{I}}_{17}$ obtained from:

$$\mathbf{R}_{11} = (16)$$
$$\mathbf{R}_{13} = (16 \quad 64 \quad 180)$$
$$\mathbf{R}_{15} = (16 \quad 64 \quad 180 \quad 420 \quad 868)$$
$$\mathbf{R}_{17} = (16 \quad 64 \quad 180 \quad 420 \quad 868 \quad 1644 \quad 2913);$$

are shown in figures 7.2 (a), (b), (c) and (d), respectively.

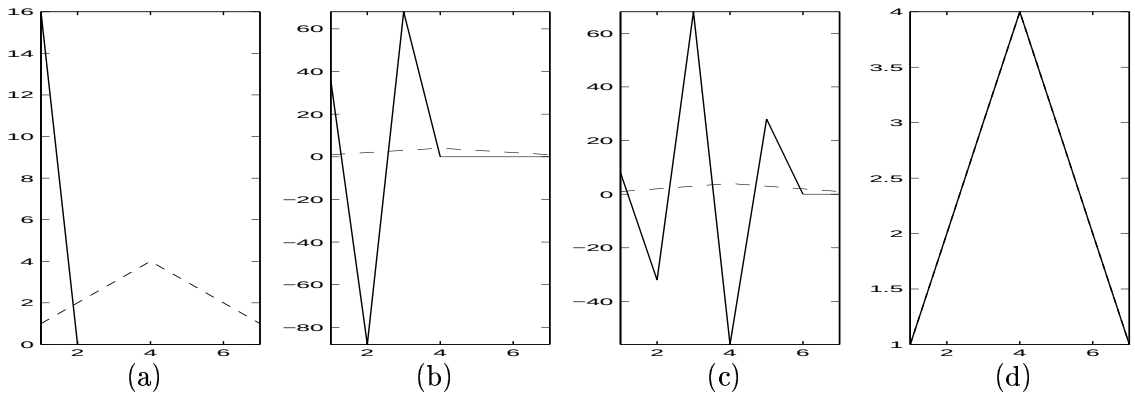

Figure 7.2: *Backprojection reconstruction from (a) 1, (b) 3, (c) 5 and (d) 7 reverse accumulation moments assuming null image values. Original image is plotted in dashed line.*

In general, it has been observed that increasing the number of accumulation moments generates more ripples in the reconstructed image, unless the number of accumulation moments equals its size.

On the other hand, the second alternative, i.e. assuming null values for unknown accumulation moments, neither allows to obtain any acceptable reconstruction, as shown in the following example.

Example 7.0.4. Given $\mathbf{I}_{17} = (1 \quad 2 \quad 3 \quad 4 \quad 3 \quad 2 \quad 1)$, the reconstructed images $\tilde{\mathbf{I}}_{17}$ obtained from:

$$\begin{aligned}
\mathbf{R}_{17} &= (16 \quad 0 \quad 0 \quad 0 \quad 0 \quad 0 \quad 0) \\
\mathbf{R}_{17} &= (16 \quad 64 \quad 180 \quad 0 \quad 0 \quad 0 \quad 0) \\
\mathbf{R}_{17} &= (16 \quad 64 \quad 180 \quad 420 \quad 868 \quad 0 \quad 0) \\
\mathbf{R}_{17} &= (16 \quad 64 \quad 180 \quad 420 \quad 868 \quad 1644 \quad 2913);
\end{aligned}$$

are shown in figures 7.3 (a), (b), (c) and (d), respectively.

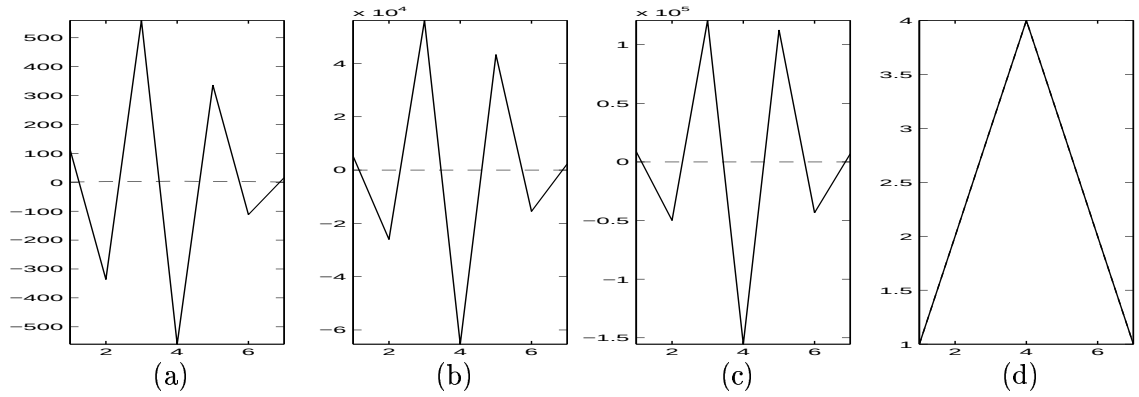

Figure 7.3: *Backprojection reconstruction from (a) 1, (b) 3, (c) 5 and (d) 7 reverse accumulation moments assuming that unknown moments are null. Original image is plotted in dashed line.*

It is possible to choose other values for unknown accumulation moments so that different reconstructed images are obtained. However, the backprojection method does not provide a criteria to choose these values in terms of a reconstruction error measure.

Nevertheless, one important point is that this process only involves subtractions. No matrix inversions are required, contrary to what happens in common reconstruction methods.

Chapter 8

A matrix-based reformulation of image series approximation

In this chapter, we introduce a matrix-based reformulation of the reconstruction of an image from a set of its projection coefficients. From this formulation, a new reconstruction method is derived: the unitary transform method. The key point of this new method is that the basis functions used in the reconstruction and those used to obtain the projection coefficients do not necessarily define the same subspace. It is proved that, when both subspaces coincide, the approximated image is the same as the one obtained using a least-squares error criterion.

Any discrete image of size $a \times b$, $\mathbf{I}_{ab}$, can be seen as a vector in $\mathbb{R}^{a \times b}$ or, alternatively, as a bidimensional function that maps all the points of the uniform lattice $\{1, 2, \ldots, a\} \times \{1, 2, \ldots, b\}$ onto real values. Then, $\mathbf{I}_{ab} \in \mathbb{R}^{a \times b}$ can be uniquely expressed as a linear combination of the functions of a basis set, i.e., a set containing ab linearly independent bidimensional functions, which will be denoted by $\{\Xi_{ab}^{k\,l}\}$, $k = 0, \ldots, a-1$ and $l = 0, \ldots, b-1$. In other words,

$$\mathbf{I}_{ab} = \sum_{k=0}^{a-1} \sum_{l=0}^{b-1} \alpha^{k\,l}\, \Xi_{ab}^{k\,l}. \tag{8.1}$$

Definition 8.0.2 (Basis matrices). The functions in any basis set are assumed to be separable and equally defined for both coordinates, i.e.,

$$\Xi_{ab}^{k\,l} = \boldsymbol{\phi}_a^k\, (\boldsymbol{\phi}_b^l)^t,$$

where $\boldsymbol{\phi}_a^k$ and $\boldsymbol{\phi}_b^l$ are vectors which will be grouped into respective matrices of the form:

$$\boldsymbol{\Phi}_{pq} = \left(\boldsymbol{\phi}_p^0 \quad \ldots \quad \boldsymbol{\phi}_p^{(q-1)}\right),$$

called *basis matrices*.

Definition 8.0.3 (Gram matrices). Given any subset of $\{\Xi_{ab}^{kl}\}$, their associated *Gram matrices* contain the inner products between its separable elements, respectively, as follows:

$$\boldsymbol{\Gamma}_q^p = (\boldsymbol{\Phi}_{pq})^t\, \boldsymbol{\Phi}_{pq}.$$

Note that $\mathbf{\Gamma}_q^p[k+1, l+1] =< \boldsymbol{\phi}_p^k, \boldsymbol{\phi}_p^l >$ and that Gram matrices become diagonal when dealing with orthogonal basis sets and the identity when the basis is orthonormalized.

Definition 8.0.4 (Projection matrices). The matrices containing the projection coefficients of an image $\mathbf{I}_{ab} \in \mathbb{R}^{a \times b}$ onto the first $m \cdot n$ elements of $\{\mathbf{\Xi}_{ab}^{k\,l}\}$ are called *projection matrices*. They can be obtained by computing:

$$\mathbf{\Omega}_{mn} = (\mathbf{\Phi}_{am})^t \; \mathbf{I}_{ab} \; \mathbf{\Phi}_{bn}. \tag{8.2}$$

Note that $\mathbf{\Omega}_{mn}[k+1, l+1] =< \mathbf{I}_{ab}, \mathbf{\Xi}_{ab}^{kl} >= (\boldsymbol{\phi}_a^k)^t \; \mathbf{I}_{ab} \; \boldsymbol{\phi}_p^l$.

Definition 8.0.5 (Expansion matrices). An image $\mathbf{I}_{ab} \in \mathbb{R}^{a \times b}$ can be partially expanded in terms of a subset of $\{\mathbf{\Xi}_{ab}^{k\,l}\}$ as:

$$\hat{\mathbf{I}}_{ab}^{mn} = \sum_{k=0}^{m-1} \sum_{l=0}^{n-1} \lambda^{k\,l} \mathbf{\Xi}_{ab}^{k\,l} = \mathbf{\Phi}_{am} \; \mathbf{\Lambda}_{mn} \; (\mathbf{\Phi}_{bn})^t, \tag{8.3}$$

where $m \leq a$, $n \leq b$, and $\mathbf{\Lambda}_{mn}[k+1, l+1] = \lambda^{k\,l}$. Note that $\hat{\mathbf{I}}_{ab}^{ab} = \mathbf{I}_{ab}$. When λ^{kl} is chosen so that the truncation error is minimized using a least-squares error criterion, $\mathbf{\Lambda}_{mn}$ denotes what it is called an *expansion matrix*.

Lemma 8.0.3. *Given an image* $\mathbf{I}_{ab}$ *and a subset of* $\{\mathbf{\Xi}_{ab}^{kl}\}$, *any expansion matrix can be expressed in terms of the corresponding projection and Gram matrices as follows:*

$$\mathbf{\Lambda}_{mn} = (\mathbf{\Gamma}_m^a)^{-1} \; \mathbf{\Omega}_{mn} \; (\mathbf{\Gamma}_n^b)^{-1}, \tag{8.4}$$

where $m \leq a$ *and* $n \leq b$.

Proof. Since $\lambda^{k\,l}$ is chosen so that the truncation error is minimized according to a least-squares error criterion, the subspaces generated by the truncation error and the truncated series are orthogonal (see figure 8.1). That is, for $p = 0, \ldots, m-1$ and for $q = 0, \ldots, n-1$,

$$< \mathbf{\Xi}_{ab}^{p\,q}, \mathbf{I}_{ab} - \sum_{k=0}^{m-1} \sum_{l=0}^{n-1} \lambda^{k\,l} \mathbf{\Xi}_{ab}^{k\,l} >= 0.$$

In other words,

$$< \boldsymbol{\phi}_a^p (\boldsymbol{\phi}_b^q)^t, \mathbf{I}_{ab} >= \sum_{k=0}^{m-1} \sum_{l=0}^{n-1} \lambda^{k\,l} < \boldsymbol{\phi}_a^p, \boldsymbol{\phi}_a^k > < (\boldsymbol{\phi}_b^q)^t, (\boldsymbol{\phi}_b^l)^t >,$$

$$\forall p = 0, \ldots, m-1, \forall q = 0, \ldots, n-1.$$

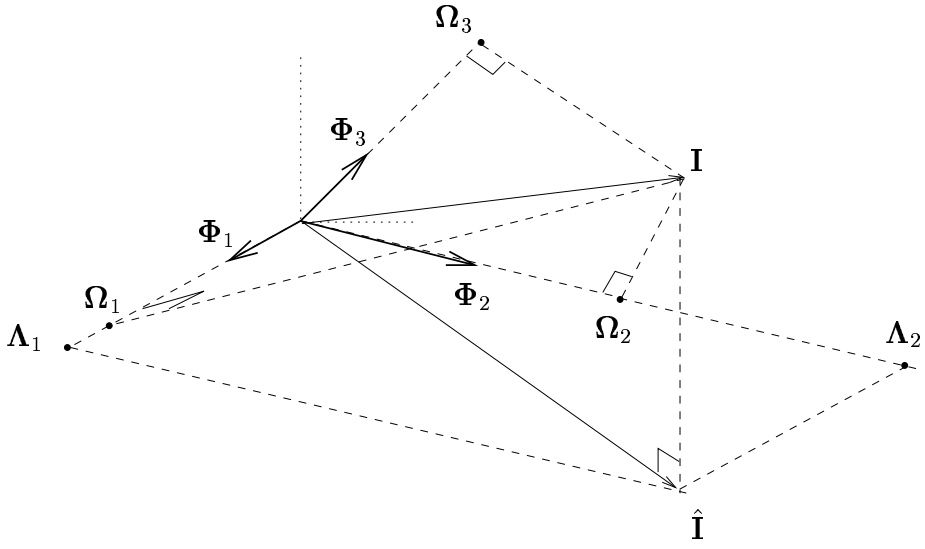

Figure 8.1: *Geometric interpretation of the least-squares error criterion.*

Then, when formulated in matrix terms, this leads to:

$$\mathbf{\Omega}_{mn} = \mathbf{\Gamma}^a_m \, \mathbf{\Lambda}_{mn} \, \mathbf{\Gamma}^b_n. \tag{8.5}$$

Since Gram matrices are obtained from functions of a basis set, they are non-singular and this proves the lemma.

□

Corollary 8.0.2 (Least-squares approximation). *The series approximation of an image, in the least-squares sense, can be expressed as:*

$$\hat{\mathbf{I}}^{mn}_{ab} = \mathbf{\Phi}_{am} \, \mathbf{\Lambda}_{mn} \, (\mathbf{\Phi}_{bn})^t = \mathbf{\Phi}_{am} \, (\mathbf{\Gamma}^a_m)^{-1} \, \mathbf{\Omega}_{mn} \, (\mathbf{\Gamma}^b_n)^{-1} \, (\mathbf{\Phi}_{bn})^t =$$

$$= \mathbf{\Phi}_{am} \, ((\mathbf{\Phi}_{am})^t \, \mathbf{\Phi}_{am})^{-1} \mathbf{\Omega}_{mn} \, ((\mathbf{\Phi}_{bn})^t \, \mathbf{\Phi}_{bn})^{-1} \, (\mathbf{\Phi}_{bn})^t = (\mathbf{\Phi}_{am})^- \, \mathbf{\Omega}_{mn} \, (\mathbf{\Phi}_{bn})^+, \tag{8.6}$$

where $(\cdot)^-$ and $(\cdot)^+$ are called the left and right Moore-Penrose pseudoinverses or generalized inverses.

The inversion of the Gram matrices requires the computation of the above pseudoinverses which are highly ill-conditioned when dealing with geometric moments. In practice, one has to rely on the singular value decomposition to obtain these pseudoinverses as explained in chapter 12.

Corollary 8.0.3. *If the basis set $\{\overline{\mathbf{\Xi}}^{kl}_{ab}\}$ is orthonormal – we use an overline to distinguish it from the general case – the least-squares approximation of the image is obtained from*

$$\overline{\mathbf{I}}^{mn}_{ab} = \overline{\mathbf{\Phi}}_{am} \, \overline{\mathbf{\Omega}}_{mn} \, (\overline{\mathbf{\Phi}}_{bn})^t \tag{8.7}$$

since

$$\overline{\mathbf{\Omega}}_{mn} = \overline{\mathbf{\Lambda}}_{mn}. \tag{8.8}$$

Lemma 8.0.4. *Given a subset of* $\{\overline{\Xi}_{ab}^{kl}\}$ *that expands a subspace of the same dimension as the one expanded by a subset of* $\{\Xi_{ab}^{kl}\}$*, then:*

$$\overline{\mathbf{\Omega}}_{mn} = ((\mathbf{\Phi}_{am})^t\ \overline{\mathbf{\Phi}}_{am})^{-1}\ \mathbf{\Omega}_{mn}\ ((\overline{\mathbf{\Phi}}_{bn})^t\ \mathbf{\Phi}_{bn})^{-1}, \tag{8.9}$$

where

$$\mathbf{\Omega}_{mn} = (\mathbf{\Phi}_{am})^t\ \mathbf{I}_{ab}\ \mathbf{\Phi}_{bn}$$

and

$$\overline{\mathbf{\Omega}}_{mn} = (\overline{\mathbf{\Phi}}_{am})^t\ \mathbf{I}_{ab}\ \overline{\mathbf{\Phi}}_{bn}.$$

Proof. Let us consider the following approximated image

$$\overline{\mathbf{I}}_{ab}^{mn} = \overline{\mathbf{\Phi}}_{am}\ \overline{\mathbf{\Omega}}_{mn}\ (\overline{\mathbf{\Phi}}_{bn})^t. \tag{8.10}$$

If we want that this image has the same projection coefficients onto $\{\Xi_{ab}^{kl}\}$ as $\mathbf{I}_{ab}$, then

$$\mathbf{\Omega}_{mn} = (\mathbf{\Phi}_{am})^t\ \mathbf{I}_{ab}\ \mathbf{\Phi}_{bn} = (\mathbf{\Phi}_{am})^t\ \overline{\mathbf{I}}_{ab}^{mn}\ \mathbf{\Phi}_{bn} = (\mathbf{\Phi}_{am})^t\ \overline{\mathbf{\Phi}}_{am}\ \overline{\mathbf{\Omega}}_{mn}\ (\overline{\mathbf{\Phi}}_{bn})^t\ \mathbf{\Phi}_{bn}, \tag{8.11}$$

from which (8.0.4) is readily obtained.

□

Corollary 8.0.4 (Unitary approximation). *The series approximation of an image can be obtained from:*

$$\overline{\mathbf{I}}_{ab}^{mn} = \overline{\mathbf{\Phi}}_{am}\ ((\mathbf{\Phi}_{am})^t\ \overline{\mathbf{\Phi}}_{am})^{-1}\ \mathbf{\Omega}_{mn}\ ((\overline{\mathbf{\Phi}}_{bn})^t\ \mathbf{\Phi}_{bn})^{-1}(\overline{\mathbf{\Phi}}_{bn})^t = \tag{8.12}$$

$$= \overline{\mathbf{\Phi}}_{am}\ (\mathbf{C}_m^a)^{-1}\ \mathbf{\Omega}_{mn}\ \left((\mathbf{C}_n^b)^t\right)^{-1}\ (\overline{\mathbf{\Phi}}_{bn})^t \tag{8.13}$$

where

$$\mathbf{C}_q^p[k+1, l+1] =< \overline{\phi}_p^k, \phi_p^l > . \tag{8.14}$$

Corollary 8.0.5. *If the subsets of* $\{\Xi_{ab}^{kl}\}$ *and* $\{\overline{\Xi}_{ab}^{kl}\}$ *span the same subspace, then* $\hat{\mathbf{I}}_{ab}^{mn} = \overline{\mathbf{I}}_{ab}^{mn}$.

$\hat{\mathbf{I}}_{ab}^{mn}$ and $\overline{\mathbf{I}}_{ab}^{mn}$ have a simple geometric interpretation, as shown in figure 8.2.

This chapter has provided a unified framework for the reconstruction of an image from a reduced set of projection coefficients in matrix terms. Former and novel reconstruction methods developed in chapters 10 and 11, respectively, are set into this context.

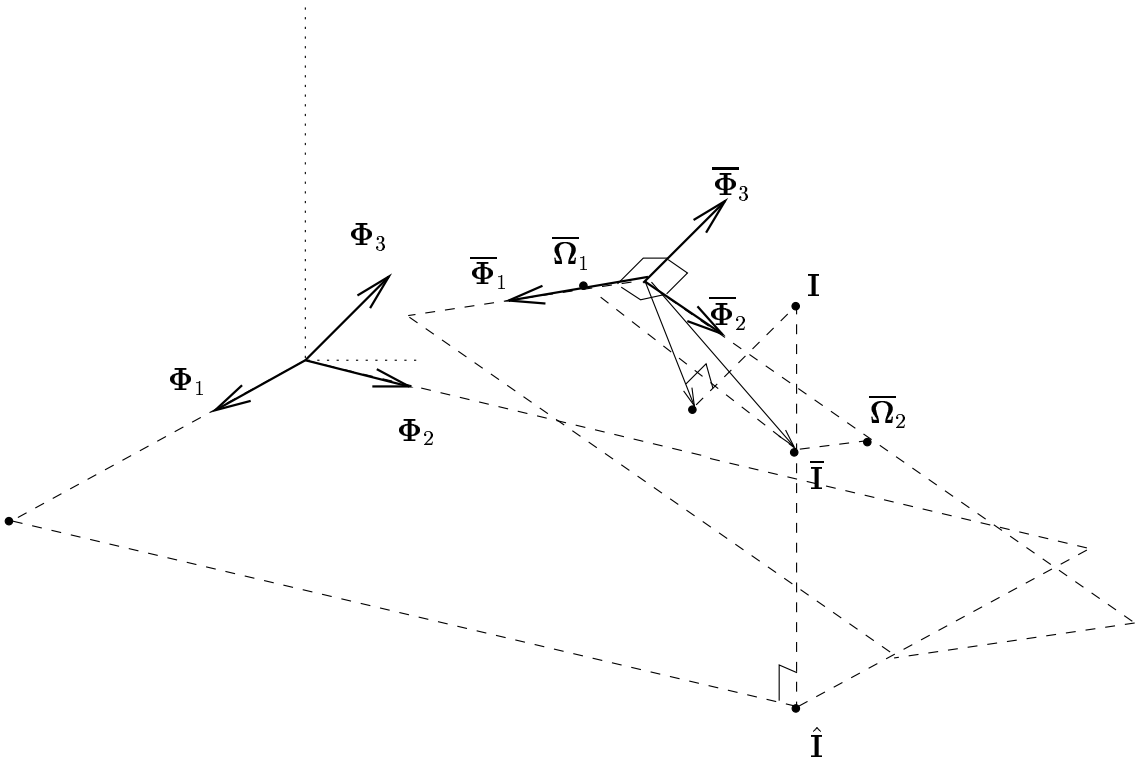

Figure 8.2: *Geometric interpretation of the unitary approximation. For clearness, the origins of both basis sets are represented separately.*

Chapter 9

Reconstructing by expressing moments as projection coefficients

9.1 Geometric and accumulation moments as projection coefficients

Geometric moments are defined in 2.2 as

$$\mu_{mn} = \sum_{x=1}^{a} \sum_{y=1}^{b} x^m y^n \mathbf{I}_{ab}[x, y]. \tag{9.1}$$

Then, they can be seen as the projection coefficients of the image onto the basis set of monomial functions, that is

$$\mathbf{\Omega}_{mn}[k+1, l+1] = \mu_{kl},$$

$$\mathbf{\Xi}^{k\,l}_{mn}[x+1, y+1] = x^k y^l,$$

and

$$\mathbf{\Phi}_{pq}[k, l] = k^{l-1},$$

for $k = 0, \ldots, m-1$ and $l = 0, \ldots, n-1$.

These basis matrices are the already introduced *Vandermonde matrices* and their associated Gram matrices correspond to what in the literature are known as *Hilbert matrices* whose general term is [105]:

$$\mathbf{\Gamma}^p_q[k+1, l+1] = \frac{1}{k+l+1}.$$

Likewise, direct and reverse accumulation moments are defined in 2.10 and 2.19 as

$$\mathbf{L}_{mn}[k, l] = \sum_{x=1}^{a} \sum_{y=1}^{b} \binom{a-x+k-1}{a-x} \binom{b-y+l-1}{b-y} \mathbf{I}_{ab}[x, y] \tag{9.2}$$

and

$$\mathbf{R}_{mn}[k,l] = \sum_{x=1}^{a}\sum_{y=1}^{b}\binom{x+k-2}{x-1}\binom{y+l-2}{y-1}\mathbf{I}_{ab}[x,y], \tag{9.3}$$

respectively.

Remark. *Since combinatorial numbers can be expressed in a polynomial form as shown in the proofs of theorems 2.2.1 and 2.3.1, i.e.*

$$r_q^p(t) = \binom{p-t+q-1}{p-t} = \frac{(-1)^{q-1}}{(q-1)!}\prod_{i=1}^{q-1}(t-p-i), \tag{9.4}$$

where the order of the polynomial is $q-1$, accumulation moments can be seen as the projection coefficients of the image onto the basis set of these polynomial functions.

Hence, for direct accumulation moments,

$$\mathbf{\Omega}_{mn}[k,l] = \mathbf{L}_{mn}[k,l],$$

$$\mathbf{\Xi}_{mn}^{k\,l}[x,y] = r_k^a(x)\, r_l^b(y)$$

and

$$\mathbf{\Phi}_{pq}[k,l] = \frac{(-1)^{l-1}}{(l-1)!}\prod_{i=1}^{l-1}(-p-i+k),$$

for $k = 0,\ldots,m-1$ and $l = 0,\ldots,n-1$.

Likewise, for reverse accumulation moments,

$$\mathbf{\Omega}_{mn}[k,l] = \mathbf{R}_{mn}[k,l]$$

and, using the same definition of the polynomials in (9.4) by simply setting $p=-1$,

$$\mathbf{\Xi}_{mn}^{k\,l}[x,y] = r_k^{-1}(-x)\, r_l^{-1}(-y)$$

and

$$\mathbf{\Phi}_{pq}[k,l] = \frac{(-1)^{l-1}}{(l-1)!}\prod_{i=1}^{l-1}(1-i-k);$$

for $k = 0,\ldots,m-1$ and $l = 0,\ldots,n-1$.

Tables 9.1 and 9.2 show some polynomials of the basis set associated with direct and reverse accumulation moments, which are plotted in figures 9.1 and 9.2, respectively. In figure 9.3, the polynomial basis up to fourth order are represented for both (a) direct and (b) reverse accumulation moments.

p=1	$\mathbf{r}_0[x] = 1$
p=2	$\mathbf{r}_0[x] = 1$ $\mathbf{r}_1[x] = -x + 3$
p=3	$\mathbf{r}_0[x] = 1$ $\mathbf{r}_1[x] = -x + 4$ $\mathbf{r}_2[x] = 0.500\,x^2 - 4.500\,x + 10$
p=4	$\mathbf{r}_0[x] = 1$ $\mathbf{r}_1[x] = -x + 5$ $\mathbf{r}_2[x] = 0.500\,x^2 - 5.500\,x + 15$ $\mathbf{r}_3[x] = -0.167\,x^3 + 3\,x^2 - 17.830\,x + 35$
p=5	$\mathbf{r}_0[x] = 1$ $\mathbf{r}_1[x] = -x + 6$ $\mathbf{r}_2[x] = 0.500\,x^2 - 6.500\,x + 21$ $\mathbf{r}_3[x] = -0.167\,x^3 + 3.500\,x^2 - 24.334\,x + 56$ $\mathbf{r}_4[x] = 0.042\,x^4 - 1.250\,x^3 + 13.958\,x^2 - 68.750\,x + 126$
p=6	$\mathbf{r}_0[x] = 1$ $\mathbf{r}_1[x] = -x + 7$ $\mathbf{r}_2[x] = 0.500\,x^2 - 7.500\,x + 28$ $\mathbf{r}_3[x] = -0.167\,x^3 + 4\,x^2 - 31.830\,x + 84$ $\mathbf{r}_4[x] = 0.042\,x^4 - 1.417\,x^3 + 17.958\,x^2 - 100.584\,x + 210$ $\mathbf{r}_6^5[x] = 0.008\,x^5 - 0.375\,x^4 - 6.708\,x^3 + 59.625\,x^2 - 263.283\,x + 462$
p=7	$\mathbf{r}_0[x] = 1$ $\mathbf{r}_1[x] = -x - 8$ $\mathbf{r}_2[x] = 0.5\,x^2 - 8.5\,x + 36$ $\mathbf{r}_3[x] = -0.167\,x^3 + 4.5\,x^2 - 40.334\,x + 120$ $\mathbf{r}_4[x] = 0.042\,x^4 - 1.583\,x^3 + 22.458\,x^2 - 140.917\,x + 330$ $\mathbf{r}_5[x] = -0.008\,x^5 + 0.417\,x^4 - 8.292\,x^3 + 82.084\,x^2 - 404.200\,x + 792$ $\mathbf{r}_6[x] = 0.001\,x^6 - 0.087\,x^5 + 2.285\,x^4 - 31.646\,x^3 + 245.214\,x^2 - 1007.767\,x + 1716$

Table 9.1: *Polynomial basis associated with the direct accumulation moments for increasing values of p.*

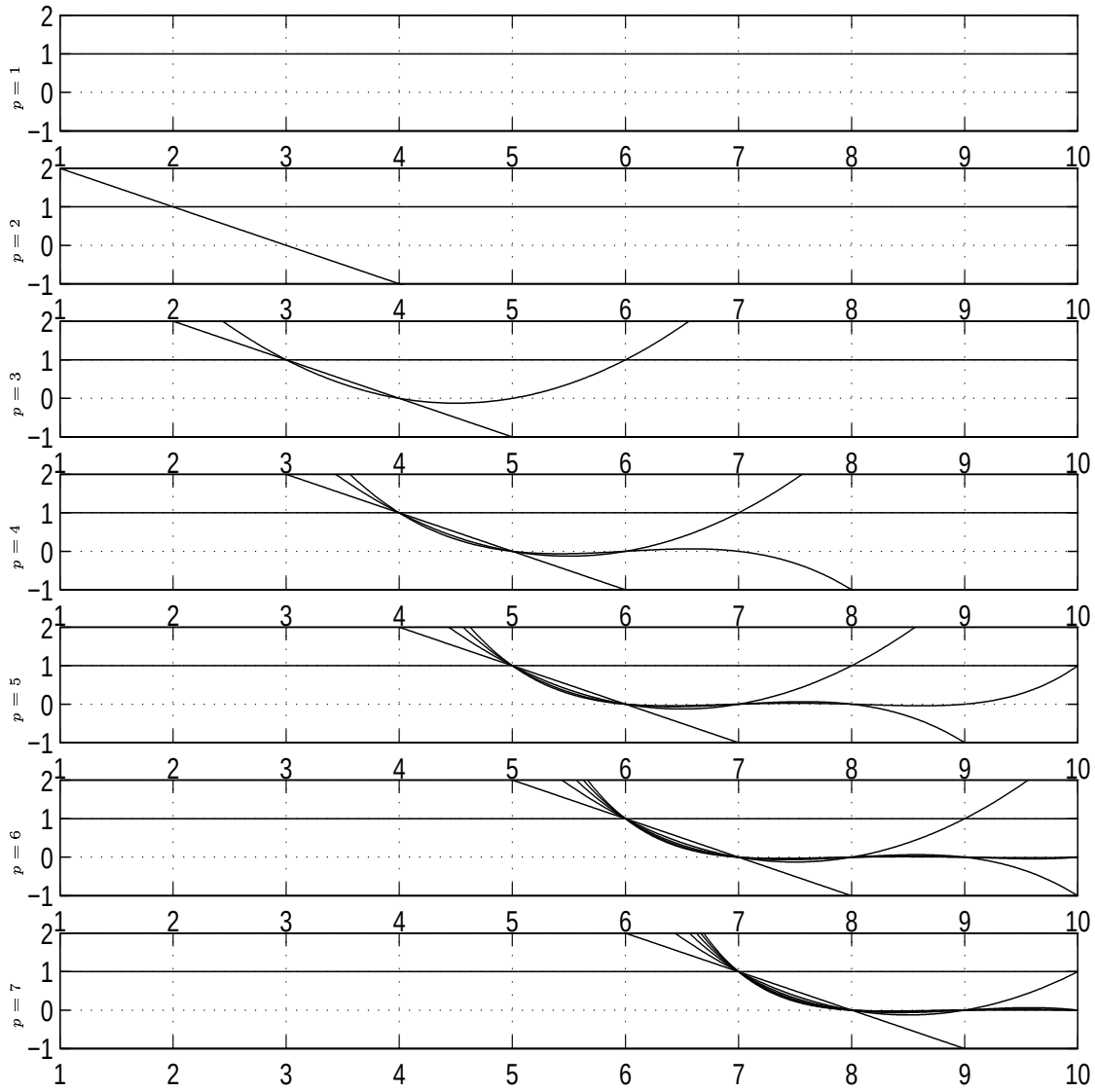

Figure 9.1: *Polynomial functions associated with the direct accumulation moments for increasing values of p.*

p=-1	$\mathbf{r}_0[x] = 1$
	$\mathbf{r}_1[x] = x$
	$\mathbf{r}_2[x] = 0.500\,x^2 + 0.500\,x$
	$\mathbf{r}_3[x] = 0.167\,x^3 + 0.500\,x^2 + 0.334\,x$
	$\mathbf{r}_4[x] = 0.042\,x^4 + 0.250\,x^3 + 0.458\,x^2 0.250\,x$
	$\mathbf{r}_5[x] = 0.008\,x^5 + 0.084\,x^4 + 0.292\,x^3 + 0.417\,x^2 + 0.200\,x$
	$\mathbf{r}_6[x] = 0.001\,x^6 + 0.0217\,x^5 + 0.118\,x^4 + 0.312\,x^3 + 0.381\,x^2 + 0.167\,x$

Table 9.2: *Polynomial basis associated with the reverse accumulation moments.*

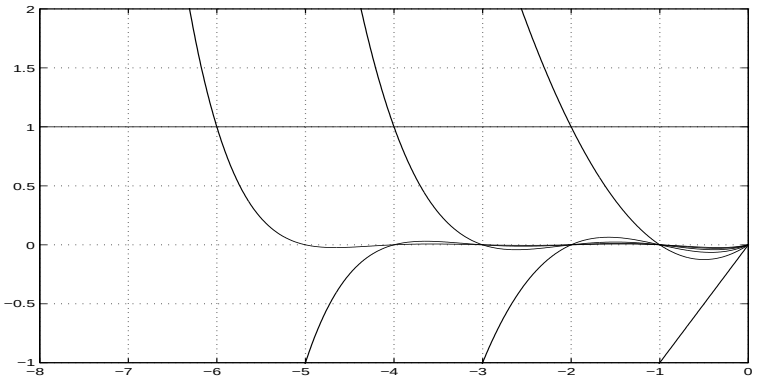

Figure 9.2: *Polynomial functions associated with reverse accumulation moments.*

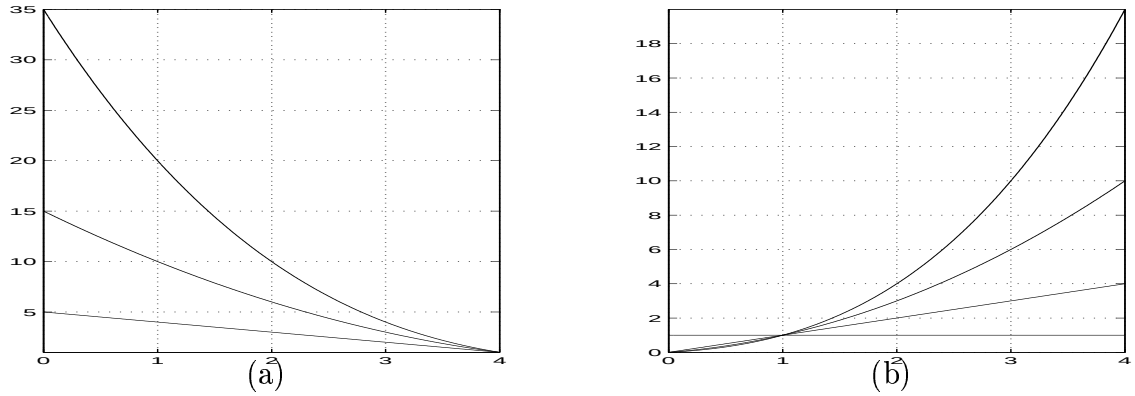

Figure 9.3: *Polynomial basis of fourth order for (a) direct and (b) reverse accumulation moments.*

Notice that the coefficients of $r_q^p(t)$ correspond to the elements of $\mathbf{G}_q^p[:,q]$, as defined in 2.16. Likewise, the coefficients of $r_q^{-1}(t)$ correspond to the elements of $\mathbf{H}_q[:,q]$, as defined in 2.23.

This interpretation shows how both geometric and accumulation moments are obtained as projection coefficients onto a polynomial basis. In fact, this is the definition of moments, which only differ in the specific polynomial basis set and the chosen coordinate system, either polar or cartesian. Therefore, although it was not so obvious that accumulation moments could be considered as proper moments when first introduced in chapter 2, here we have provided a formal justification.

9.2 Ill-posedness

Inverse problems, that is, reconstructing an image from a finite set of its projection coefficients are usually ill-posed problems in the Hadamard sense [4]: either the solution is not unique, leading to an ambiguous reconstruction, or it does not exist or it does not depend continuously on the input data.

In this section, we set the problem of reconstructing an image from a finite set of its moments in terms of the matrix formulation introduced in chapter 8. In this context, given a finite set of either geometric or accumulation moments, the reconstruction problem consists in obtaining an image matrix $\mathbf{I}_{ab}$ so that any of the following relationships is verified:

$$\begin{aligned} \mathbf{M}_{mn} &= (\mathbf{V}_{am})^t\, \mathbf{I}_{ab}\, \mathbf{V}_{bn}; \\ \mathbf{L}_{mn} &= (\mathbf{Q}_{am})^t\, \mathbf{I}_{ab}\, \mathbf{Q}_{bn}; \\ \mathbf{R}_{mn} &= (\mathbf{P}_{am})^t\, \mathbf{I}_{ab}\, \mathbf{P}_{bn}. \end{aligned} \tag{9.5}$$

If $a = m$ and $b = n$, then

$$\mathbf{I}_{ab} = \left((\mathbf{V}_a)^t\right)^{-1} \mathbf{M}_{ab} \left(\mathbf{V}_b\right)^{-1} = \left((\mathbf{Q}_a)^t\right)^{-1} \mathbf{L}_{ab} \left(\mathbf{Q}_b\right)^{-1} = \left((\mathbf{P}_a)^t\right)^{-1} \mathbf{R}_{ab} \left(\mathbf{P}_b\right)^{-1}. \tag{9.6}$$

In [88, pp. 90-91], a method to obtain the inverses of square Vandermonde matrices is provided. Square Pascal-like matrices are also invertible using this method since we have proved in theorems 2.2.1 and 2.3.1, respectively, that they are connected to Vandermonde matrices through triangular matrices.

However, in common applications, the number of available moments is lower than image dimensions, i.e. $m < a$ and $n < b$, so that only an approximated image can be obtained. In this case, the reconstructed image is not unique and the reconstruction is an ill-posed problem.

Non-unicity of the solution is easily proved if the equations in (9.5) are expressed in terms of a set of $m \cdot n$ linear equations with $a \cdot b$ unknowns of the form:

$$\boldsymbol{\omega}_{m\cdot n} = \mathbf{K}_{m\cdot n\ a\cdot b}\, \mathbf{i}_{a\cdot b}, \tag{9.7}$$

where $\boldsymbol{\omega}$ and $\mathbf{i}$ are columnwise vectors obtained by sequentially reading each row of the projection matrix and $\mathbf{I}_{ab}$, respectively; and $\mathbf{K}_{m\cdot n\ a\cdot b}$ is obtained from the Kronecker product of the basis matrices, as shown in chapter 6, that is

$$\mathbf{K}_{m\cdot n\ a\cdot b} = (\boldsymbol{\Phi}_{a\cdot m})^t \otimes (\boldsymbol{\Phi}_{b\cdot n})^t.$$

The rank of $\mathbf{K}_{m\cdot n\ a\cdot b}$ is, at most, $m \cdot n$. Then, the set of equations in (9.7) is rank-deficient and the solution is not unique [30]. Therefore, selective-solution methods are required, which impose $a \cdot b - m \cdot n$ linearly independent constraints so that the solution becomes unique. In chapter 8, it is shown that traditional least-squares reconstruction methods solve the ill-posedness by assuming constraints on the expansion coefficients. On the contrary, the unitary transform reconstruction method that we introduce in chapter 11 assumes constraints that can be interpreted in terms of image parameters, which is a much useful approach.

9.3 Ill-conditioning

In this section, we deal with ill-conditioning. We analyze the underlying reason why reconstructing an image from a set of its moments is, in general, an ill-conditioned problem; this means that, small perturbations in the data generate large errors in the reconstructed image which prevent us from obtaining an effective solution.

Here, we assume that moments are not affected by measurement errors. Then, we will see that perturbations are only due to *roundoff errors*.

Roundoff errors are the consequence of using a limited number of digits to approximate a number which requires more than this limit of digits for its exact specification. This error is introduced because of the fact that a computer is capable of supplying only a certain number of digits in effecting arithmetic operations. In particular, most common computers (IBM PC, most UNIX workstations, or Macintosh) use an IEEE arithmetic format that is based on a 64-bits floating-point representation of the numbers; specifically, 11 bits are used for the exponent, 52 bits, for the mantissa (the fraction), and 1 bit, for the sign [23, chapter 4]. Then, the exponent ranges from 1 to 2046, where $2046 = 2^{11} - 2$, but it is normalized from -1023 to 1022. As a consequence, the largest representable floating point number is $1.797693134862316 \times 10^{308}$ and the smallest positive floating point number is $2.225073858507201 \times 10^{-308}$. Since the mantissa is specified by 52 bits, the *computer integer resolution*, i.e. the maximum unsigned floating point integer, is $\eta = 2^{53} - 1 = 9.007199254740991 \times 10^{15}$. Therefore, any pair of numbers that have the same exponent but their mantissa differ below η are represented by the same value in the computer and roundoff error is introduced. Hence, the order in which additions are carried out is important since the associative law $(n_1 \oplus n_2) \oplus n_3 = n_1 \oplus (n_2 \oplus n_3)$, where the symbols $\oplus$ denotes computer addition, does not always hold [39, pp. 5-23].

In particular, geometric moments are obtained by the following addition:

$$\mathbf{M}_{mn}[k+1,l+1] = 1^k 1^l \mathbf{I}_{ab}[1,1] + 1^k 2^l \mathbf{I}_{ab}[1,2] + \ldots + 1^k a^l \mathbf{I}_{ab}[1,b] + \ldots + a^k b^l \mathbf{I}_{ab}[a,b].$$

Assuming a square image of size a and $0 \leq \mathbf{I}_a[k,l] \leq 255$, the maximum order $m_{\max} = n_{\max}$ ensuring exact moment computation independently of the algorithm, for the worst possible case in which $\mathbf{I}_a[1,1] = 1$ and $\mathbf{I}_a[a,a] = 255$, is obtained when $255a^{2m_{\max}} < \eta$. Then,

$$m_{\max} < \frac{\ln(\frac{\eta}{255})}{2\ln(a)}. \tag{9.8}$$

Figure 9.4 shows these values for increasing image sizes a.

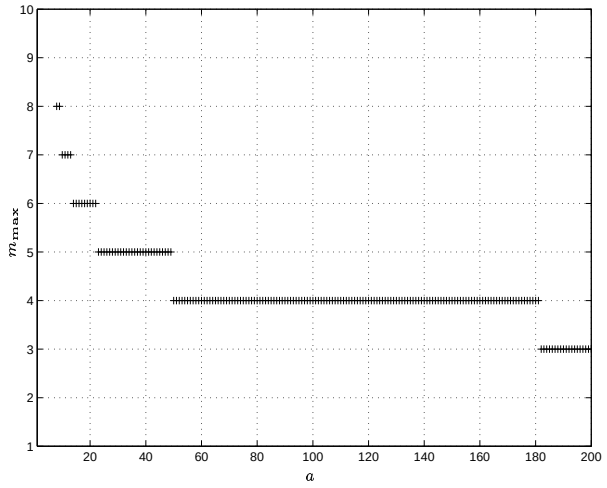

Figure 9.4: *Maximum order of moment m_{max} computable without roundoff error for increasing values of the image size a, when the computer integer resolution is $\eta = 2^{53} - 1$.*

Aside from the roundoff error in the value of moment, the inverse process, that is reconstructing an image from a set of its moments, is also perturbed by roundoff errors. Let us assume a number of moments equal to the image size. Then, the inverse process involves inverting the Vandermonde matrix. A measure of the roundoff error introduced in this process is plotted in figure 9.5 where the mean square error of $\mathbf{V}_m (\mathbf{V}_m)^{-1}$ with respect to the identity matrix $\mathbf{1}_m$, for different values of m, is evaluated.

The influence of roundoff errors in the reconstruction process is analyzed in terms of the perturbation theory. Let us consider the linear set of equations in (9.7) where subscripts are now ignored for simplicity of notation,

$$\boldsymbol{\omega} = \mathbf{K}\,\mathbf{i}. \tag{9.9}$$

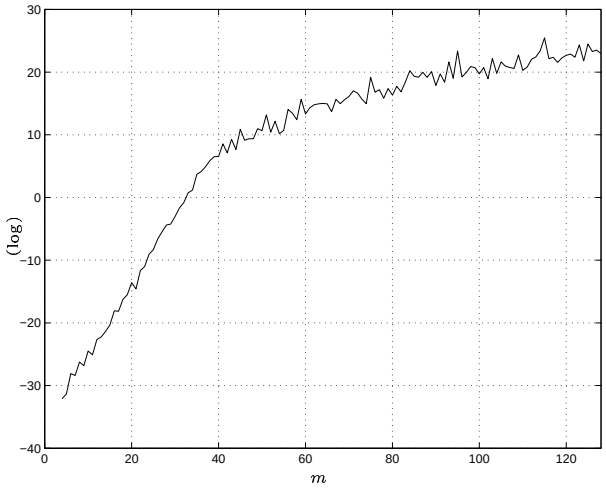

Figure 9.5: *Roundoff error in the inversion of Vandermonde matrices* $\mathbf{V}_m$ *for increasing values of* m.

An elementary formulation of perturbation theory tell us that if the matrix $\mathbf{K}$ and the vector $\boldsymbol{\omega}$ are perturbed by small amounts $\boldsymbol{\delta}\mathbf{K}$ and $\boldsymbol{\delta\omega}$, respectively, we have that [30]:

$$\begin{aligned} \frac{\|\boldsymbol{\delta}\mathbf{i}\|}{\|\mathbf{i}\|} &\leq \frac{\|\boldsymbol{\delta}\mathbf{K}\|}{\|\mathbf{K}\|}\chi(\mathbf{K}), \qquad \text{if } \frac{\|\boldsymbol{\delta}\mathbf{K}\|}{\|\mathbf{K}\|} \ll 1; \\ \frac{\|\boldsymbol{\delta}\mathbf{i}\|}{\|\mathbf{i}\|} &\leq \frac{\|\boldsymbol{\delta\omega}\|}{\|\boldsymbol{\omega}\|}\chi(\mathbf{K}), \qquad \text{if } \frac{\|\boldsymbol{\delta\omega}\|}{\|\boldsymbol{\omega}\|} \ll 1; \end{aligned} \tag{9.10}$$

where $\boldsymbol{\delta i}$ is the change produced in $\mathbf{i}$, and $\chi(\mathbf{K})$ is the condition number of matrix $\mathbf{K}$ with respect to inversion. The condition number is so-called because it quatitatively describes the ill condition or bad behaviour of matrix $\mathbf{K}$. It is defined as follows [30]:

$$\chi(\mathbf{K}) = \|\mathbf{K}\|\|(\mathbf{K})^{-1}\|,$$

where $\|\cdot\|$ is the norm of the corresponding matrix, that is, a number that gives a measure of the magnitude of the matrix. In particular, the norm that measures the largest amount by which a vector is amplified by matrix multiplication corresponds to the spectral norm, defined as:

$$\|\mathbf{K}\| = \max \frac{\|\mathbf{K}\,\boldsymbol{\omega}\|}{\|\boldsymbol{\omega}\|} = \sqrt{\lambda_{\max}},$$

where $\lambda_{\max}$ is the largest eigenvalue of $(\mathbf{K})^t\,\mathbf{K}$; then,

$$\|(\mathbf{K})^{-1}\| = \frac{1}{\sqrt{\lambda_{\min}}},$$

where $\lambda_{\min}$ is the corresponding minimum eigenvalue. Thus, by adopting the spectral norm,

$$\chi(\mathbf{K}) = \sqrt{\frac{\lambda_{\max}}{\lambda_{\min}}}. \tag{9.11}$$

Remark. *The sensitivity of the inverse problem with regard to perturbations in the data can be bounded by the condition number of its associated matrix using (9.10).*

Therefore, perturbation theory provides an understanding of the possibility of obtaining an effective solution of a linear inverse problem.

In figure 9.6, the mean square error in the reconstruction of uniformly distributed random images of different sizes is plotted. It is clearly shown that, increasing matrix

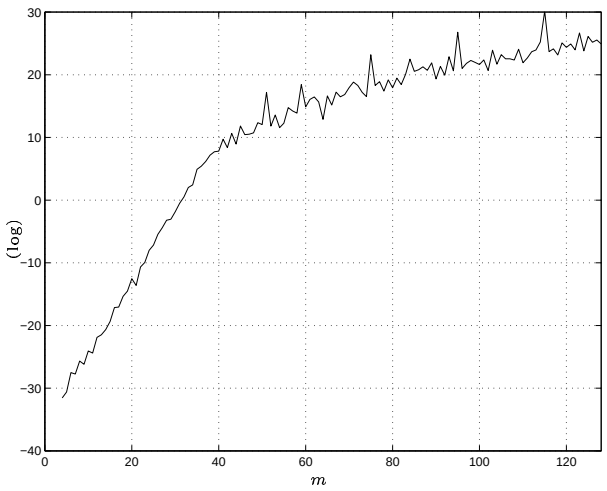

Figure 9.6: *Mean square error in the reconstruction of a uniformly distributed random square image of size m.*

dimensions lead to roundoff errors that generate numerical instabilities in the inverse process and, consequently, large errors in the reconstructed image.

Figure 9.7 shows the condition number of Vandermonde matrices for increasing matrix dimensions m. The maximum computer integer resolution $\eta = 2^{53}-1 = 9.007199254740991 \times 10^{15}$ is also plotted. It can be seen that the condition number can be empirically approximated as follows:

$$\chi(\mathbf{V}_m) = \begin{cases} 10^{\frac{37\,m}{80}} = \mathrm{e}^{\frac{37\ln(10)\,m}{80}} & \text{for } m = 1, \ldots, 40; \\ 10^{\frac{37}{2}} & \text{for } m \geq 40. \end{cases} \tag{9.12}$$

Then, for $m = 35$, the condition number of the corresponding Vandermonde matrix $\mathbf{V}_m$ overpasses the maximum computer integer resolution. Notice that, in figure 9.6, the error of reconstructing a uniformly distributed random image is significant for $m \geq 35$.

Hence, although the condition number only provides a bound of the sensibility of the linear set of equations to perturbations, the analysis of figure 9.6 reveals that this bound is very close to empirical results. As a consequence, although the approximation

error is supposed to diminish as order increases, there exists a limit in the number of useful moments due to numerical considerations. In chapter 12, it is shown how using the singular value decomposition can palliate the roundoff error introduced in the inverse process.

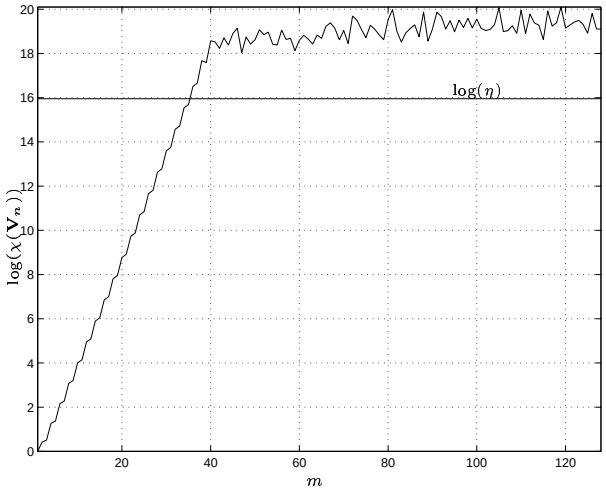

Figure 9.7: *Condition number of the Vandermonde matrix* $\mathbf{V}_m$ *for increasing size* m *and a computer integer resolution* $\eta = 2^{53} - 1$.

Roundoff errors can be modeled as white Gaussian noise [50]. In this sense, an interesting analysis on the signal-to-noise rate versus the maximum order of moment used in the reconstruction, when white Gaussian noise is added to the signal, can be found in [108].

Finally, notice that the inherent problem in reconstructing an image from a finite set of moments comes from the projection basis set itself. An analysis of the basis set functions reveals that monomials – associated with the geometric moments – and $r_q^p(t)$ – associated with the accumulation moments– differ very little, respectively, as order increases; in other words, they are nearly parallel.

Chapter 10

Drawbacks of former reconstruction methods

In this chapter, former reconstruction methods are analyzed. There exist two basic approaches. On one hand, the Legendre method, which is based on the least-squares approximation of the image using Legendre polynomials. On the other hand, the variational methods, which are based on the bayesian theory; they obtain either the image that maximizes the entropy or the one that minimizes the divergence, depending on the adopted optimization function.

We show in this chapter how Legendre polynomials are not orthogonal in the discrete domain, contrary to what is assumed by some authors. Therefore image reconstruction using these polynomials is incorrect. Proper orthogonal polynomials are used in chapter 11. We also show how the explicit exponential form of the image that is obtained when the entropy is maximized using Lagrange multipliers, is not always a solution. The reason is that this method assumes a continuous optimization domain and this is not always the case.

10.1 The Legendre method

Image reconstruction from a finite set of geometric moments using the Legendre method was first formulated in [106]. This method is based on the approximation of the image as a linear combination of orthogonal polynomial functions. Polynomials are the most intuitive choice among possible orthogonal basis functions because they can be easily related to the monomial functions that are used to obtain geometric moments. Moreover, since they expand the same subspace, as derived next, the reconstructed image is a least-squares approximation of the original one, as it was proved in chapter 8.

Proposition 10.1.1. *Any polynomial* $\mathbf{p}_r^l$ *of degree* l*, can be expressed as a unique linear*

combination of the orthogonal polynomials $\{\overline{\mathbf{p}}_r^k\}$, $0 < k \leq l$. *That is,*

$$\mathbf{p}_r^l[t] = \sum_{k=0}^{l} c^{k\,l}\ \overline{\mathbf{p}}_r^k[t], \qquad for \quad t = 1, 2, \ldots, r;$$

where

$$c^{k\,l} = < \overline{\mathbf{p}}_r^k, \mathbf{p}_r^l > .$$

Proof. The set of orthogonal polynomials $\{\overline{\mathbf{p}}_r^k\}$, $0 < k \leq l$, define a basis in the vector space of polynomials of order l [26]. Then, the finite series expansion of any polynomial of order l leads to the above result.

□

Corollary 10.1.1. *Sets of polynomials up to the same order expand the same subspace.*

Using corollary 8.0.4, an approximation of the image can be obtained from

$$\overline{\mathbf{I}}_{ab}^{mn} = \overline{\mathbf{P}}_{am}\ (\mathbf{C}_m^a)^{-1}\ \mathbf{M}_{mn}\ \left((\mathbf{C}_n^b)^t\right)^{-1}\ (\overline{\mathbf{P}}_{bn})^t,$$

where $\mathbf{C}_q^p[k+1, l+1] = c^{kl}$, as defined in proposition 10.1.1.

Because of corollary 10.1.1, the reconstructed image is a least-squares approximation. Notice that this method assumes null projection coefficients onto the Legendre polynomials of order higher than the maximum order of available moments. Thus, this solves the ill-posedness and the solution becomes unique.

10.1.1 The incorrectness of the Legendre method

Legendre and Zernike polynomials were first proposed in [106] for image reconstruction and invariant parameters determination. They are orthogonal polynomials for continuous variables in rectangular and polar coordinates, respectively. Extensive information on these polynomials can be found in [86].

Remark. *Legendre and Zernike polynomials are not orthogonal polynomials for discrete variables.*

Their non-orthogonality can be verified by computing their associated Gram matrix, as shown in the following example. Nevertheless, a formal analysis on classical orthogonal polynomials of a discrete variable can be found in [78].

Example 10.1.1. Legendre polynomials up to fourth order are:

$$\overline{\mathbf{p}}_r^{\,0}[t] = 1$$
$$\overline{\mathbf{p}}_r^{\,1}[t] = t$$
$$\overline{\mathbf{p}}_r^{\,2}[t] = \frac{3}{2}t^2 - \frac{1}{2}$$
$$\overline{\mathbf{p}}_r^{\,3}[t] = \frac{5}{2}t^3 - \frac{3}{2}t$$
$$\overline{\mathbf{p}}_r^{\,4}[t] = \frac{35}{8}t^4 - \frac{30}{8}t^2 + \frac{3}{8}$$

Then, assuming r=5 and evaluating t in the polynomial domain, that is $t = \{-1, -\frac{1}{2}, 0, \frac{1}{2}, 1\}$,

$$\mathbf{P}_{55} = \begin{pmatrix} 1 & -1 & 1 & -1 & 1 \\ 1 & -0.5 & -0.13 & 0.44 & -0.29 \\ 1 & 0 & -0.5 & 0 & 0.38 \\ 1 & 0.5 & -0.13 & -0.44 & -0.29 \\ 1 & 1 & 1 & 1 & 1 \end{pmatrix},$$

and the associated Gram matrix is

$$\mathbf{\Gamma}_5 = \begin{pmatrix} 5 & 0 & 1.25 & 0 & 1.80 \\ 0 & 2.5 & 0 & 1.56 & 0 \\ 1.25 & 0 & 2.28 & 0 & 1.88 \\ 0 & 1.56 & 0 & 2.38 & 0 \\ 1.8 & 0 & 1.88 & 0 & 2.31 \end{pmatrix}.$$

Since the resulting Gram matrix is not diagonal, the basis functions are not orthogonal. Nevertheless, notice that polynomials of even and odd order are mutually orthogonal, which justifies some resemblance of the reconstructed image with respect to the original one. Moreover, as the order of the polynomials increases, their Gram matrices tends to a diagonal matrix. This is shown in figure 10.1, where the mean square error between the Gram matrix $\mathbf{\Gamma}_m$ and the identity matrix $\mathbf{1}_m$, for increasing dimensions m, is plotted.

Remark. *Discrete image reconstruction from a finite set of geometric moments using Legendre or Zernike polynomials is not correct.*

This remark has not been previously reported in the literature concerning image reconstruction from a finite set of geometric moments. Indeed, in [81] (and other papers by the same author, [82] and [61]), the reconstruction error was justified as the error introduced by assuming constant values of Legendre polynomials inside each pixel area, instead of the non-orthogonality of Legendre polynomials for discrete variable.

However, the error introduced due to this non-orthogonality is negligible, as shown in the following examples.

Example 10.1.2. Figure 10.2 shows the reconstructed images using Legendre polynomials, from geometric moments up to order (a) 1, (b) 3, (c) 5 and (d) 7.

Example 10.1.3. In figure 10.3, the reconstruction of letter "E" is done using Legendre polynomials from increasing number of moments.

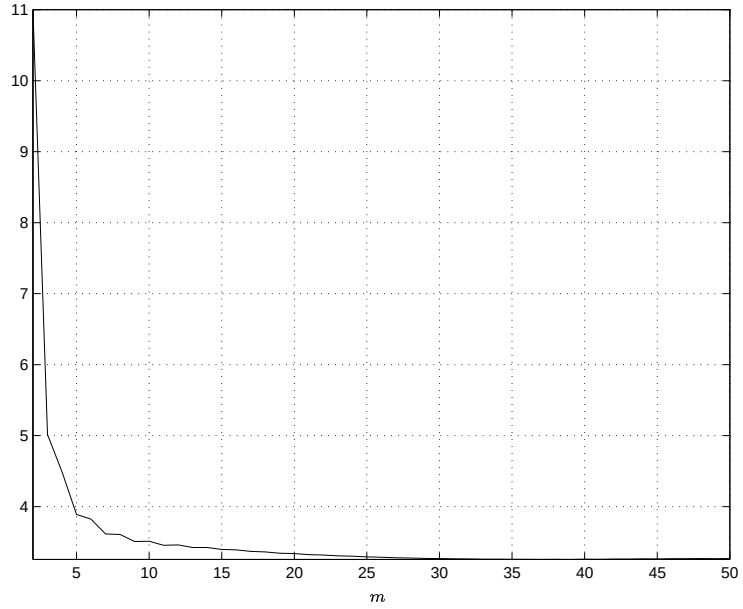

Figure 10.1: *Mean square error between the Gram matrices associated with Legendre polynomials and the identity matrices for increasing dimension m.*

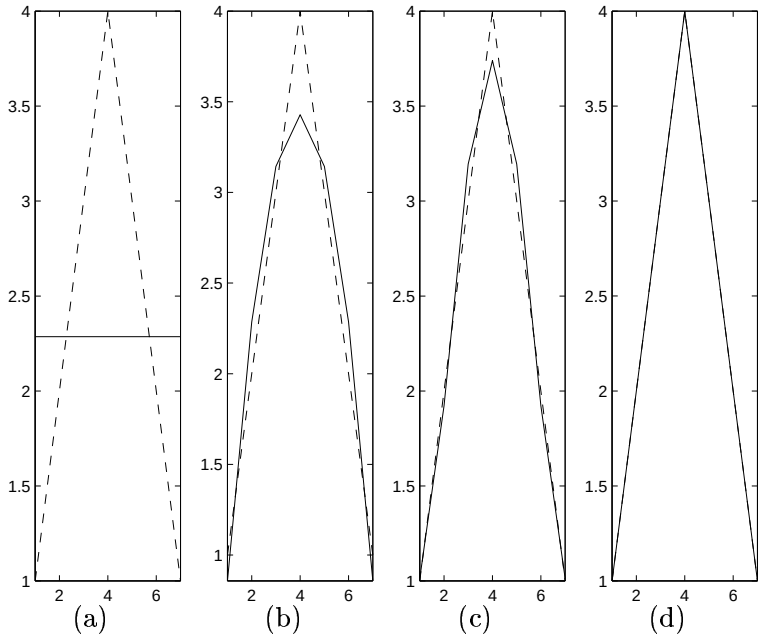

Figure 10.2: *Reconstructed images using Legendre polynomials from (a) 1, (b) 3, (c) 5 and (d) 7 geometric moments. The original 7×1 image is plotted in dashed line.*

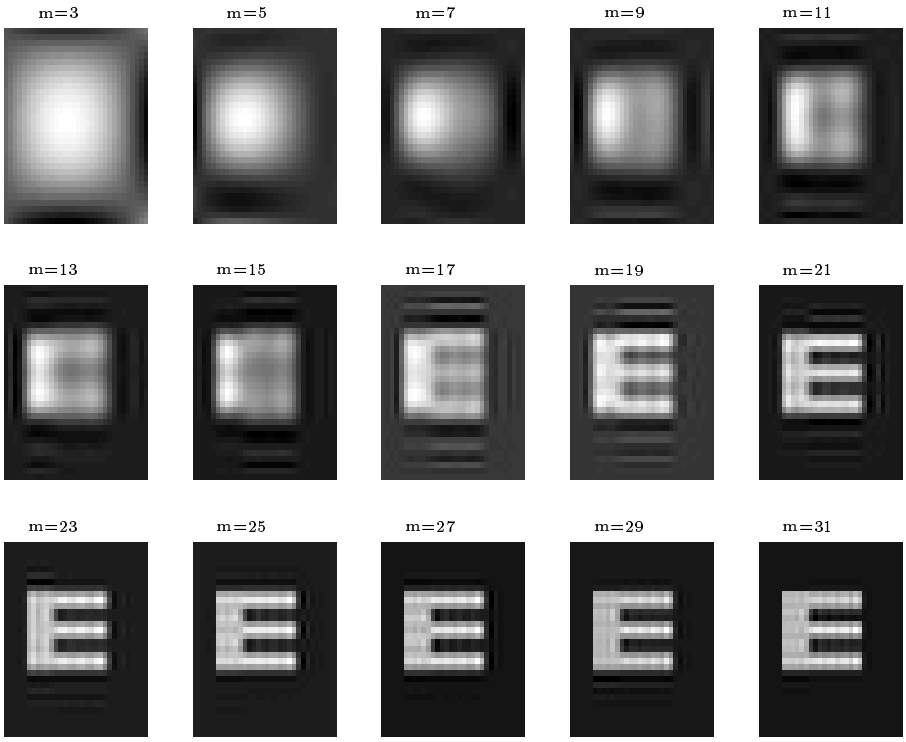

Figure 10.3: *Reconstructed images using Legendre polynomials for increasing values of geometric moments m of a 32×32 image.*

10.2 The variational method

A bayesian interpretation of the reconstruction problem can be formulated in terms of entropy. The concept of entropy is related to the degree of uncertainty of a random process. An intuitive understanding of uncertainty led to its mathematical definition, which is uniquely stated, except for a constant factor, as

$$H = -\sum_{x=1}^{a}\sum_{y=1}^{b} \mathbf{I}_{ab}[x,y]\,\ln\big(\mathbf{I}_{ab}[x,y]\big)$$

where $\mathbf{I}_{ab}[x,y]$ is assumed to be a probability distribution function.

Maximum entropy methods (MEM) have been proposed as an approach to the problem of inversion, given a priori information [88]. In this context, reconstructing an image from a finite set of geometric moments can be translated into the context of estimating the probability distribution function, given a finite set of constraints, by maximizing the entropy. That is,

$$\mathbf{I}_{ab} \quad \text{such that} \quad \max\{H\} \text{ or } \min\{-H\}$$

subjected to the following constraints:

1. the image is positive, that is,

   $$\mathbf{I}_{ab}[x,y] > 0, \qquad \text{for} \quad x = 1,\ldots,a \quad \text{and} \quad y = 1,\ldots,b;$$

2. the geometric moments up to order $(m-1, n-1)$ of the obtained image coincide with the given moments, that is

   $$\overline{\mathbf{M}}_{mn} = (\mathbf{V}_{am})^t\ \mathbf{I}_{ab}\ \mathbf{V}_{bn}$$

   where $\overline{\mathbf{M}}_{mn}$ is the normalized geometric moment matrix such that the area is the unity, that is $\overline{\mathbf{M}}_{mn}[1,1] = 1$.

Results are obtained using variational techniques involving Lagrange multipliers λ^{kl}, that is, minimizing

$$\sum_{x=1}^{a}\sum_{y=1}^{b} \mathbf{I}_{ab}[x,y]\,\ln\big(\mathbf{I}_{ab}[x,y]\big) + \sum_{k=0}^{m-1}\sum_{l=0}^{n-1} \lambda^{kl}\,\Big(\sum_{x=1}^{a}\sum_{y=1}^{b} \mathbf{I}_{ab}[x,y]\,x^k y^l - \mathbf{M}_{mn}[k+1,l+1]\Big).$$

It has been proved [80, pp. 569-577] that the solution to this equation can be expressed as an exponential function of the form:

$$\mathbf{I}_{ab}[x,y] = A\ e^{\{-\lambda^{11}\,xy - \cdots - \lambda^{mn}\,x^m\,y^n\}},$$

where λ^{kl} can be obtained from the set of non-linear equations obtained when this image is included in the equations defined by the above constraints, i.e. those that the geometric

moment impose. This is the basic result used in [79] for image reconstruction from a finite set of geometric moments.

A more general concept used to solve the problem at hand is the Kullback-Leibler distance or cross-entropy, which measures the distance between two probability density functions. Its generalization to the case of other functions than probability densities is known as I-divergence. This is the variational approach introduced in [70]. I-Divergence is defined as

$$\sum_{x=1}^{a}\sum_{y=1}^{b}\Big(\mathbf{I}_{ab}[x,y]\,\ln\Big(\frac{\mathbf{I}_{ab}[x,y]}{\mathbf{I}^0_{ab}[x,y]}\Big)+\mathbf{I}^0_{ab}[x,y]-\mathbf{I}_{ab}[x,y]\Big),$$

where $\mathbf{I}^0_{ab}$, is an a priori estimate of $\mathbf{I}_{ab}$. Then, the variational method associated with the divergence consists of minimizing this function subjected to the set of known moments. Notice that the method is equivalent to MEM if a constant a priori estimates of $\mathbf{I}^0_{ab}$ are assumed.

10.2.1 Considerations about the optimization domain

Solving the variational method through Lagrange multipliers permits to obtain an explicit form of the reconstructed image in terms of an exponential function. However, the method implicitly assumes a continuous domain of the function to be minimized because it involves derivatives. This is not always the case as shown in the following example.

Example 10.2.1. Let $\mathbf{I}_{13} = (0 \quad 0 \quad 1)$. Then, $\mathbf{M}_{12}[1,1] = 1$ and $\mathbf{M}_{12}[1,2] = 3$. If we want to reconstruct an image from these moments using the variational method, the Lagrange multipliers approach provides a reconstructed image of the form:

$$\tilde{\mathbf{I}}_{13}[k] = \mathrm{e}^{-(\lambda_0 k+\lambda_1 k^2)}, \qquad \text{for } k = 1,2,3.$$

Including this image into the equations defined by the constraints, i.e. those that the geometric moments impose, leads to:

$$\begin{aligned} uw + uw^2 + uw^3 &= 1\\ uw + 2uw^2 + 3uw^3 &= 3, \end{aligned}$$

where $u = \mathrm{e}^{-\lambda_0 k}$ and $v = \mathrm{e}^{-\lambda_1 k^2}$. It can be shown that this set of polynomial equations is incompatible: there are not real values for u and v that simultaneously satisfy them.

The reason is easy to understand when analyzing the domain of the optimization function. On one hand, the solution to the set of constraint equations

$$\begin{aligned} \tilde{\mathbf{I}}_{13}[1] + \tilde{\mathbf{I}}_{13}[2] + \tilde{\mathbf{I}}_{13}[3] &= 1\\ \tilde{\mathbf{I}}_{13}[1] + 2\tilde{\mathbf{I}}_{13}[2] + 3\tilde{\mathbf{I}}_{13}[3] &= 3 \end{aligned}$$

is a line in the three-dimensional space of the image which, in parametric formulation, can be expressed as.

$$(\tilde{\mathbf{I}}_{13}[1], \tilde{\mathbf{I}}_{13}[2], \tilde{\mathbf{I}}_{13}[3]) = (0,0,1) + t(1,-2,1).$$

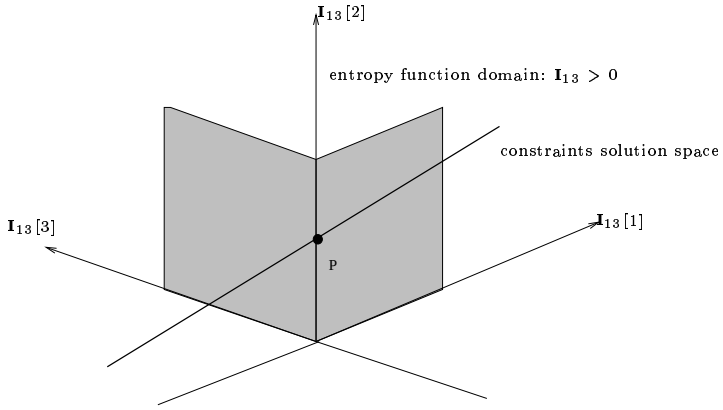

Figure 10.4: *Geometric representation of the optimization domain of example 10.2.1.*

On the other hand, the entropy function is defined for $0 \leq \tilde{\mathbf{I}}_{13}[k] \leq 1$. Then, the geometric representation of this domain shows that their intersection is a single point (see figure 10.4). Therefore, it can never be obtained by variational methods because they involve derivatives and a continuous domain is required.

Chapter 11

Novel reconstruction methods

We have just shown that none of the former reconstruction methods is fully satisfactory. In this chapter, using the matrix-based reformulation of image series expansion introduced in chapter 8, we straightforwardly obtain a set of unified approaches to solve the problem of reconstructing an image from a finite set of its moments.

Ill-posedness is solved imposing null value to those coefficients of the orthogonal basis set used in the reconstruction that have higher order than the maximum order of available moments. It is shown how specific orthogonal basis sets allow to translate this requirement into visual constraints over the image such as its bandwidth or spatial resolution. None of the former methods provided the proper setting to introduce these constraints.

11.1 Least-squares reconstruction using Chebyshev polynomials

Since different sets of polynomials up to the same order expand the same subspace (corollary 10.1.1), the unitary approximation in corollary 8.0.4 provides a least-squares reconstruction if the orthogonal basis set corresponds to orthogonal polynomials. This is the underlying idea of the Legendre method. However, proper polynomials must be used instead of the erroneously adopted Legendre and Zernike ones.

Lemma 11.1.1 (Orthogonal polynomials in $\mathbb{R}^{a\times b}$). *The only possible orthogonal polynomials in the vector space of discrete images of size $a \times b$ are the Chebyshev polynomials.*

Proof. In [78], a unified approach to different types of orthogonal polynomials is provided. In particular, orthogonal polynomials of a discrete variable are obtained as solutions of the following difference equation:

$$\triangle[\sigma(x)\rho(x) \bigtriangledown y(x)] + \lambda\rho(x)y(x) = 0,$$

were $\sigma(x)$ is a polynomial of at most second degree; λ is a constant; $\rho(x)$ is a function that verifies $\triangle[\sigma(x)\rho(x)] = \tau(x)\rho(x)$, where $\tau(x)$ is a polynomial of at most first degree;

and

$$\triangle y(x) = y(x+1) - y(x),$$
$$\triangledown y(x) = y(x) - y(x-1).$$

Then, it is proved that the polynomial solutions are defined by the finite difference form of the Rodrigues formula, i.e.

$$p^k(x) = \frac{B_k}{\rho(x)} \ \triangle^k \left[\rho(x) \prod_{l=0}^{k-1} \sigma(x-k)\right]. \tag{11.1}$$

These polynomials are unique orthogonal polynomials, up to a normalizing factor, if both the support region and the weighting function $\rho(x)$ are fixed.

Since geometric moments are defined over a uniform lattice in $[1, a] \times [1, b]$ and the weighting function is the unity, the only possible orthogonal polynomials are the Chebyshev polynomials, as proved in [78, pp. 30-44].

□

Definition 11.1.1 (Chebyshev polynomials of discrete variables). The Chebyshev polynomial of order k is defined as

$$\mathbf{p}_N^k[x] = \begin{cases} 1 & \text{if} \quad k = 0, \\ \frac{(-1)^k}{k!} \ \triangle^k \left[\prod_{l=0}^{k-1}(x-l)(N-1-x+l)\right] & \text{if} \quad k = 1, \ldots, N-1, \end{cases} \tag{11.2}$$

for $x = 0, 1, \ldots, N-1$.

Lemma 11.1.2 (Recurrence relation of Chebyshev polynomials). *Chebyshev polynomials of discrete variables verify the following recurrence relation:*

$$x \ \mathbf{p}_N^k[x] = \alpha^k \mathbf{p}_N^{k+1}[x] + \beta^k \mathbf{p}_N^k[x] + \gamma^k \mathbf{p}_N^{k-1}[x], \tag{11.3}$$

where

$$\alpha^k = \frac{k+1}{2(2k+1)}; \tag{11.4}$$
$$\beta^k = \frac{N-2}{2}; \tag{11.5}$$
$$\gamma^k = \frac{k((N-1)^2 - k^2)}{2(2k+1)}. \tag{11.6}$$

Proof. In fact, recurrence relation is a common property for all orthogonal polynomials [78, pp. 14]. Value for parameters $\alpha^k, \beta^k$and γ^k are derived in [78, pp. 36-44].

□

Figure 11.1 shows the normalized Chebyshev polynomials for $N = 5$.

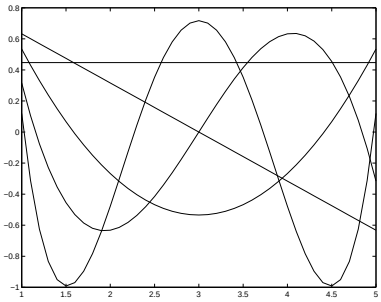

Figure 11.1: *Normalized Chebyshev polynomials for* $N = 5$.

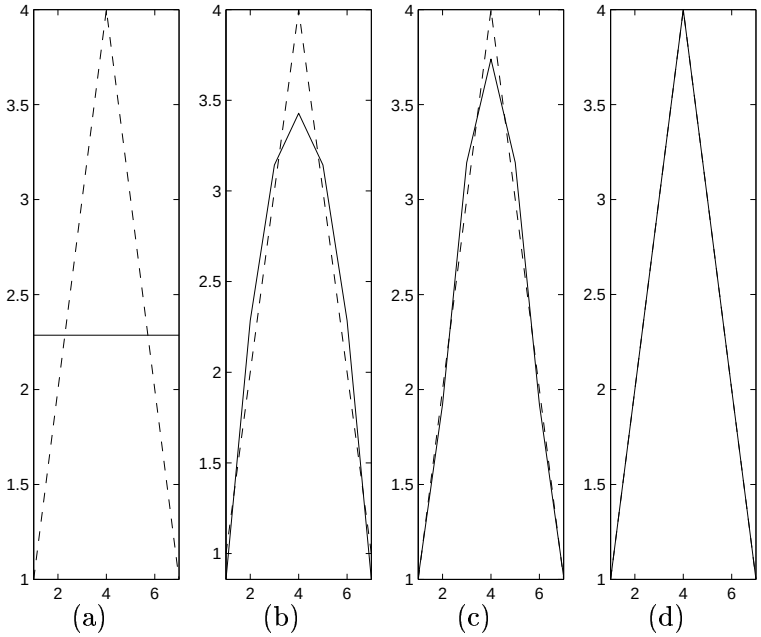

Figure 11.2: *Reconstructed images using Chebyshev polynomials from (a) 1, (b) 3, (c) 5 and (d) 7 moments. Original* 1×7 *image is plotted in dashed line.*

Example 11.1.1. In figure 11.2, a normalized version of the Chebyshev polynomials compiled in table 11.1.1 are used to reconstruct the original image shown in dashed line, for (a) $N = 1$, (b) $N = 3$, (c) $N = 5$ and (d) $N = 7$. It can be seen that, using the same number of geometric moments as pixels in the image, the original image is perfectly reconstructed.

A comparison between the reconstructed images in figure 11.2– using Chebyshev polynomials – and figure 10.2 – using Legendre polynomials – reveals that, although the Legendre polynomials are not orthogonal in the discrete domain, they can be used in the reconstruction process. In fact, the mean square reconstruction error in these particular examples nearly coincides, as shown in figure 11.3.

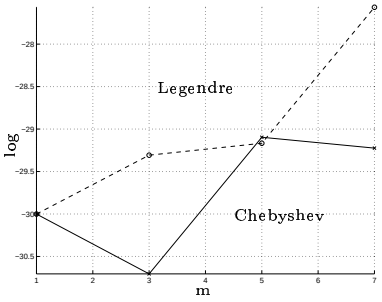

Figure 11.3: *Comparison of the mean square reconstruction error using Legendre and Chebyshev polynomials in figures 10.1.2 and 11.1.1, respectively.*

Example 11.1.2. In figure 11.4, the reconstruction of letter "E" is done using Chebyshev polynomials for increasing number of moments.

Remark. *The same results are obtained if corollary 8.0.2 is used instead of corollary 8.0.4 when Chebyshev polynomials are considered. That is,*

$$\overline{\mathbf{I}}_{ab}^{mn} = \overline{\mathbf{P}}_{am}\,(\mathbf{C}_m^a)^{-1}\,\mathbf{M}_{mn}\,\left((\mathbf{C}_n^b)^t\right)^{-1}\,(\overline{\mathbf{P}}_{bn})^t = (\mathbf{V}_{am})^-\,\mathbf{M}_{mn}\,(\mathbf{V}_{bn})^+ = \hat{\mathbf{I}}_{ab}^{mn}. \quad (11.7)$$

In figure 8.2, the geometric interpretation of the unitary transform reconstruction clearly shows that, if both the projection basis and the orthogonal reconstruction basis belong to the same vector space (a plane in the figure), then the reconstructed images obtained, using either a least-squares approximation or a unitary approximation, coincide. Since both basis are polynomials, by corollary 10.1.1, this remark becomes obvious.

Remark. *Since accumulation moments are also obtained from projections onto a polynomial basis set, as shown in section 9.1, the least-squares approximated image obtained from a reduced set of accumulation moments of an image is the same as the one obtained from the same amount of its geometric moments. Then,*

$$\overline{\mathbf{I}}_{ab}^{mn} = (\mathbf{Q}_{am})^-\,\mathbf{L}_{mn}\,(\mathbf{Q}_{bn})^+ = (\mathbf{P}_{am})^-\,\mathbf{R}_{mn}\,(\mathbf{P}_{bn})^+ = (\mathbf{V}_{am})^-\,\mathbf{M}_{mn}\,(\mathbf{V}_{bn})^+. \quad (11.8)$$

N=1	$\mathbf{p}_1^0[x] = 1$
N=2	$\mathbf{p}_2^0[x] = 1$ $\mathbf{p}_2^1[x] = 2x - 1$
N=3	$\mathbf{p}_3^0[x] = 1$ $\mathbf{p}_3^1[x] = 2x - 2$ $\mathbf{p}_3^2[x] = 6x^2 - 12x + 2$
N=4	$\mathbf{p}_4^0[x] = 1$ $\mathbf{p}_4^1[x] = 2x - 3$ $\mathbf{p}_4^2[x] = 6x^2 - 18x + 6$ $\mathbf{p}_4^3[x] = 20x^3 - 90x^2 + 94x - 6$
N=5	$\mathbf{p}_5^0[x] = 1$ $\mathbf{p}_5^1[x] = 2x - 4$ $\mathbf{p}_5^2[x] = 6x^2 - 24x + 12$ $\mathbf{p}_5^3[x] = 20x^3 - 120x^2 + 172x - 24$ $\mathbf{p}_5^4[x] = 70x^4 - 560x^3 + 1370x^2 - 1000x + 24$
N=6	$\mathbf{p}_6^0[x] = 1$ $\mathbf{p}_6^1[x] = 2x - 5$ $\mathbf{p}_6^2[x] = 6x^2 - 30x + 20$ $\mathbf{p}_6^3[x] = 20x^3 - 150x^2 + 274x - 60$ $\mathbf{p}_6^4[x] = 70x^4 - 700x^3 + 2150x^2 - 2000x + 120$ $\mathbf{p}_6^5[x] = 252x^5 - 3150x^4 + 13720x^3 - 24150x^2 + 14048x + 120$
N=7	$\mathbf{p}_7^0[x] = 1$ $\mathbf{p}_7^1[x] = 2x - 6$ $\mathbf{p}_7^2[x] = 6x^2 - 36x + 30$ $\mathbf{p}_7^3[x] = 20x^3 - 180x^2 + 400x - 120$ $\mathbf{p}_7^4[x] = 70x^4 - 840x^3 + 3110x^2 - 3540x + 360$ $\mathbf{p}_7^5[x] = 252x^5 - 3780x^4 + 19740x^3 - 41580x^2 + 28968x + 720$ $\mathbf{p}_7^6[x] = 924x^6 - 16632x^5 + 112560x^4 - 352800x^3 + 501396x^2 - 250488x + 720$

Table 11.1: *Chebyshev polynomials for increasing values of N.*

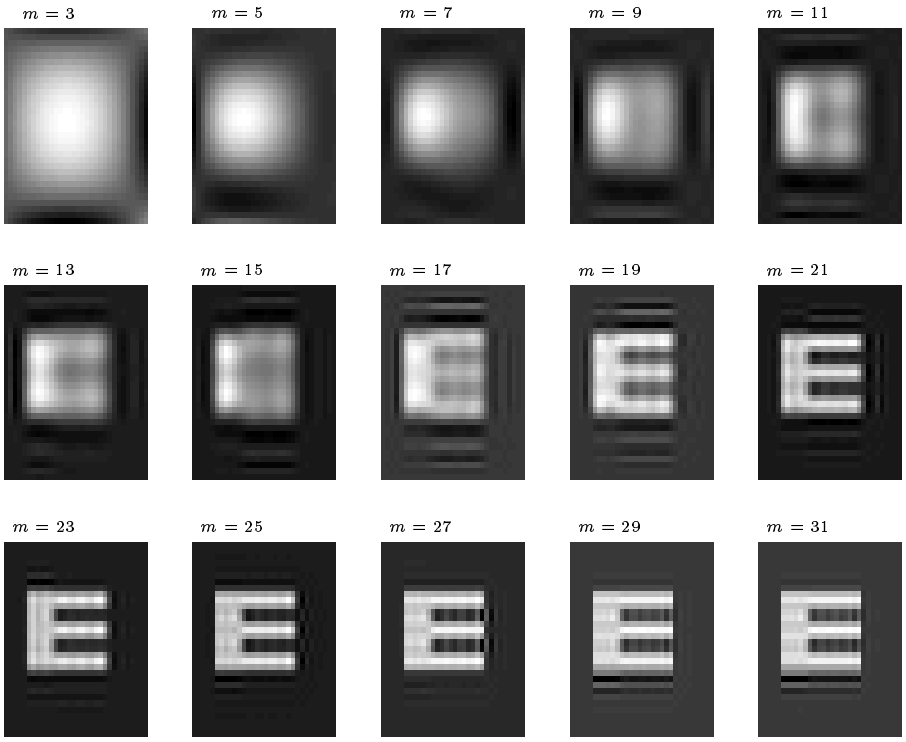

Figure 11.4: *Reconstructed images using Chebyshev polynomials from moments of increasing order of a* 32×32 *image.*

Notice that the ill-posedness of the reconstructing problem is solved by assuming that the coefficients obtained as the projection of the image onto Chebyshev polynomials of order higher than the maximum order of available moments are null.

11.2 The unitary transform method

By lemma 8.0.4, given the Vandermonde matrix $\mathbf{V}_{pq}$, associated with the monomial basis set and $\overline{\mathbf{\Phi}}_{pq}$, associated with any separable orthogonal basis set,

$$\overline{\mathbf{\Omega}}_{mn} = ((\mathbf{V}_{am})^t \, \overline{\mathbf{\Phi}}_{am})^{-1} \, \mathbf{M}_{mn} \, ((\overline{\mathbf{\Phi}}_{bn})^t \, \mathbf{V}_{bn})^{-1}. \tag{11.9}$$

Then, the image is reconstructed from

$$\overline{\mathbf{I}}_{ab}^{mn} = \overline{\mathbf{\Phi}}_{am} \, ((\mathbf{V}_{am})^t \, \overline{\mathbf{\Phi}}_{am})^{-1} \, \mathbf{M}_{mn} \, ((\overline{\mathbf{\Phi}}_{bn})^t \, \mathbf{V}_{bn})^{-1} \, (\overline{\mathbf{\Phi}}_{am})^t. \tag{11.10}$$

As in the previous section, the unitary transform method obtains an approximation of the image by its truncated series expansion onto an orthonormal basis set. The only difference is that both the projection and the reconstruction subspaces are not the same. Then, the coefficients associated with those reconstruction functions of order higher than the maximum order of available moments are assumed to be null. All the others are obtained from an approximated image whose moments are known. A geometric interpretation was provided in chapter 8 (figure 8.2).

A desirable property for the basis functions of the series approximation of an image is that they concentrate most of the information in a reduced amount of coefficients since only a finite number of them are used. What information means depends on the interpretation of the basis; however, most common applications refer to bandwidth or spatial resolution, which are associated with the Fourier and Haar coefficients, respectively. Then, setting a relationship between these coefficients and moments provides a straightforward interpretation of the information contained in higher-order moments, as well as a novel method for reconstructing an image from a given set of moments [65]. None of the former methods provided the proper setting to introduce these constraints.

11.2.1 Reconstructing a band-limited image

In terms of the Fourier transform coefficients of the image, the band-limiting assumption means that Fourier coefficients of order greater or equal to (m, n) are null.

Fourier coefficients are normally defined as

$$c_{k,l} = \frac{1}{\sqrt{ab}} \sum_{x=1}^{a} \sum_{y=1}^{b} \mathbf{I}_{ab} \, \mathrm{e}^{-j2\pi \left(\frac{(x-1)(k-1)}{a} + \frac{(y-1)(l-1)}{b} \right)}.$$

Nevertheless, a relocation of these coefficients into a matrix $\mathbf{C}_{mn}$ is carried out here so that increasing indexes correspond to higher frequency coefficients. In this case,

$$\mathbf{C}_{mn}[k,l] = \frac{1}{\sqrt{ab}} \sum_{x=1}^{a} \sum_{y=1}^{b} \mathbf{I}_{ab}\, \mathrm{e}^{-j2\pi\left(\frac{(x-1)(k-\frac{(m-1)}{2}-1)}{a}+\frac{(y-\frac{(n-1)}{2}-1)(l-1)}{b}\right)}. \tag{11.11}$$

Then, Fourier coefficients can be seen as the projection coefficients of the image onto complex exponential functions of the form:

$$\overline{\mathbf{\Phi}}_{pq}[k,l] = \frac{1}{p}\, \mathrm{e}^{-j2\pi\left(\frac{(k-1)(l-\frac{(q-1)}{2}-1)}{p}\right)}.$$

Considering orthogonal basis matrices of this form into (11.10), a low-pass approximation of the original image is obtained from a finite set of geometric moments.

Example 11.2.1. In figure 11.5, the band-limited reconstruction of letter "E" is done using the unitary transform method with Fourier coefficients and moments of increasing order.

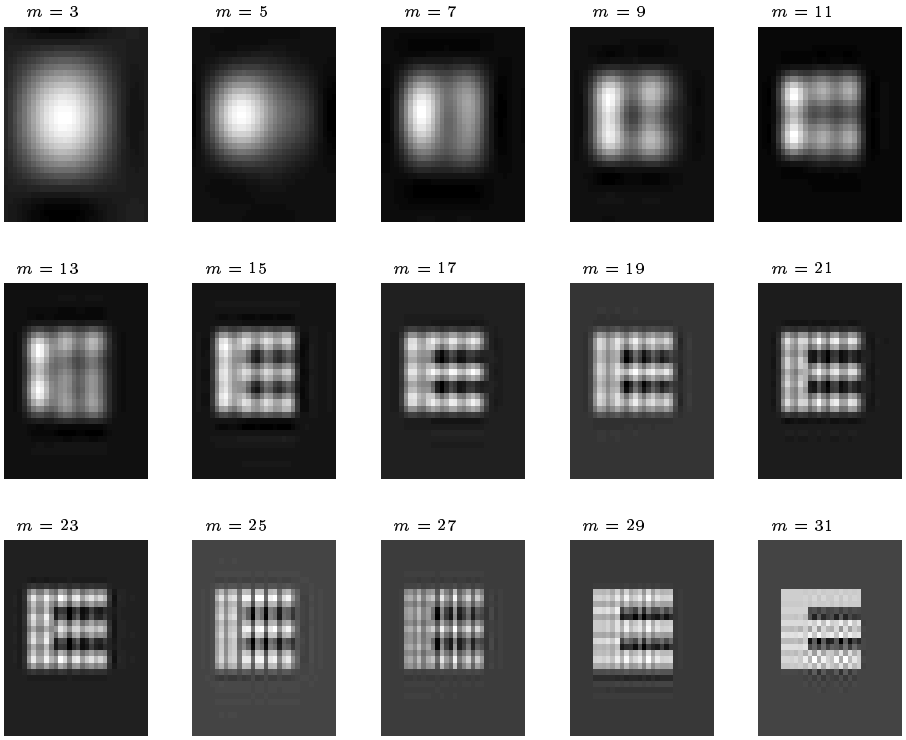

Figure 11.5: *Band-limited reconstruction of a* 32×32 *image using the unitary method from moments of increasing order.*

Remark. *A band-limited image can be perfectly reconstructed, using this method, when the number of moments obtained from the image is equal or greater than the number of its significant discrete Fourier spectrum coefficients.*

Likewise, a high-pass approximation could be obtained if the basis function associated with higher frequencies were considered instead.

11.2.2 Reconstructing a resolution-limited image

Limiting the resolution of an approximated image means eliminating those regions of smaller size than a given one. In terms of Haar transforms, this requirement becomes trivial since its main characteristic is the direct relationship between the number of coefficients and the spatial resolution of the signal.

Figure 11.6 shows the effect of limiting the resolution of a function using the Haar transform, when a reduced set of p coefficients is considered.

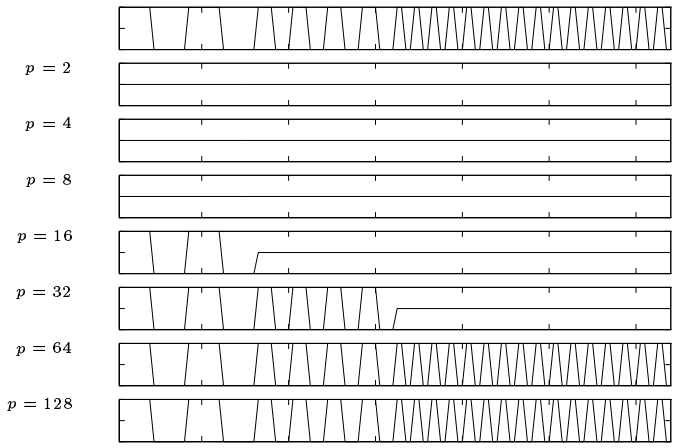

Figure 11.6: *Effect of limiting the spatial resolution of a function using a finite set of its Haar coefficients.*

Haar coefficients are obtained from the projection of the image onto the Haar functions $h_k^N(z)$, which are defined over the closed interval $z \in [0,1]$, and for $k = 0, 1, 2, \ldots, n-1$, where $N = 2^n$. Since any integer k can uniquely be decomposed as

$$k = 2^p + q - 1, \qquad \text{where} \quad \begin{cases} \text{either} & 1 \leq q \leq 2^p \text{ and } 1 \leq p \leq n-1, \\ \text{or} & q = 0, 1 \text{ and } p \neq 0. \end{cases}$$

Haar functions are defined as:

$$h_0^N(z) = h_{00}^N(z) = \frac{1}{\sqrt{N}},$$

and

$$h_k^N(z) = h_{pq}^N(z) = \frac{1}{\sqrt{N}} \begin{cases} 2^{\frac{p}{2}} & \text{if } \frac{q-1}{2^p} \leq z < \frac{q-\frac{1}{2}}{2^p}, \\ -2^{\frac{p}{2}} & \text{if } \frac{q-\frac{1}{2}}{2^p} \leq z < \frac{q}{2^p}, \\ 0 & \text{otherwise.} \end{cases}$$

Then,

$$\overline{\mathbf{\Phi}}_{pq}[k,l] = h_l^p(k). \tag{11.12}$$

Considering orthogonal basis matrices of this form in equation (11.10), a resolution-limited approximation of the original image is obtained from a finite set of geometric moments.

Example 11.2.2. In figure 11.7, the resolution-limited reconstruction of letter "E" is done using the unitary transform method with Haar coefficients and moments of increasing order.

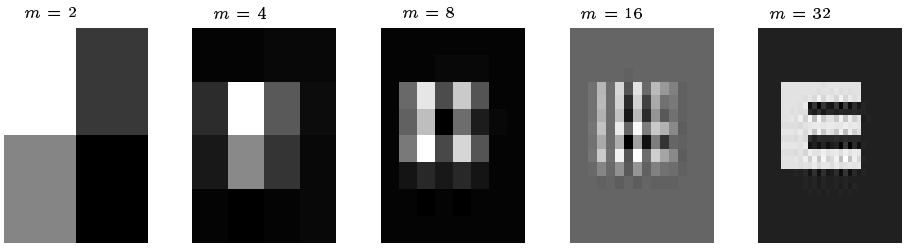

Figure 11.7: *Resolution-limited reconstruction of a* 32×32 *image using the unitary method from moments of increasing order.*

Setting to zero Haar coefficients of higher order allows reconstructing a resolution-limited image from a finite set of its moments.

Remark. *A resolution-limited image can be perfectly reconstructed, using the unitary method, when the number of moments obtained from the image is equal or higher than the number of its significant discrete Haar coefficients.*

Finally, in figure 11.8, it is shown a comparison for the novel reconstruction methods that we have introduced in this chapter, for the particular case of the letter "E" used in the previous examples. The comparison is done in terms of the logarithm of the mean square error:

$$10 \log\Big(\frac{\sum_{x=1}^{a}\sum_{y=1}^{b}(\mathbf{I}_{ab}[x,y] - \hat{\mathbf{I}}_{ab}[x,y])^2}{\sum_{x=1}^{a}\sum_{y=1}^{b}(\mathbf{I}_{ab}[x,y])^2}\Big). \tag{11.13}$$

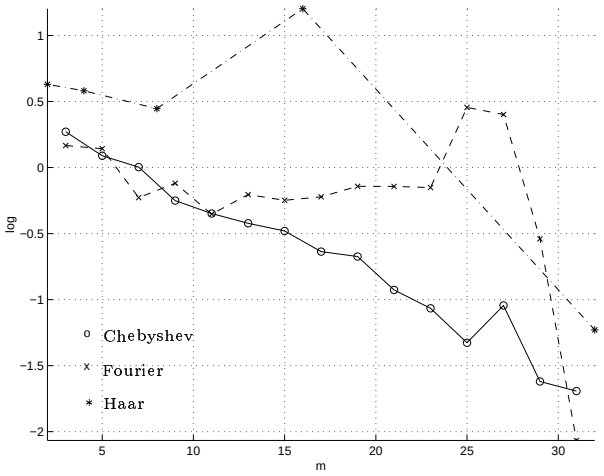

Figure 11.8: *Mean square error of the reconstructed images in figures 11.4, 11.5 and 11.7.*

Chapter 12

Computational considerations

We have just introduced, in the previous chapter, novel reconstruction methods that solve the ill-posedness of the reconstruction problem under a unified approach. In this chapter, we deal with some computational considerations related to reduce the dimensionality of the problem, that is, the amount of data involved in computations. Dimensionality can be reduced by taking advantage of the separability of the basis functions. We propose to uncouple the problem and parallelize each uncoupled system prior to solve it through an iterative method that provides the closest solution to the initial guess [95]. Then, assuming null initialization, the solution to the direct set of equations defined by known moments is the one of minimum energy.

A different approach is attained through the singular value decomposition. This method consist of diagonalizing a matrix through orthogonal ones [30]. The elements of the diagonal matrix are the singular values in decreasing value order. Then, setting to zero those singular values that are too small reduces roundoff errors.

12.1 Uncoupling and parallelizing

In general, image processing imposes large memory requirements, not only for image storage but for the intermediate steps in their manipulations. Therefore, algorithms that avoid manipulating the complete image at once are generally pursued. In this sense, the following properties provide the necessary key points for decomposing the reconstruction problem into simpler ones. In our case, this is possible because the basis functions are separable.

Property 12.1.1 (Separability). *Given separable projection basis, image reconstruction from a set of projections, that is solving*

$$\mathbf{\Omega}_{mn} = (\mathbf{\Phi}_{am})^t \, \mathbf{I}_{ab} \, \mathbf{\Phi}_{bn},$$

can be uncoupled into two steps:

1. *obtain the intermediate variable* $\mathbf{F}_{mb}$ *from*

$$\mathbf{\Omega}_{mn} = \mathbf{F}_{mb}\ \mathbf{\Phi}_{bn};$$

2. *obtain the image* $\mathbf{I}_{ab}$*, from*

$$\mathbf{F}_{mb} = (\mathbf{\Phi}_{am})^t\ \mathbf{I}_{ab}.$$

This property provides a way to translate the problem of solving a set of $m \cdot n$ linear equations with $a \cdot b$ unknows into two problems of lower dimension.

Property 12.1.2 (Parallelizability). *Each row in the step 1 and each column in the step 2 can be expressed as*

$$\mathbf{\Omega}_{mn}[k,:] = \mathbf{F}_{mb}[k,:]\ \mathbf{\Phi}_{bn}, \tag{12.1}$$

for $k = 1, \ldots, m$*, and*

$$\mathbf{F}_{mb}[:,l] = (\mathbf{\Phi}_{am})^t\ \mathbf{I}_{ab}[:,l], \tag{12.2}$$

for $l = 1, \ldots, n$*, respectively. This defines an independent set of equations that can be solved separately. Equation (12.1) defines a set of* n *equations, one for each possible value of* k*; and equation (12.2) a set of* m *equations, one for each possible value of* l*.*

This property allows parallel implementations of the inverse problem.

12.2 Iteratively reconstructing

We propose an iterative algorithms based on Kaczmarz method [95] for solving a linear set of equations. This method is generally known as the algebraic reconstruction technique (ART) among the tomographic community since first introduced in [36].

Given a linear set of equations,

$$\mathbf{y}_p = \mathbf{A}_{pq}\ \mathbf{x}_q,$$

each equation

$$\mathbf{y}_p[k] = \sum_{l=1}^{q} \mathbf{A}_{pq}[k,l]\ \mathbf{x}_q[l], \qquad \text{for} \quad k = 1, \ldots, p,$$

defines an hyperplane in the q-dimensional space, where q is the number of unknowns. Therefore, a vector of unknowns $(\mathbf{x}_q[1], \ldots, \mathbf{x}_q[q])$ is represented by a point in this space. The method iteratively projects an initial q-dimensional point onto each one of the hyperplanes defined by each linear equation, as shown in figure 12.1. That is,

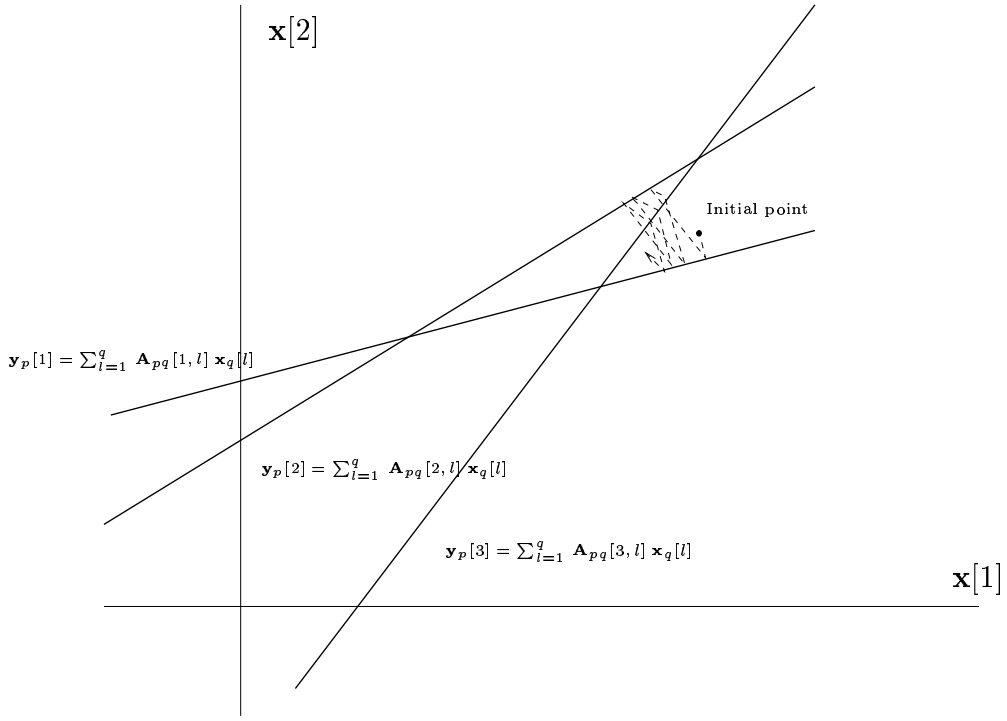

Figure 12.1: *Space of unknowns. Each equation defines an hyperplane (represented by a line in the two-dimensional space).*

$$\mathbf{x}_p^i = \mathbf{x}_p^{i-1} - \lambda^i\, \mathbf{A}_{pq}[k,:]\, \frac{(\mathbf{x}_p^{i-1}\, \mathbf{A}_{pq}[k,:] - \mathbf{y}_q[k])}{\mathbf{A}_{pq}[k,:]\, (\mathbf{A}_{pq}[k,:])^t}, \tag{12.3}$$

where i refers to the iteration index, k, to the selected equation in the set and λ^i, to a relaxation parameter.

The rate of convergence of the algorithm intuitively depends on how parallel are the hyperplanes. Since the hyperplanes are obtained from ill-conditioned matrices, they are likely to be nearly parallel, providing a slow rate of convergence.

The solution obtained in this way corresponds to the one which is closest to the initial guess in a least-squares error sense [95, pp. 415-425]. Hence, a null initialization selects a minimum energy solution.

Remark. *Applying this iterative method to the direct formulation of the reconstruction problem, $\mathbf{\Omega}_{mn} = \mathbf{\Phi}_{am}^t\, \mathbf{I}_{ab}\, \mathbf{\Phi}_{bn}$, a null initialization provides a unique solution: the minimum energy image with the desired moments.*

Notice that a straightforward application of this iterative method implies $m \cdot n$ equations and $a \cdot b$ unknowns, as described in chapter 9. Then, the so-called space of unknowns is ab-dimensional. Since each coordinate of these space will be updated at each iteration and the number of iterations depends on the conditioning of the problem, it results in a great amount of operations. Nevertheless, the separability of the problem, in the terms

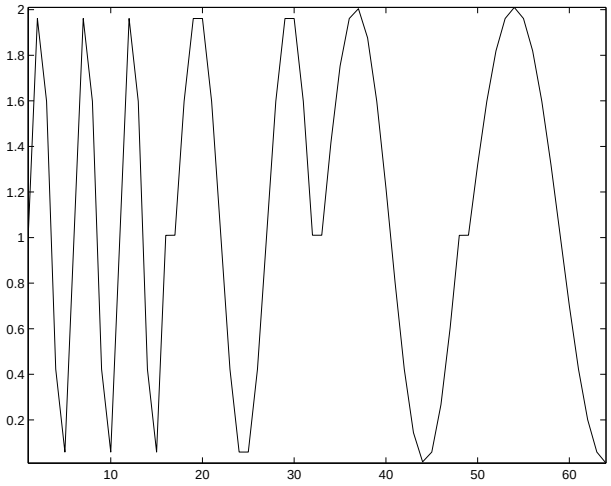

Figure 12.2: *Original function.*

given in the previous section, can be used to reduce computational overhead. Unfortunately, this is not possible in tomographic applications where the underlying projection basis set is not separable.

Therefore, properties 12.1.1 and 12.1.2, respectively, can be straightforwardly introduced in the iterative reconstruction methods. They allow to reduce the dimensionality of the space of unknowns. That is, instead of dealing with the whole image as a vector of dimension ab, rows and columns are treated independently and the maximum dimension of the space of unknowns is either b or a, in the first and second step respectively. This is formalized in algorithm 12.1.

Example 12.2.1. The function in figure 12.2 has been reconstructed using algorithm 12.1. We have used different values for the convergence factor, ϵ, – i. e. the factor that decides when to stop this iterative algorithm depending on the root-mean-square error between the solution of two consecutive steps of the iteration, that is,

$$\text{evaluate\_error}(\mathbf{x}_p, \mathbf{t}_p) = \sqrt{\frac{(\mathbf{x}_p - \mathbf{t}_p)^t \, (\mathbf{x}_p - \mathbf{t}_p)}{(\mathbf{x}_p)^t \mathbf{x}_p}},$$

where $\mathbf{x}_p$ and $\mathbf{t}_p$ refer to the current and previous solution values after an iteration of the algorithm.

The results are plotted in figure 12.3 for geometric moments (in solid line), direct accumulation moments (in dotted line) and reverse accumulation moments (in dashdotted line). An amount of moments equal to the image dimensions has been considered.

The number of iterations of the algorithm and the relative error of the moments obtained from the reconstructed image with respect to those of the original one, for different values of the convergence factor, are shown in figures 12.4a and 12.4b, respectively.

Algorithm: iterative_reconstruction
Input: $\mathbf{\Omega}_{mn}, \mathbf{\Phi}_{am}, \mathbf{\Phi}_{bn}, a, b, \epsilon$
Output: $\mathbf{I}_{ab}$

Initialize $\mathbf{X}_{bm}$
$\mathbf{F}_{mb} \leftarrow$ solve_uncoupled_set$(\mathbf{X}_{bm}, \mathbf{\Omega}_{mn}, \mathbf{\Phi}_{bn}, m, \epsilon)$

Initialize $\mathbf{X}_{ab}$
$(\mathbf{I}_{ab})^t \leftarrow$ solve_uncoupled_set$(\mathbf{X}_{ab}, (\mathbf{F}_{mb})^t, \mathbf{\Phi}_{am}, b, \epsilon)$

$\mathbf{I}_{ab} \leftarrow \left((\mathbf{I}_{ab})^t\right)^t$

Algorithm: solve_uncoupled_set
Input: $\mathbf{X}_{pr}, \mathbf{B}_{rq}, \mathbf{A}_{pq}, r, \epsilon$
Output: $\mathbf{C}_{rp}$

FOR k=1 TO r
    $\mathbf{x}_p \leftarrow \mathbf{X}_{pr}[:, k]$
    $\mathbf{y}_q \leftarrow (\mathbf{B}_{rq}[k, :])^t$
    $\mathbf{x}_p \leftarrow$ solve_parallelized_set$((\mathbf{A}_{pq})^t, \mathbf{x}_p, \mathbf{y}_q, \epsilon)$
    $\mathbf{C}_{rp}[k, :] \leftarrow (\mathbf{x}_p)^t$
ENDFOR

Algorithm: solve_parallelized_set
Input: $\mathbf{x}_p, \mathbf{A}_{pq}, \mathbf{y}_q$
Output: $\mathbf{x}_p$

Initialize $\mathbf{x}_p$
WHILE error $>$ criterion
        $\mathbf{t}_p \leftarrow \mathbf{x}_p$
        FOR i=1 TO p
            $\mathbf{x}_p \leftarrow$ update$(\mathbf{x}_p, \mathbf{A}_{pq}, \mathbf{y}_q, i)$
        ENDFOR
        error $\leftarrow$ evaluate_error$(\mathbf{x}_p, \mathbf{t}_p)$
ENDWHILE

Algorithm 12.1: *Iterative reconstruction.*

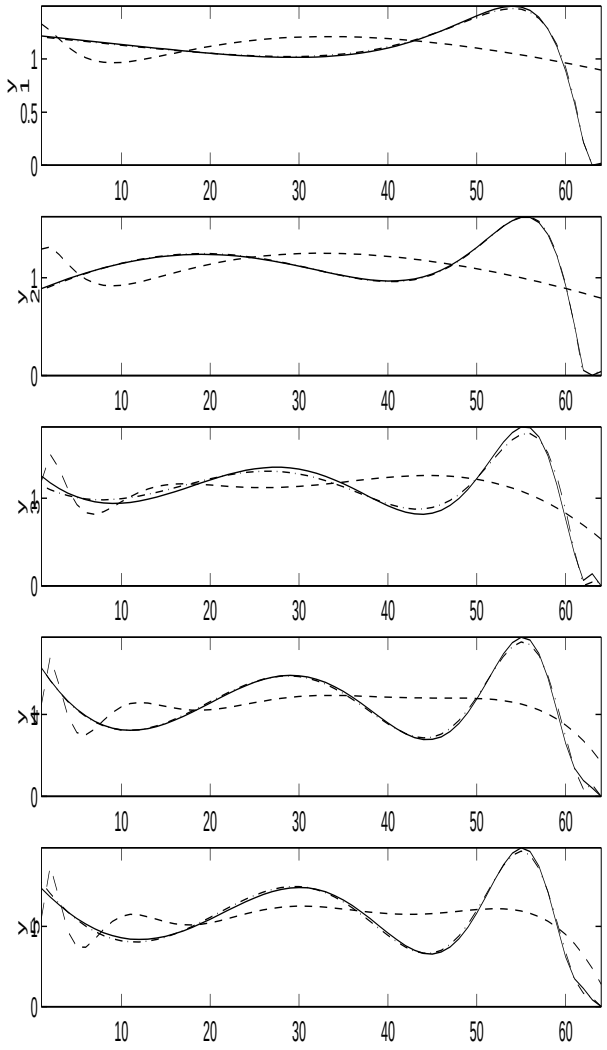

Figure 12.3: *Reconstructed images using the proposed iterative algorithm, for an amount of moments equal to image dimensions, and different values of the convergence factor ϵ, i.e. (a) 10^{-1}, (b) 10^{-2}, (c) 10^{-3}, (d) 10^{-4}, (e) 10^{-5}. The reconstructions using the geometric and the reverse accumulation moments, in solid and dashdotted lines, respectively, are nearly overlapped.*

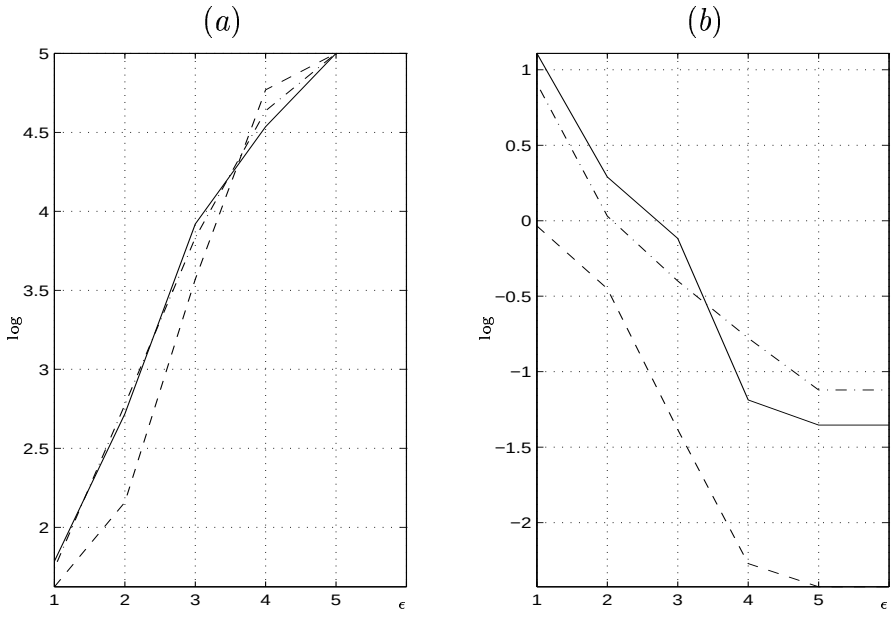

Figure 12.4: *(a) The number of iterations and (b) the error of the moments obtained from the reconstructed image with respect to those of the original one, in figure 12.3. Solid lines refer to geometric moments, dashdotted lines to reverse accumulation moments and dashed ones to direct accumulation moments.*

Although the algorithm always converges, the number of iterations exponentially increases as the parameter ϵ decreases.

Notice that in figure 12.4b, for a fixed ϵ, the direct accumulation moments provide a better reconstruction than geometric or direct accumulation moments, in terms of the error of the moments of the reconstructed image with respect to the original one.

Multiple variations of this simple iterative algorithm have been introduced in the literature concerning the adequate relaxation parameter, the optimal order to access the set of linear equations, the convergence factor and the initial guess of the iteration [10, 38, 37, 45, 44, 17, 76]. However, there exists a consensus about the specific image-dependence of this parameters.

It is worth to mention that the relaxation parameter has a statistical interpretation. This interpretation derives from the correspondence between the estimate-maximize (EM) formulation, which is a general method for solving maximum likelihood (ML) estimation problems given incomplete data [20], and the formulation of the Kaczmarz method [95]. Experimental results developed in [37] to determine the optimal value of this parameter show its dependence on the level of noise. In particular, for the case of white Gaussian noise, it is proved to be related to the noise covariance associated with the equations in each iteration [20]. Since roundoff error can be modeled as white Gaussian noise, as already mentioned in chapter 9, this parameter is related to numerical instabilities.

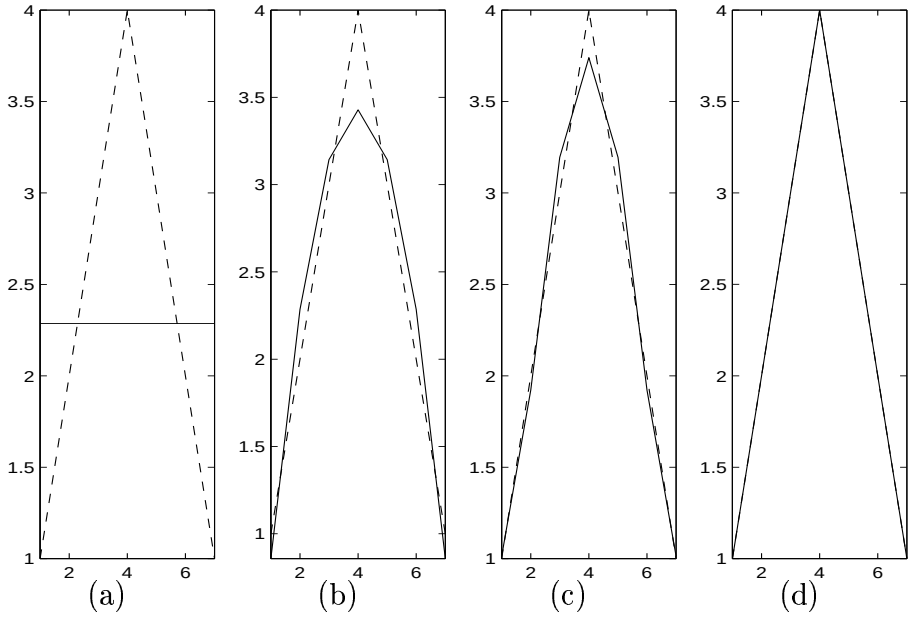

Figure 12.5: *Reconstructed images using SVD from (a) 1, (b) 3, (c) 5 and (d) 7 geometric moments. Original* 1×7 *image is plotted in dashed line.*

12.3 Singular value decomposing

Inverting ill-conditioned matrices requires preconditioning, that is, eliminating numerical instabilities. For non-square matrices, a generalized inverse is normally used. In chapter 8, it has been shown that this pseudoinverse allows to obtain the least-squares approximation of an image. The pseudoinverse of a matrix can be obtained from its singular values [34, chapter 11]. For example the left pseudoinverse of $\mathbf{A}_{mn}$ is obtained as

$$(\mathbf{A}_{mn})^{-} = \mathbf{U}_m \begin{pmatrix} \mathbf{D}_{pp}^{-1} & \mathbf{0}_{n-p,n-p} \\ \mathbf{0}_{m-p,m-p} & \mathbf{0}_{n-p,n-p} \end{pmatrix} (\mathbf{W}_n)^t; \tag{12.4}$$

where $\mathbf{D}_{pp}^{-1}[k,k] = \frac{1}{\sigma_k}$ and σ_k are the singular values of $\mathbf{A}_{mn}$ such that $\sigma_1 \geq \cdots \geq \sigma_p \geq 0$,; and, $\mathbf{U}_m$ and $\mathbf{V}_n$ are orthogonal matrices.

Then, the singular values are the elements of a diagonal matrix obtained from diagonalizing a real matrix $\mathbf{A}_{mn}$ using the orthogonal matrices $\mathbf{U}_m$ and $\mathbf{W}_n$ [30, pp. 69-72]. These singular values are the positive square roots of the eigenvalues (which are non negatives) of $(\mathbf{A}_{mn})^t\mathbf{A}_{mn}$. The columns of $\mathbf{U}_m$ are called the left singular vectors of $\mathbf{A}_{mn}$ (the ortogonal eigenvectors of $\mathbf{A}_{mn}(\mathbf{A}_{mn})^t$) and the columns of $\mathbf{W}_n$ are called the right singular vectors of $\mathbf{A}_{mn}$ (the ortogonal eigenvectors of $(\mathbf{A}_{mn})^t\mathbf{A}_{mn}$) [49].

Example 12.3.1. In figure 12.5, it is shown how the reconstruction of the image in dashed line using the SVD is the same as the one obtained from the least-squares approximation in chapter 11.

The SVD allows to reduce numerical instabilities by setting to zero those singular

values that are too small [88, pp. 676-706]. But, how small is small? A plausible answer seems to be to consider as small those values smaller than m times the computer numerical precision ξ, where m refers to matrix dimensions. The numerical precision is defined as the distance from 1.0 to the next largest floating point number, that is, for the case of the 64-bits floating-point IEEE format (see section 9.3), $\xi = 2^{-52} = 2.220446049250313 \times 10^{-16}$. However, a more accurate answer would depend on the application.

To evaluate the performance of the SVD in reducing numerical instabilities, a pseudoinverse is obtained treating as zero those singular values that are smaller than a given threshold t; in particular, $t = m\,\xi\,\sigma_1$, where σ_1 is the largest singular value of the matrix. Figure 12.6 shows the mean square error of $\mathbf{V}_m\,(\mathbf{V}_m)^-$ with respect to the identity matrix $\mathbf{1}_m$ for increasing values of m. Comparing these results with the ones obtained for the ordinary inverse in figure 9.5, it is shown that the computation of the pseudoinverse clearly reduces roundoff errors in the reconstruction process. Figure 12.7 shows the mean square error of reconstructing uniformly distributed random square images for increasing values of m using pseudoinverses. Again, results improve with regard to the ones in figure 9.6 where the ordinary inverses are used.

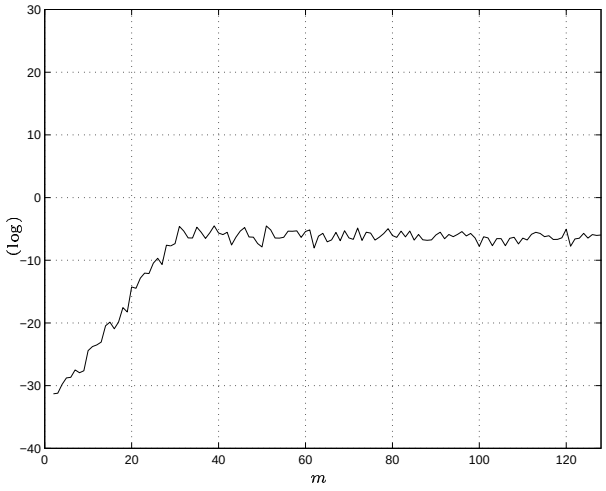

Figure 12.6: *Roundoff error in the Vandermonde matrix pseudoinverses* $(\mathbf{V}_m)^-$ *for a threshold* $t = m\,\xi\,\sigma_1$, *where* σ_1 *is the largest singular value of* $\mathbf{V}_m$ *and* $\xi = 2^{-52}$.

12.4 Reconstruction error

In this section, we analyze the error in the reconstructed image. Aside from the roundoff error analyzed in chapter 9, there exist two other sources of error: (a) the reconstruction error due to the fact that the number of moments is lower than the image size; and (b) the reconstruction error due to noisy data.

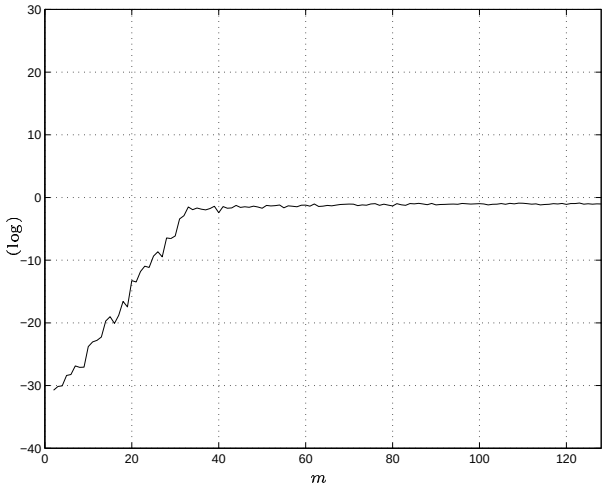

Figure 12.7: *Mean square error in the reconstruction of uniformly distributed random square image of size m using Vandermonde matrix pseudoinverses.*

Let us consider the linear reconstruction problem in the general form:

$$\hat{\mathbf{i}}_{a\cdot b} = (\mathbf{K}_{a\cdot b\cdot m\cdot n})^{-}\ \hat{\boldsymbol{\omega}}_{m\cdot n}, \tag{12.5}$$

where, according to the unified approach of chapter 11, the pseudoinverse $(\mathbf{K}_{a\cdot b\cdot m\cdot n})^{-}$ can be written as:

$$(\mathbf{K}_{a\cdot b\cdot m\cdot n})^{-} = \left(\overline{\boldsymbol{\Phi}}_{am}\ ((\boldsymbol{\Phi}_{am})^{t}\ \overline{\boldsymbol{\Phi}}_{am})^{-1}\right)\ \otimes\ \left(\overline{\boldsymbol{\Phi}}_{bn}\ ((\boldsymbol{\Phi}_{bn})^{t}\ \overline{\boldsymbol{\Phi}}_{bn})^{-1}\right). \tag{12.6}$$

Then, as stated in section 9.3, a bound of the sensitivity of the reconstructed image with regard to perturbations in the data can be derived from the condition number of the involved matrix as follows:

$$\frac{\|\boldsymbol{\delta}\hat{\mathbf{i}}\|}{\|\hat{\mathbf{i}}\|} \leq \frac{\|\boldsymbol{\delta}\mathbf{K}\|}{\|\mathbf{K}\|}\chi(\mathbf{K}), \qquad \text{where } \frac{\|\boldsymbol{\delta}\mathbf{K}\|}{\|\mathbf{K}\|} \ll 1;\ \text{and}$$

$$\frac{\|\boldsymbol{\delta}\hat{\mathbf{i}}\|}{\|\hat{\mathbf{i}}\|} \leq \frac{\|\boldsymbol{\delta}\boldsymbol{\omega}\|}{\|\boldsymbol{\omega}\|}\chi(\mathbf{K}), \qquad \text{where } \frac{\|\boldsymbol{\delta}\boldsymbol{\omega}\|}{\|\boldsymbol{\omega}\|} \ll 1.$$

Therefore, the reconstruction error can be analized in terms of the condition number of matrix $\mathbf{K}_{a\cdot b\cdot m\cdot n}$. Figure 12.8 plots this value in function of the available number of moments and different reconstruction basis matrices. The maximum computer integer resolution $\eta = 2^{53} - 1 = 9.007199254740991 \times 10^{15}$ is also plotted.

The influence of the condition number is shown in the following example.

Example 12.4.1. Let us consider the reconstruction of letter "A". Figures 12.9, 12.10, 12.11 and 12.12 show the results for different order of moments, using Chebyshev polynomial, Fourier, Haar and monomial basis, respectively. A comparison in terms of the mean square reconstruction error is shown in figure 12.13.

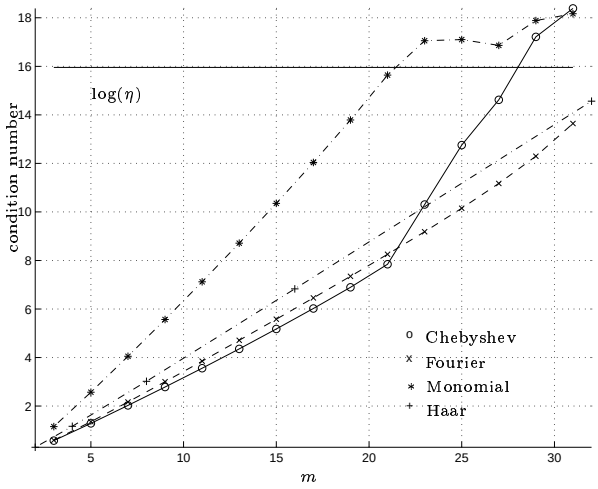

Figure 12.8: *Condition number of matrix* $\mathbf{K}$.

It can be seen that the reconstruction error decreases as the order of moments increases. This outlines the fact that the reconstruction error is mainly a truncation error, i.e. the error introduced by the fact that the number of moments is lower than the image size. Since we have used pseudoinverses instead of ordinary inverses to reduce ill-conditioning, these result proves that roundoff error can be palliated using the singular value decomposition and eliminating those singular values below a given threshold.

Example 12.4.2. This example shows the effect of noisy data. Figures 12.14, 12.15, 12.16 and 12.17 show the reconstruction of the same image as in the previous example from a set of moments obtained from a noisy image. In particular, zero mean gaussian white noise with 0.01 variance has been added. A comparison of the mean square reconstruction error is shown in figure 12.18.

In this case, the error do not, in general, continuously decreases as the order of moments increases. There exists a particular order, that depends on the basis used in the reconstruction, for which the reconstruction error has its minimum value. Notice that monomial basis are more insensitive to noisy data. Therefore, although the monomial basis and the Chebyshev polynomial basis should provide the same reconstructed image – both basis define the same subspace and are supossed to reconstruct the image contained in this subspace – the latter is more sensitive to perturbations in the data.

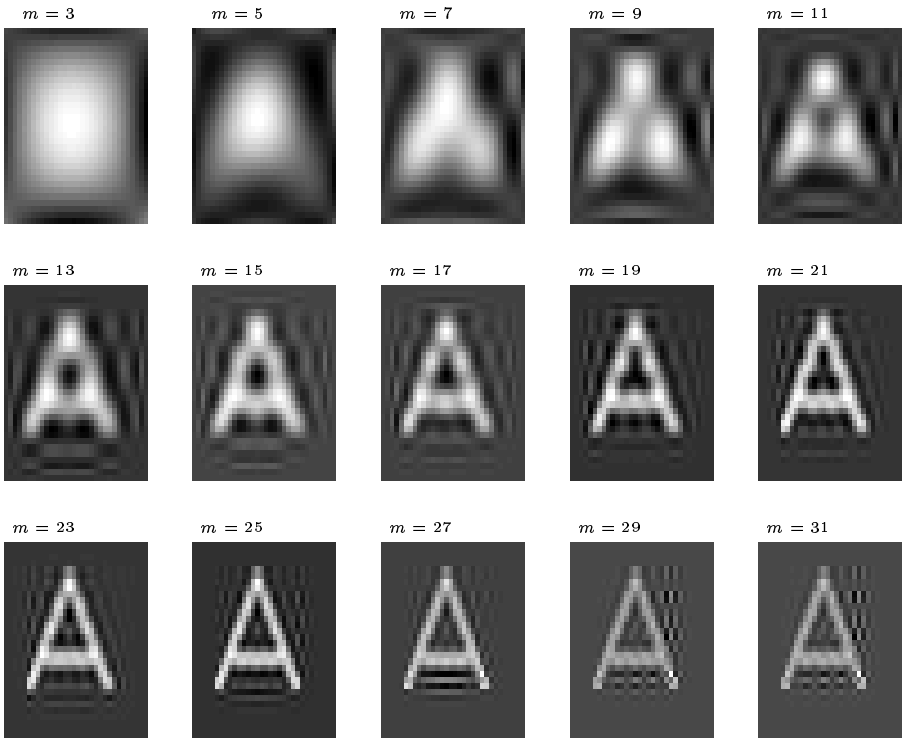

Figure 12.9: *Reconstructed images using the Chebyshev polynomial basis for increasing number of moments of a* 32×32 *image.*

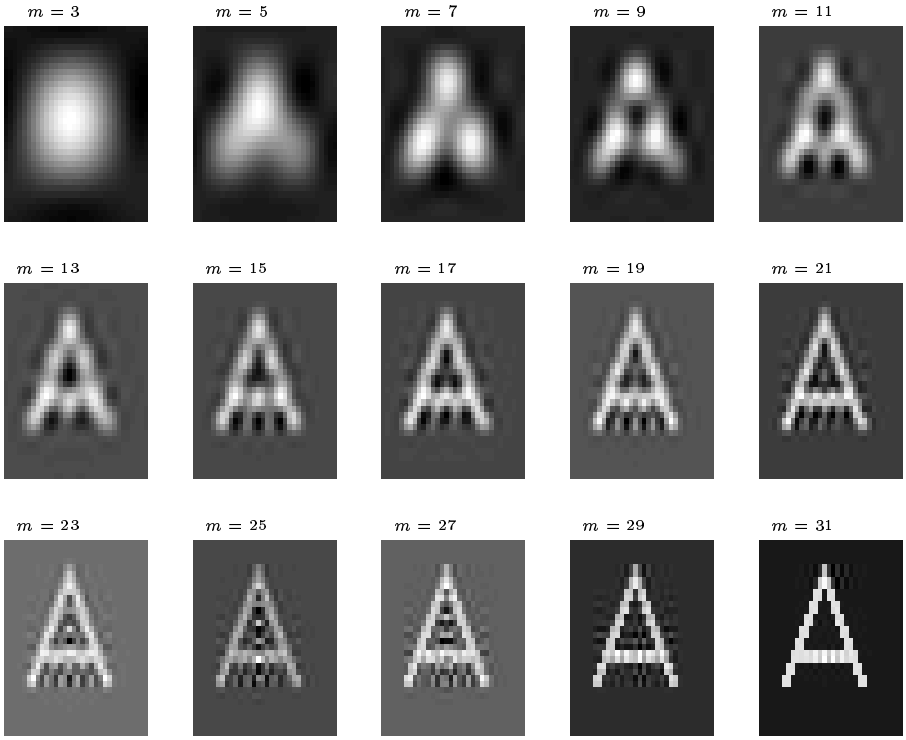

Figure 12.10: *Reconstructed images using the Fourier basis for increasing number of moments of a* 32×32 *image.*

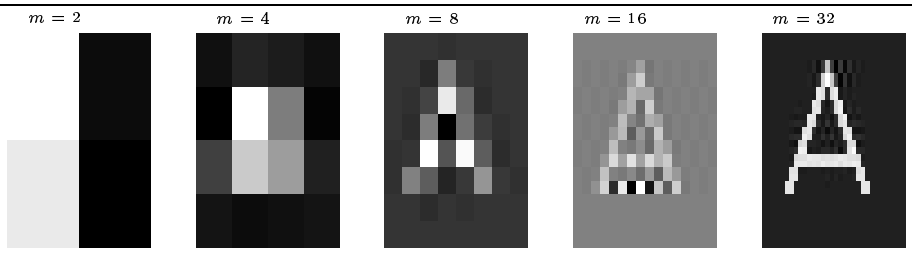

Figure 12.11: *Reconstructed images using the Haar basis for increasing number of moments of a* 32×32 *image.*

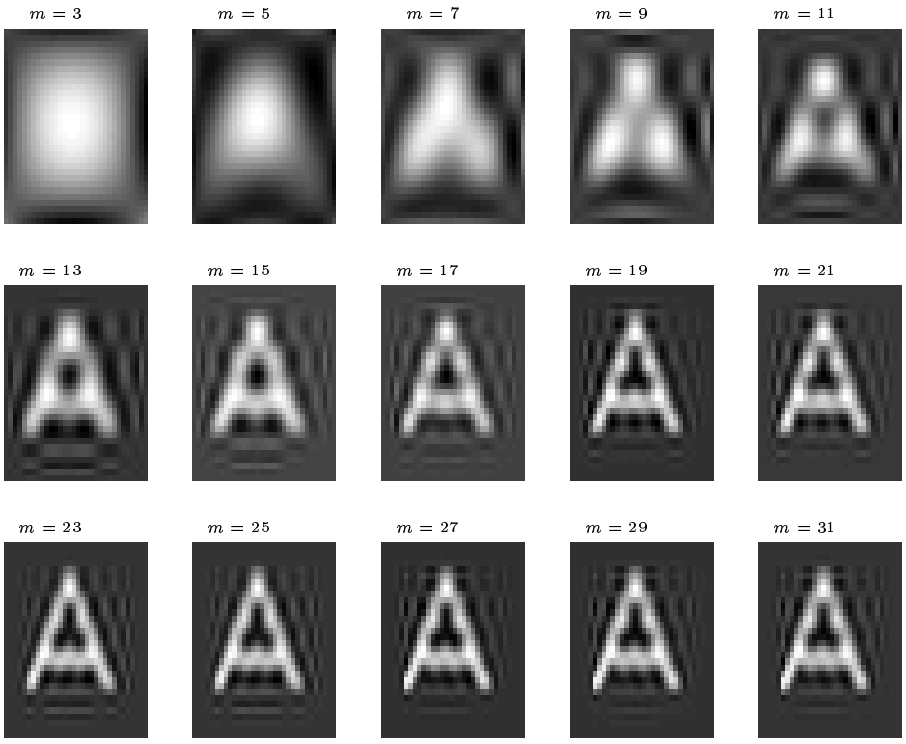

Figure 12.12: *Reconstructed images using the monomial basis for increasing number of moments of a* 32×32 *image.*

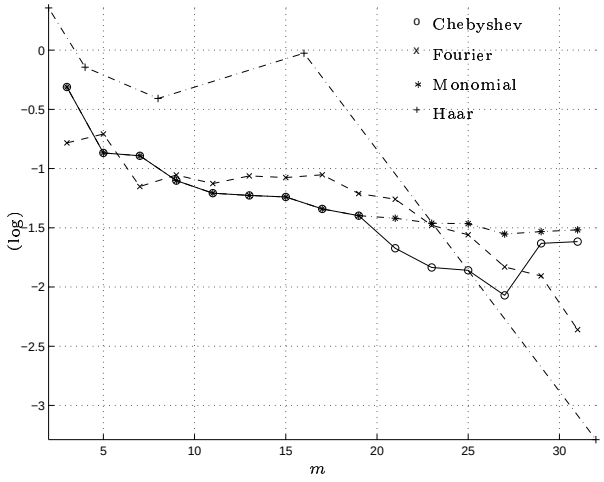

Figure 12.13: *Mean square error of the reconstructed images in figures 12.9, 12.10, 12.11 and 12.12.*

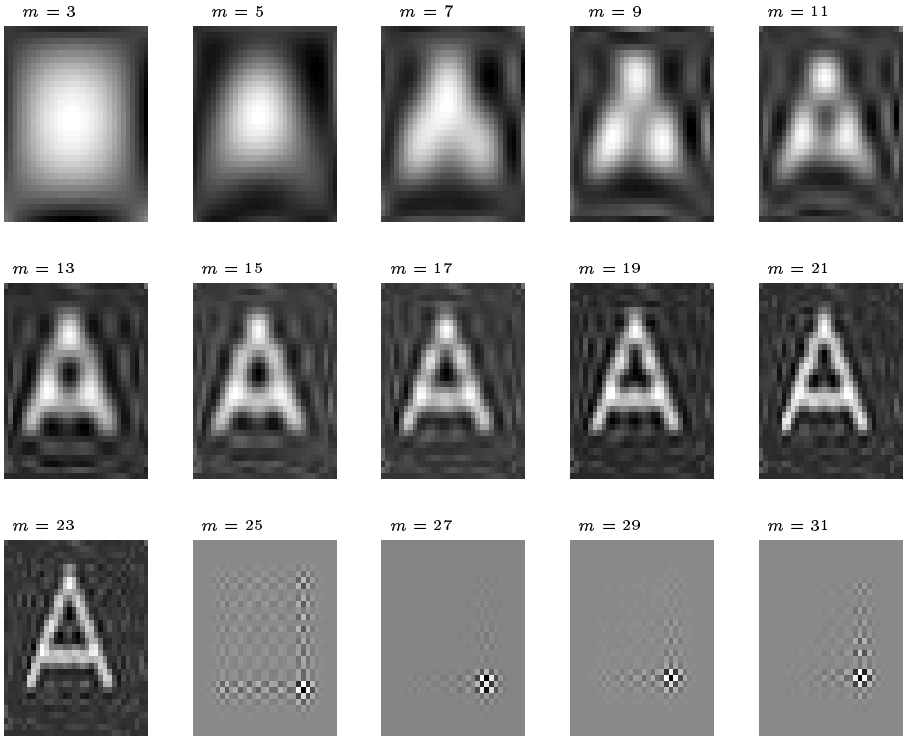

Figure 12.14: *Reconstructed images using the Chebyshev polynomial basis for increasing number of moments of a* 32×32 *image.*

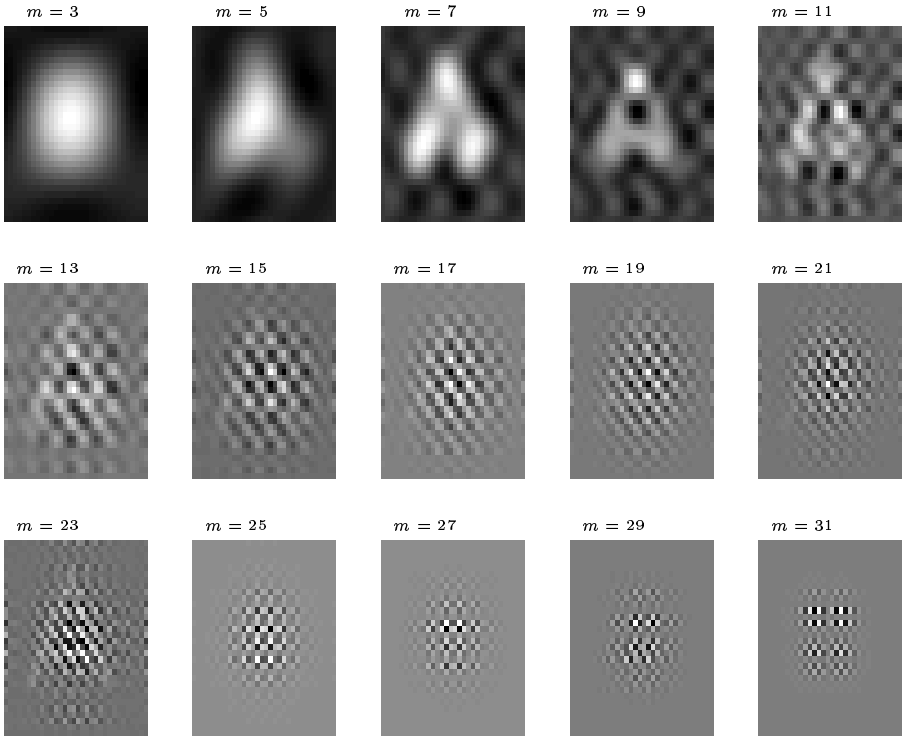

Figure 12.15: *Reconstructed images using the Fourier basis for increasing number of moments of a* 32×32 *image.*

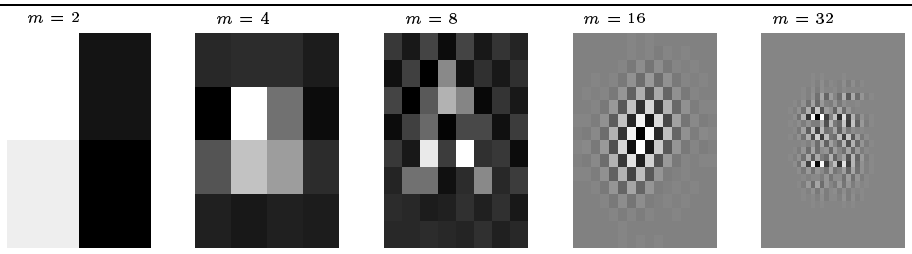

Figure 12.16: *Reconstructed images using the Haar basis for increasing number of moments of a* 32×32 *image.*

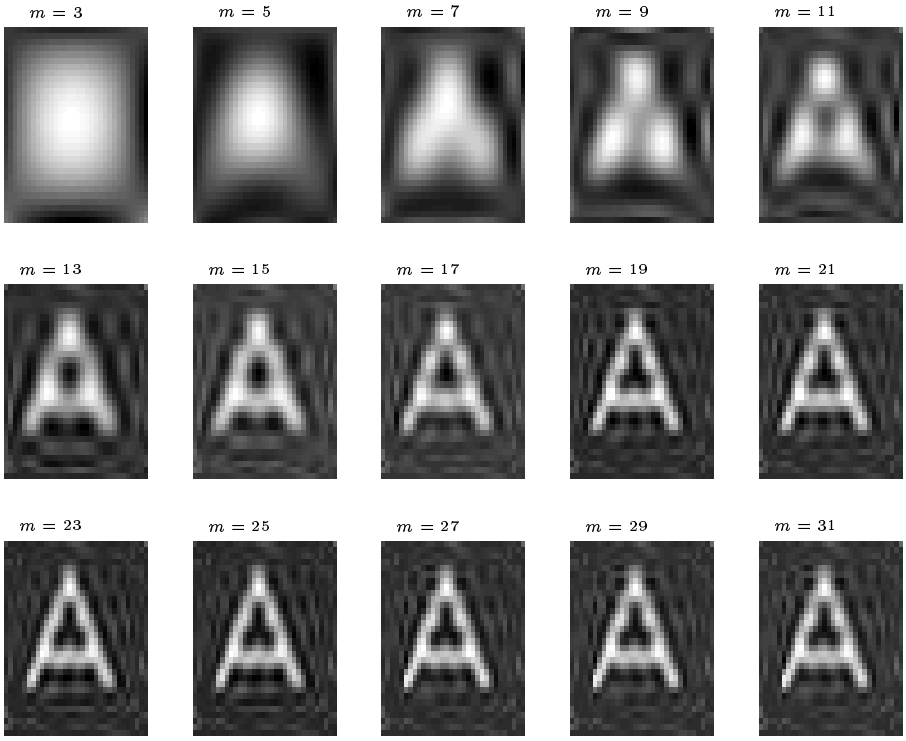

Figure 12.17: *Reconstructed images using the monomial basis for increasing number of moments of a* 32×32 *image.*

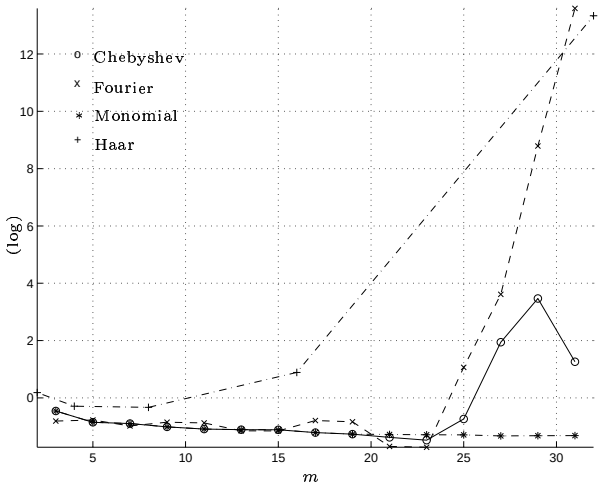

Figure 12.18: *Mean square error of the reconstructed images in figures 12.14, 12.15, 12.16 and 12.17.*

Chapter 13

The binary case

Since the reconstruction methods introduced in previous chapters are limited to gray-level images, if a binary image is required it is necessary to binarize the approximated image. However, the binarization process do not normally preserve moments. Therefore, it seems reasonable to consider specific methods for reconstructing a binary image from a finite set of its moments.

When dealing with binary images, the reconstruction problem can be translated into the context of constraint satisfaction problems (CSP). For the particular case of global constraints such as moments, obtaining a solution is often computationally very expensive. Hence, we particularize the general problem to the one of reconstructing a binary image having a given area and centroid, that is, moments up to first order. To this end, we have devised a recursive algorithm of linear complexity with respect to the area of the region to be reconstructed.

13.1 Setting the problem as a CSP

Reconstructing a binary image requires solving equation (8.2) subject to the constraint

$$\mathbf{I}_{ab}[x, y] \in \{0, 1\}.$$

Therefore, solving the inverse problem for binary images fits into the context of constraint satisfaction problems (CSP), which involve finding values for variables subject to constraints on acceptable combination of values.

The variables of the problem are the pixels of the image, their domain of potential values is $\{0, 1\}$, and the constraints are the set of linear equations defined by the known moments. These equations are of the form of pseudoboolean linear constraints since coefficients are integer values and variables are 0 or 1 [3]. Then, a solution is specified by the assignment of a value to each variable such that constraints are satisfied.

The process of searching for a solution satisfying these pseudoboolean linear constraints can be represented by a search tree, where each level of the tree corresponds to

a variable and nodes to the assignment of values to variables. A search path is the set of assignment values along a branch of the tree. A solution is obtained when exploring a search path such that their nodes are consistent, that is, the values assigned to the variables satisfy the constraints.

Any algorithm that expands the complete search tree is NP-complete, which means that its cost increases exponentially with the problem dimensions. Therefore, complete expansion must be avoided. Pruning techniques that eliminate a subtree of the search space, either based on already assigned variables (retrospective techniques) or not yet assigned variables (prospective techniques) along the current search path, have been proposed in the literature (see [24] for a review). Also, ordering techniques based on some heuristic that directs the sequence in which variables, values and constraints are considered during the search have extensively been developed. A measure of the effort for CSP algorithms is the number of constraint checks, that is the number of times that a basic question of the form: "is value x_1 of variable x consistent with value y_1 of variable y?" occurs.

In the next section, it is proved that obtaining a binary image of a given area and centroid, that is, of particular values of the accumulation moments up to first order, do not require to expand the search tree. Its complexity is linear with the area.

Since the solution to this problem is, in general, not unique, it is possible to consider additional constraints so that it satisfies some desired properties; for instance, connectivity, thinness, closed contours or higher order moments. In this case, the search tree must be pruned while searching. A measure of the efficiency of the algorithms in this case is the number of constraint checks, that is, the analysis of consistency of variables at each node with respect to other variables. Obviously, the deeper in the search tree we explore before a partial solution is rejected, the more costly is the algorithm.

Constraints are defined as m-ary when they involve m variables. Local constraints are at most 8-ary, since they represent a relationship between a pixel and its neighborhood. On the other hand, global constraints might relate a pixel with all the others in the image; therefore, they are ab-ary. Then, more efficient algorithms can be envisaged for local constraints than for global ones.

13.2 Partial constraint satisfaction

Definition 13.2.1 (Index vector). Given the columnwise form of a binary image $\mathbf{i}_{ab}$, the vector $\mathbf{p}_c$ containing those positions k that verify $\mathbf{i}_{ab}[k] = 1$ such that $\mathbf{p}_c[l] < \mathbf{p}_c[l+1]$, for $1 \leq l \leq c$, is defined as *the index vector* associated with $\mathbf{i}_{ab}$.

Lemma 13.2.1. *Given a binary image $\mathbf{I}_{ab}$, its index vector and its direct accumulation moments up to first order satisfy*

$$\sum_{l=1}^{c} \mathbf{p}_c[l] = \mathbf{R}_{mn}[1,2] + b\,\mathbf{R}_{mn}[2,1] - b\,\mathbf{R}_{mn}[1,1], \tag{13.1}$$

where $c = \mathbf{R}_{mn}[1,1]$.

Proof. From equation (2.19), the reverse accumulation moments up to first order can be expressed in terms of the image as:

$$\mathbf{R}_{mn}[1,1] = \sum_{r=1}^{a}\sum_{s=1}^{b} \mathbf{I}_{ab}[r,s]$$

$$\mathbf{R}_{mn}[1,2] = \sum_{r=1}^{a}\sum_{s=1}^{b} \binom{s}{s-1} \mathbf{I}_{ab}[r,s]$$

$$\mathbf{R}_{mn}[2,1] = \sum_{r=1}^{a}\sum_{s=1}^{b} \binom{r}{r-1} \mathbf{I}_{ab}[r,s]$$

Using the columnwise form of the binary image $\mathbf{i}_{ab}$, obtained by sequentially reading each row of $\mathbf{I}_{ab}$, this set of linear equations can be expressed in matrix fom as follows:

$$\begin{pmatrix} \mathbf{R}_{mn}[1,1] \\ \mathbf{R}_{mn}[1,2] \\ \mathbf{R}_{mn}[2,1] \end{pmatrix} = \begin{pmatrix} 1 & \dots & 1 & 1 & \dots & 1 & \dots & 1 & \dots & 1 \\ 1 & \dots & b & 1 & \dots & b & \dots & 1 & \dots & b \\ 1 & \dots & 1 & 2 & \dots & 2 & \dots & a & \dots & a \end{pmatrix} \mathbf{i}_{ab}. \tag{13.2}$$

Then, it is easy to verify that

$$\mathbf{R}_{mn}[1,2] + b\,\mathbf{R}_{mn}[2,1] - b\,\mathbf{R}_{mn}[1,1] = \begin{pmatrix} 1 & 2 & \dots & \dots & ab \end{pmatrix} \mathbf{i}_{ab}.$$

In other words, a linear combination of the accumulation moments up to first order is the projection of the columnwise form of the image onto the vector of natural numbers. Therefore,

$$\sum_{k=1}^{ab} k\,\mathbf{i}_{ab}[k] = \sum_{k \text{ such that } \mathbf{i}_{ab}[k]=1} k \quad = \sum_{l=1}^{c} \mathbf{p}_c[l],$$

where c is the number of 1's in the image, i.e. $c = \mathbf{R}_{mn}[1,1]$. This proves the lemma. □

Corollary 13.2.1. *By lemma 13.2.1 and corollary 2.3.1,*

$$\sum_{l=1}^{c} \mathbf{p}_c[l] = \mathbf{M}_{mn}[1,2] + b\,\mathbf{M}_{mn}[2,1] - b\,\mathbf{M}_{mn}[1,1], \tag{13.3}$$

where $c = \mathbf{M}_{mn}[1,1]$.

A geometric interpretation of lemma 13.2.1 leads to the following result.

Corollary 13.2.2. *Given the c-dimensional lattice of all possible index vectors associated with binary images of area c, the index vectors that are associated with binary images of the same centroid are located onto an hyperplane of the form*

$$\mathbf{p}_c^s[1] + \mathbf{p}_c^s[2] + \cdots + \mathbf{p}_c^s[c] = s,$$

where s depends on the centroid.

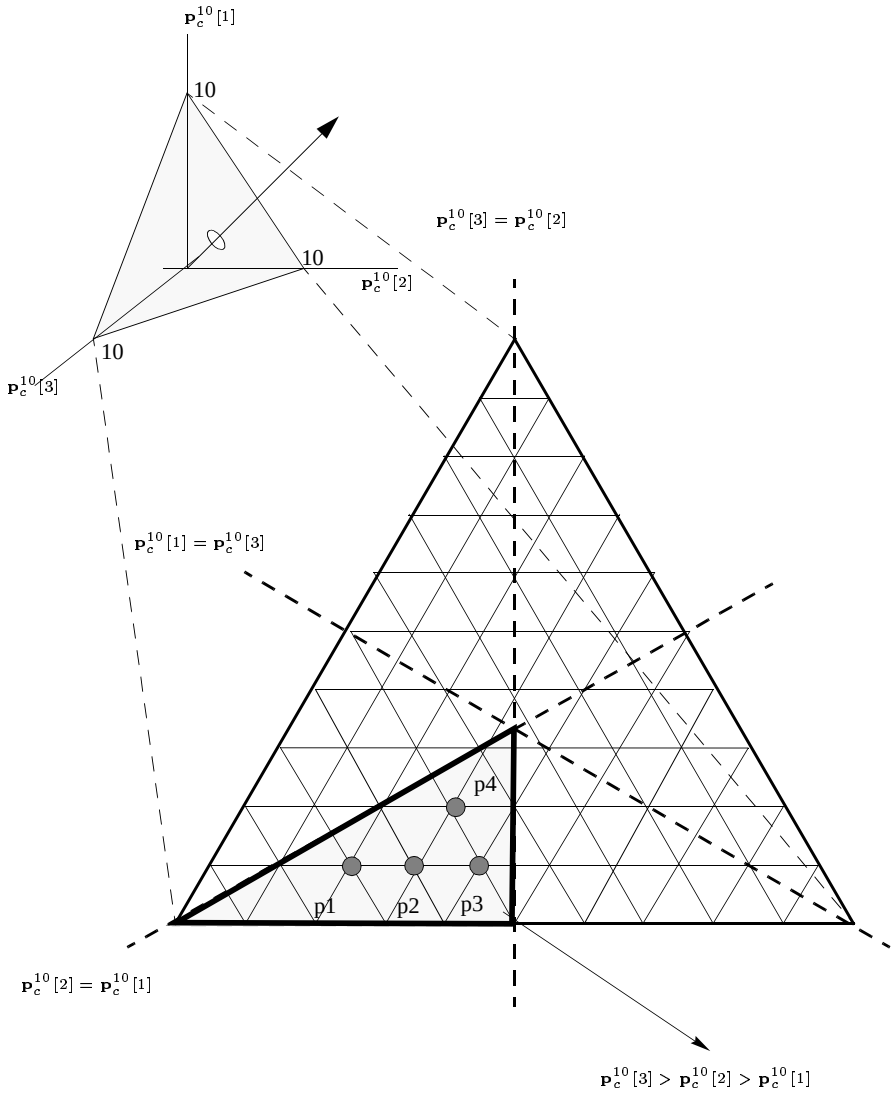

Figure 13.1: *Hyperplane of constant addition* $s = 10$ *and* $c = 3$.

Figure 13.1 exemplifies this interpretation.

Lemma 13.2.2. *The range of values of* $\mathbf{p}_c^s[c]$ *of all index vectors that verify* $\sum_{l=1}^{c} \mathbf{p}_c^s[l] = s$ *is composed by the integers in the interval* $\left[\check{\mathbf{p}}_c^s[c], \hat{\mathbf{p}}_c^s[c]\right]$, *where*

$$\hat{\mathbf{p}}_c^s[c] = min\Big(s - \frac{c(c-1)}{2}, ab\Big), \tag{13.4}$$

$$\check{\mathbf{p}}_c^s[c] = \begin{cases} \hat{\mathbf{p}}_c^s[c] - \lfloor d \rfloor, & if \quad \hat{\mathbf{p}}_c^s[c] - \lfloor d \rfloor \geq c - 1 + f + \left\lceil \frac{1}{c-1} \lfloor d \rfloor \right\rceil \\ \hat{\mathbf{p}}_c^s[c] - \lfloor d \rfloor + 1, & otherwise, \end{cases} \tag{13.5}$$

$$d = \hat{\mathbf{p}}_c^s[c] - \frac{1}{c}\Big(s - \frac{(c-1)(c-2)}{2}\Big), \tag{13.6}$$

and

$$f = \frac{s - \hat{\mathbf{p}}_c^s[c]}{c-1} - \frac{c}{2}. \tag{13.7}$$

Proof. Since

$$\mathbf{p}_c^s[c] = s - \sum_{l=1}^{c-1} \mathbf{p}_c^s[l], \tag{13.8}$$

then, for a fixed value of s, the maximum value of $\mathbf{p}_c^s[c]$, $\hat{\mathbf{p}}_c^s[c]$ is attained when all other coordinates $\mathbf{p}_c^s[l]$ are minimum, i.e. $\mathbf{p}_c^s[l] = l$, for $l = 1, \ldots, c-1$. Then,

$$\sum_{l=1}^{c-1} \mathbf{p}_c^s[l] = \frac{c(c-1)}{2}.$$

However, since the index vector refers to locations of the columnwise form of the image, there exists a constraint on its maximum value, that is

$$\hat{\mathbf{p}}_c^s[c] \leq ab,$$

where $a \times b$ is the image size. Hence,

$$\hat{\mathbf{p}}_c^s[c] = \min\Big(s - \frac{c(c-1)}{2}, ab\Big).$$

On the other hand, the expression of the minimum value $\check{\mathbf{p}}_c^s[c]$ can be derived from modeling the problem in terms of the collision of two mobiles. Figure 13.2 sketchs the model. Let $\mathbf{p}_c^s[c]$ be mobile 1 and all the other $\left[\mathbf{p}_c^s[c-1], \mathbf{p}_c^s[c-2], \ldots, \mathbf{p}_c^s[1]\right]$ be linked in a single mobile 2. Their initial positions are defined by the situation in which $\mathbf{p}_c^s[c] = \hat{\mathbf{p}}_c^s[c]$.

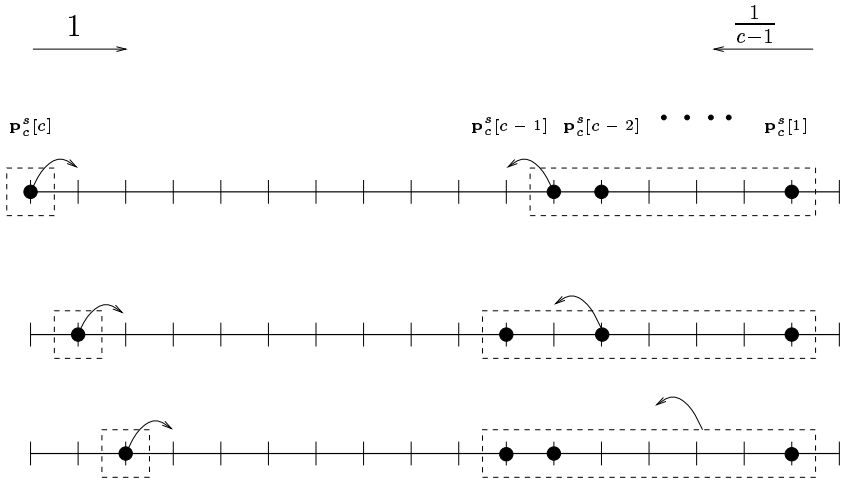

Figure 13.2: *Kinematic model to obtain* $\check{\mathbf{p}}_c^s[c]$.

Notice that, if $\hat{\mathbf{p}}_c^s[c] = ab$ the front position of mobile 2 is $c-1+f$, where f is a constant offset required to each element of mobile 2 so that equation (13.8) is satisfied. Then,

$$f = \frac{s - \hat{\mathbf{p}}_c^s[c]}{c-1} - \frac{c}{2}.$$

Their speed are measured in terms of integers per jump. Assuming that mobile 1 can move at 1 integer per jump, mobile 2 moves at $\frac{1}{c-1}$ integers per jump because equation (13.8) must always be satisfied. Then, at the collision point,

$$\hat{\mathbf{p}}_c^s[c] - d = c - 1 + \text{offset} + \lceil \frac{1}{c-1}\, d \rceil; \tag{13.9}$$

from which

$$d = \hat{\mathbf{p}}_c^s[c] - \frac{1}{c}\big(s - \frac{(c-1)(c-2)}{2}\big). \tag{13.10}$$

Since the number of jumps must be an integer, let it round to the nearest integer towards zero, i.e. $\lfloor d \rfloor$. Then, if

$$\hat{\mathbf{p}}_c^s[c] - \lfloor d \rfloor \geq c - 1 + \text{offset} + \left\lceil \frac{1}{c-1} \lfloor d \rfloor \right\rceil, \tag{13.11}$$

it means that mobile 1 can perform $\lfloor d \rfloor$ jumps without colliding with mobile 2. Then, to avoid any collision, the number of jumps must be $\lfloor d \rfloor - 1$. Therefore,

$$\check{\mathbf{p}}_c^s[c] = \begin{cases} \hat{\mathbf{p}}_c^s[c] - \lfloor d \rfloor, & \text{if equation (13.11) is satisfied,} \\ \hat{\mathbf{p}}_c^s[c] - \lfloor d \rfloor + 1, & \text{otherwise.} \end{cases}$$

Notice that, since the speed of mobile 1 is 1 integer per jump, every integer value included in between $\check{\mathbf{p}}_c^s[c]$ and $\hat{\mathbf{p}}_c^s[c]$ determine the coordinates of index vectors on plane s. Then, the range of values of $\mathbf{p}_c^s[c]$ is completly defined and lemma 13.2.2 is proved. □

Property 13.2.1 (Recursivity). *Given c and s, it is possible to obtain all index vectors of dimension c on the hyperplane s by recursively applying lemma 13.2.2, for $i = c, c-1, \ldots, 1$, so that, for each value $\mathbf{p}_i^{s_i,k}[i] = \check{\mathbf{p}}_i^{s_i}[i] + k$ in $[\check{\mathbf{p}}_i^{s_i}[i], \hat{\mathbf{p}}_i^{s_i}[i]]$, the range of values of coordinate $\mathbf{p}_i^{s_i}[i-1]$ is obtained from lemma 13.2.2 when*

$$s = s_i - \mathbf{p}_i^{s_i,k}[i]$$
$$c = i,$$

where $s_c = s$.

This is formalized in algorithm 13.1.

```
Algorithm: binary_images_of_given_area_and_centroid
Input:   s, c
Output: {PATHS}

  {path } ← {∅}
  {PATHS} ← {∅}
  {PATHS} ← hyperplane (s, c, {path},{PATHS} )

---------------------------------------------------

Algorithm: hyperplane
Input:   s, c,{path},{PATHS}
Output: {PATHS}

  IF c ≠ 1
    {R} ← obtain_range(c, s)
    WHILE {R} ≠ {∅}
          p ← {R}
          {R} ← {R} − p
          s ← s − p
          c ← c − 1
          {path} ← {path} ∪ p
          {PATHS} ← hyperplane (s, c, {path},{PATHS} )
    ENDWHILE
  ELSE
    {path} ← {path} ∪ s
    {PATHS} ← {PATHS} ∪ {path}
  ENDIF
```

Algorithm 13.1: *Reconstruction of binary images of given area and centroid.*

Example 13.2.1. Figure 13.3 shows the complete set of binary images of equal area and centroid for $c = 9$ and $s = 5$.

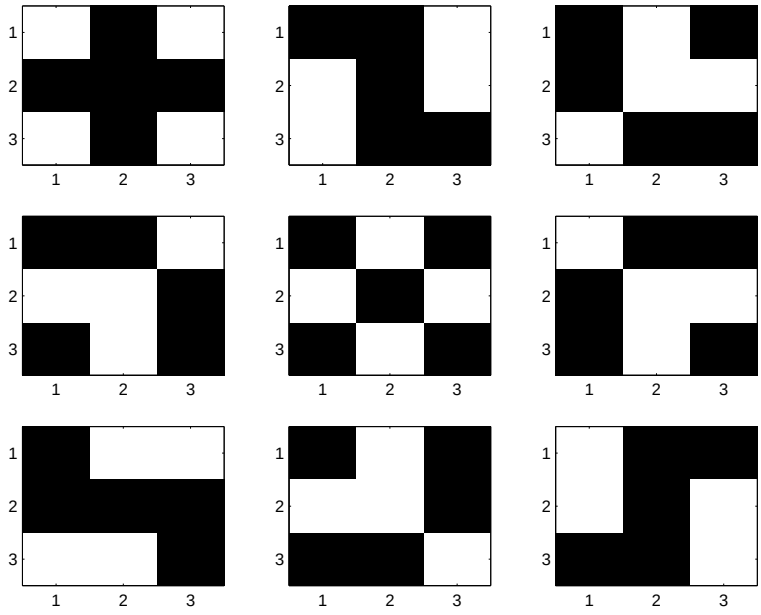

Figure 13.3: *Complete set of binary images for* $c = 9$ *and* $s = 5$.

This algorithm allows to straightforwardly obtain one solution with a cost that increases linearly with the area of the pattern to reconstruct. However, if the complete set of solutions is required, the number of solutions increases exponentially with the image size. This suggests that local constraints are a must if binary images are required (see [94] for details).

Chapter 14

Conclusions

14.1 Contributions

This section briefly enumerates the contributions achieved in this thesis.

1. The definition of a new set of global features, the accumulation moments, whose main characteristics can be summarized in four points:

   - they are related to the geometric moments through a one-to-one linear transformation so that the information contained in a finite set of geometric moments is equivalent to that contained in the accumulation moments of the same order;
   - they can be obtained using $O(a^2m)$ additions, where a and m refer to the image size and the amount of required moments, respectively;
   - they can be implemented using a simple hardware scheme of a basic structure formed by a bit-serial adder and a feedback loop that includes shift registers; and
   - they can be used to accelerate the computation of geometric moments, its associated invariants, and the actualization of moments in a sliding window.

   Thus, any application involving geometric moments can benefit from the use of accumulation moments due to their computational advantages.

2. The statement of the incorrectness of former methods used to reconstruct an image from a reduced set of its moments in assuming that:

   - the Legendre polynomials are orthogonal in the discrete domain; and
   - the solution to the Maximum Entropy reconstruction method is always an exponential function, as derived from the application of Lagrange multipliers.

   However, we have shown that the errors due to the non-orthogonality of the Legendre polynomials is almost negligible as their order increases.

3. The introduction of a new reconstruction method: the backprojection reconstruction method, that only requires $O(m^3)$ subtractions, where m refers to the number of available moments.

4. A matrix-based reformulation of image series approximation from a finite set of projection coefficients upon which two novel reconstruction methods have been proposed:

   - the Chebyshev method, based on orthogonal polynomials of discrete variables, which provides a least-squares reconstructed image. In this case, ill-posedness is solved by assuming that the coefficients obtained from projecting the image onto the polynomial of order higher than the maximum order of available moments are null; and
   - the unitary transform method, based on orthogonal functions, which allows to reconstruct a band-limited or resolution-limited image if Fourier or Haar basis functions are used, respectively.

   Moreover, these methods are general for any set of projection coefficients and any set of orthogonal functions.

The results have been implemented using MATLAB and IEEE floating-point standard arithmetic. Numerical considerations have been taken into account to palliate the ill-conditioning due to roundoff error. Under this consideration, it has been shown that, in the reconstruction process, the truncation error decreases as the number of available moments increases. However, if zero mean gaussian white noise is added to the input data, the ill-conditioning of the linear set of equations amplifies these perturbations. In this case, there exists a particular order of moment, that depends on the basis set used in the reconstruction, for which the reconstruction error has its minimum value.

14.2 Open problems and future research

We have detected some points for future research, connected to our work, that deserve further attention. We include some examples:

1. **Hardware implementation**

   A hardware implementation scheme for accumulation moment computation has been proposed. Since there exist multiple real-time applications that use geometric moments, it seems interesting to effectively implement the proposed hardware.

2. **Moment-invariant low-pass filters**

   It is possible to obtain moment-invariant low-pass filters. For instance, we have proved that a transfer function of the form $H(s) = 1 - (G(s))^n$, where

   $$G(s) = \frac{as + b}{s^2 + as + b},$$

is a moment-invariant low-pass filter that preserves moments up to order $2n$ (there exists some other implementations of these kinds of filters used to generate orthogonal wavelets [35]). If the resulting image is subsampled without aliasing, it has the same moments as the original one. Therefore, it should be possible to obtain the geometric moments of the original image at a lower cost. However, since these filters are not ideal, noise is introduced due to aliasing. Hence, it is possible to compute moments from a subsampled moment-invariant low-pass filtered image if a tradeoff between accuracy and speed of computation is accepted.

3. **Tomographic applications**

   In [70], a relationship between the geometric moments of an image and those of its Radon coefficients has been stated. Radon coefficients are defined as

   $$g(t,\theta) = \int\int f(x,y)\,\delta(t - x\cos\theta - y\sin\theta)\,dx\,dy.$$

   That is, for a fixed θ, the Radon coefficients are the accumulated values of the image along the $\pi+\theta$ direction. When θ ranges from 0 to 2π, a set of accumulation values for different directions is obtained. Notice, from this observation, that accumulation moments and Radon coefficients are intuitively related. Therefore, it seems interesting to exploit this relationship to apply the reconstruction methods proposed in this thesis to tomographic data.

4. **Local constraints in binary image reconstruction**

   A recursive algorithm that sequentially generates all possible binary images that have the same area and centroid has been proposed. The sequential nature of the algorithm allows to introduce local constraints that exploit the neighborhood relationship so that it is possible to efficiently generate images eliminating meaningless solutions prior to its completion. Therefore local constraints such as connectivity, thinness or closed contours can be easily considered.

Bibliography

[1] Ayache, N. Medical computer vision, virtual reality and robotics. *Image and Vision Computing 13*, 4 (May 1995), 295–313.

[2] Bamieh, B., and de Figueiredo, R. J. P. A general moment-invariants/attributed-graph method for three-dimensional object recognition from a single image. *IEEE Journal of Robotics and Automation 2*, 1 (Mar. 1986), 31–41.

[3] Barth, P. *Logic-based 0-1 constraint programming.* Kluwer Academic Press, Boston, 1996.

[4] Bertero, M., Poggio, T. A., and Torre, V. Ill-posed problems in early vision. *Proceedings of the IEEE 76*, 8 (Aug. 1988), 869–889.

[5] Bhattacharya, D., and Sinha, S. Invariance of stereo images via the theory of complex moments. *Pattern Recognition 30*, 9 (1997), 1373–1386.

[6] Brochard, J., Coutin, L., and Leard, M. Modelling of rigid objects by bidimensional moments. Applications to the estimation of 3D rotations. *Pattern Recognition 29*, 6 (1996), 889–902.

[7] Bronshtein, I., and Semendiaev, K. *Manual de matemáticas*, forth ed. Mir, Moscow, 1982.

[8] Burlina, P., and Chellapa, R. Spatio-temporal moments and generalized spectral analysis of divergent images for motion estimation. In *Proceedings of the ICIP-94* (Austin, TX, Nov.13-16, 1994), vol. 1, pp. 328–332.

[9] Burns, J. B. Recognition via consensus of local moments of brightness and orientation. In *IEEE Int. Conf. on Computer Vision and Pattern Recognition* (San Francisco, CA, June 18-20, 1996), pp. 891–898.

[10] Byrne, C. L. Block-iterative methods for image reconstruction from projections. *IEEE Transactions on Image Processing 5*, 5 (May 1996), 792–794.

[11] Carlbon, I., Terzopoulos, D., and Harris, K. M. Computer-assisted registration, segmentation, and 3D reconstruction from images of neuronal tissue sections. *IEEE Transactions on Medical Imaging 13*, 2 (June 1994), 351–362.

[12] Casasent, D., and Psaltis, D. Position, rotation and scale invariant optical correlation. *Applied Optics 15*, 7 (1976), 1795–1799.

[13] CHEDED, L. On quantization and its impact on the exact recovery of high order moments. In *Proceeding of the IEEE Int. Conf. on Acoustics, Speech and Signal Processing* (1995), vol. 3, pp. 1816–1819.

[14] CHEN, C.-C. Improved moment invariants for shape discrimination. *Pattern Recognition 26*, 5 (1993), 683–686.

[15] CHEN, Y. Q. *Novel Techniques for Image Texture Classification.* PhD thesis, ECS Dept. Faculty of Engineering and Applied Science, University of Southampton, Mar. 1995.

[16] CHUNG, K.-L. Computing horizontal/vertical convex shape's moments on reconfigurable meshes. *Pattern Recognition 29*, 10 (1996), 1713–1717.

[17] COMBETTES, P. L. Convex set theoretic image recovery by extrapolated iterations of parallel subgradient projections. *IEEE Transactions on Image Processing 6*, 4 (Apr. 1997), 493–506.

[18] DAI, M., BAYLOU, P., AND NAJIM, M. An efficient algorithm for computation of shape moments from run-length codes or chain codes. *Pattern Recognition 25*, 10 (1992), 1119–1128.

[19] DEN ELSEN, P. A. V., MAINTZ, J. B. A., POL, E.-J. D., AND VIERGEVER, M. A. Automatic registration of CT and MR brain images using correlation of geometrical features. *IEEE Transactions on Medical Imaging 14*, 2 (June 1995), 384–396.

[20] FEDER, M., AND WEINSTEIN, E. Parameter estimation of superimposed signals using the EM algorithm. *IEEE Transactions on Acoustics, Speech, and Signal Processing 36*, 4 (Apr. 1988), 477–489.

[21] FLUSSER, J., AND SUK, T. Pattern recognition by affine moment invariants. *Pattern Recognition 26*, 1 (1993), 167–174.

[22] FOLEY, J. D., VAN DAM, A., FEINER, S. K., AND HUGHES, J. F. *Computer graphics, principles and practice*, second ed. Addison-Wesley, Reading, Massachusetts, 1990.

[23] FORTNER, B. *The data handbook: A guide to understanding the organization and visualization of technical data*, second ed. Springer–Verlag, 1995.

[24] FREUDER, E. C., AND WALLACE, R. J. Partial constraint satisfaction. *Artificial Intelligence 58*, 1-3 (Dec. 1992), 21–70.

[25] GALVEZ, J. M., AND CANTON, M. Normalization and shape recognition of three-dimensional objects by 3D moments. *Pattern Recognition 26*, 5 (1993), 667–681.

[26] G.BROIDA, J., AND WILLIAMSON, S. G. *A Comprehensive introduction to linear algebra.* Addison-Wesley, Redwood City, CA., 1989.

[27] Ghosal, S., and Mehrotra, R. Orthogonal moment operators for subpixel edge detection. *Pattern Recognition 26*, 2 (1993), 295–306.

[28] Ghosal, S., and Mehrotra, R. A moment-based unified approach to image feature detection. *IEEE Transactions on Image Processing 6*, 6 (June 1997), 781–793.

[29] Golub, G. H., Milanfar, P., and Varah, J. A stable numerical method for inverting shape from moments. Submitted to SIAM Journal on Scientific Computing. Also available at http://aeol-www.sri.com/staff/peyman/publications.html, Oct. 1997.

[30] Golub, G. H., and van Loan, C. F. *Matrix computations*, third ed. The Johns Hopkins University Press, Baltimore, Maryland, 1996.

[31] Gruber, M., and Hsu, K.-Y. Moment-based image normalization with high noise-tolerance. *IEEE Transactions on Pattern Analysis and Machine Intelligence 19*, 2 (Feb. 1997), 136–139.

[32] Hamitouche, C., Jacq, J. J., and Roux, C. 3D Segmentation of anisotropic structures using suitable moment-based 3D surface detection. In *Proceedings of the 16th Int. Conf. on New Opportunities for Biomedical Engineers* (New York, NY, 1994), vol. 1, pp. 696–7.

[33] Hatamian, M. A real-time two-dimensional moment generating algorithm and its single chip implementation. *IEEE Transactions on Acoustics, Speech, and Signal Processing 34*, 3 (June 1986), 546–553.

[34] Haykin, S. *Adaptive filter theory*. Prentice-Hall Inc., 1996.

[35] Herley, C., and Vetterli, M. Wavelets and recursive filter banks. *IEEE Transactions on Signal Processing 41*, 8 (Aug. 1993), 2536–2556.

[36] Herman, G. T. *Image reconstruction from projections. The fundamentals of computerized tomography*. Academic Press Inc., 1980.

[37] Herman, G. T., and Meyer, L. B. Algebraic reconstruction techniques can be made computationally efficient. *IEEE Transactions on Medical Imaging 12*, 3 (Sept. 1993), 600–609.

[38] Herman, G. T., and Odhner, D. Performance evaluation of an iterative image reconstruction algorithm for positron emission tomography. *IEEE Transactions on Medical Imaging 10*, 3 (Sept. 1991), 336–346.

[39] Hildebrand, F. B. *Introduction to numerical analysis*, second ed. Dover Publications, Inc., 1974.

[40] Hu, M.-K. Visual pattern recognition by moment invariants. *IRE Transactions on Information Theory* (1962), 179–187.

[41] Ibañez, L., Hamitouche, C., and Roux, C. Moment-based operator for sub-voxel surface extraction in medical imaging. In *Proceedings of the IEEE Int. Conf. on Image Processing* (Lausanne, Switzerland, Sept. 1996), vol. 2, pp. 277–280.

[42] Jiang, X. Y., and Bunke, H. Simple and fast computation of moments. *Pattern Recognition 24*, 8 (1991), 801–896.

[43] Johnston, B., Atkins, M. S., Mackiewich, B., and Andersom, M. Segmentation of multiple sclerosis lesions in intensity corrected multispectral MRI. *IEEE Transactions on Medical Imaging 15*, 2 (Apr. 1996), 154–169.

[44] Kaufman, L., and Neumaier, A. Regularization of ill-posed problems by envelope guided conjugate gradients. Submitted. Also available at http://solon.cma.univie.ac.at/ neum/papers.html.

[45] Kaufman, L., and Neumaier, A. Regularization by envelope guided conjugate gradients. *IEEE Transactions on Medical Imaging 15* (1996), 385–389. Available at http://solon.cma.univie.ac.at/ neum/papers.html.

[46] Kellerer, H. G. Uniqueness in bounded moment problems. *Transactions of the American Mathematical Society 336*, 2 (Apr. 1993), 727–757.

[47] Khare, A., and T.Yoshikawa. Finite word length effects on moment of impulse response of digital filter. *Electronics Letters 28*, 3 (Jan. 1992), 306–307.

[48] Kirsch, A. *An Introduction to the mathematical theory of inverse problems.* No. 120 in Applied mathematical sciences. Springer, New York, 1996.

[49] Klema, V. C., and Laub, A. J. The singular value decomposition: Its computation and some applications. *IEEE Transactions on Automatic Control 25*, 2 (1980), 164–176.

[50] Kontro, J., Kallio$\ddot{j}$arvi, K., and Neuvo, Y. Floating-point arithmetic in signal processing. In *Proc. of the Int. Symposium on Circuits and Systems* (San Diego, CA, May 1992), pp. 1784–1791.

[51] Lee, C.-Y., and Cooper, D. B. Structure from motion: A region based approach using affine transformations and moment invariants. In *Proceedings of the IEEE Int. Conf. on Robotics and Automation* (Atlanta, GA, May 2-4, 1993), vol. 3, pp. 120–127.

[52] Leu, J.-G. Computing a shape's moments from its boundary. *Pattern Recognition 24*, 10 (1991), 949–957.

[53] Li, B.-C. The moment calculation of polyhedra. *Pattern Recognition 26*, 8 (1993), 1229–1233.

[54] Li, B.-C. A new computation of geometric moments. *Pattern Recognition 26*, 1 (1993), 109–113.

[55] Li, B.-C. High-order moment computation of gray-level images. *IEEE Transactions on Image Processing 4*, 4 (Apr. 1995), 502–505.

[56] Li, B.-C., and de Ma, S. Efficient computation of 3D moments. In *Proceedings of the 12th Int. Conf. on Pattern Recognition* (Jerusalem, Israel, Oct.9-13, 1994), vol. 1, pp. 22–26.

[57] Li, B.-C., and Shen, J. Fast computation of moment invariants. *Pattern Recognition 24*, 8 (1991), 807–813.

[58] Li, B.-C., and Shen, J. Pascal triangle transform approach to the calculation of 3D moments. *Computer Vision, Graphics, and Image Processing: Graphical Models and Image Processing 54*, 4 (July 1992), 391–307.

[59] Li, B.-C., and Shen, J. Two-dimensional local moment, surface fitting and their fast computation. *Pattern Recognition 27*, 6 (1994), 785–790.

[60] Li, Y. Reforming the theory of invariant moments for pattern recognition. *Pattern Recognition 25*, 7 (1992), 723–730.

[61] Liao, S. X., and Pawlak, M. On image analysis by moments. *IEEE Transactions on Pattern Analysis and Machine Intelligence 18*, 3 (Mar. 1996), 254–266.

[62] Madych, W. R. Image reconstruction in Hilbert space. In *Proceedings of the Conf. on Mathematical Methods in Tomography* (Oberwolfach, Germany, June 5-11 1990), no. 1497 in Lecture notes in mathematics.

[63] Markandey, V., and de Figueiredo, R. J. P. Robot sensing techniques based on high-dimensional moment invariants and tensors. *IEEE Transactions on Robotics and Automation 8*, 2 (Apr. 1992), 186–194.

[64] Marroquin, J., Mitter, S., and Poggio, T. Probabilistic solution of ill-posed problems in computational vision. *Journal of the American Statistical Association 82*, 397 (Mar. 1987), 76–89.

[65] Martínez, J., Ros, J., and Thomas, F. On the information contained in high-order geometric moments. In *European Workshop on Hazardaous Robotics* (Barcelona, Spain, Nov. 25-26, 1996), pp. 87–91.

[66] Martínez, J., Staffetti, E., and Thomas, F. A recursive updating rule for efficient computation of linear moments in sliding-window applications. In *Proceedings of the 13th. Int. Conf. on Pattern Recognition* (Vienna, Austria, Aug. 25-29, 1996), vol. 2, pp. 295–299.

[67] Martínez, J., and Thomas, F. Accumulation moments. A brief account of their theory and applications. Submitted.

[68] Martínez, J., and Thomas, F. A reformulation of gray-level image geometric moment computation for real-time applications. In *Proceedings of the IEEE Int. Conf. on Robotics and Automation* (Minneapolis, Minnessota, Apr. 22-28, 1996), vol. 3, pp. 2315–2320.

[69] MARTÍNEZ, J., AND THOMAS, F. Fast actualization of moments in sliding window applications. In *Proc. of EUSIPCO. Accepted* (Greece, Sept. 8-11, 1998).

[70] MILANFAR, P. *Geometric estimation and reconstruction from tomographic data.* PhD thesis, Dept. of EECS at Massachusetts Institute of Technology, June 1993.

[71] MILANFAR, P., KARL, W. C., WILLSKY, A. S., AND VERGHESE, G. C. Moment-based geometric image reconstruction. In *Proceedings ICIP-94: IEEE Int. Conf. on Image Processing* (Austin, Texas, Nov. 13-16, 1994), vol. 2, pp. 825–829.

[72] MILANFAR, P., KARL, W. C., AND WILSKY, A. S. Reconstructing binary polygonal objects from projections: A statistical view. *Computer Vision, Graphics, and Image Processing: Graphical Models and Image Processing 56*, 5 (Sept. 1994), 371–391. Also available at http://aeol-www.sri.com/staff/peyman/publications.html.

[73] MILANFAR, P., KARL, W. C., AND WILSKY, A. S. Reconstructing polygons from moments with connections to array processing. *IEEE Transactions on Signal Processing 43*, 2 (Feb. 1995), 432–443. Also available at http://aeol-www.sri.com/staff/peyman/publications.html.

[74] MIRTICH, B. Fast and accurate computation of polyhedral mass properties. *Journal of Graphics Tools 1*, 2 (1996), 31–50.

[75] MUKUNDAN, R., AND RAMAKRISHNAN, K. R. Fast computation of Legendre and Zernike moments. *Pattern Recognition 28*, 9 (1995), 1433–1442.

[76] NAGY, J. G., PLEMMONS, R. J., AND TORGERSEN, T. C. Iterative image restoration using approximate inverse preconditioning. *IEEE Transactions on Image Processing 5*, 7 (July 1996), 1151–1162.

[77] NGUYEN, T. B., AND OOMMEN, B. J. Moment-preserving piecewise linear approximations of signals and images. *IEEE Transactions on Pattern Analysis and Machine Intelligence 19*, 1 (Jan. 1997), 84–91.

[78] NIKIFOROV, A. F., SUSLOV, S. K., AND UVAROV, V. B. *Classical orthogonal polynomials of a discrete variable.* Springer Series in Computational Physics. Springer–Verlag, Berlin, 1991.

[79] PAPADEMETRIOU, R. C. Reconstructing with moments. In *Proceedings of the 11th Int. Conf. on Pattern Recognition* (The Hague, The Netherlands, Aug. 30 - Sept. 3, 1992), vol. C, pp. 476–480.

[80] PAPOULIS, A. *Probability, random variables, and sthocastic processes*, third ed. McGraw-Hill Series in Electrical Engineering: Communication and Signal Processing. McGraw–Hill Books Co., Singapore, 1991.

[81] PAWLAK, M. On the reconstruction aspects of moment descriptors. *IEEE Transactions on Information Theory 38*, 6 (Nov. 1992), 1698–1708.

[82] Pawlak, M., and Liao, S. X. On image analysis by orthogonal moments. In *Proceedings of the 11th Int. Conf. on Pattern Recognition* (The Hague, The Netherlands, Aug. 30 - Sept. 3, 1992), vol. C, pp. 549–552.

[83] Pei, S.-C., and Lin, C.-N. Image normalization for pattern recognition. *Image and Vision Computing 13*, 10 (Dec. 1995), 711–723.

[84] Pei, S.-C., and Liou, L.-G. Using moments to acquire the motion parameters of a deformable object without correspondences. *Image and Vision Computing 12*, 8 (Oct. 1994), 475–485.

[85] Philips, W. A new fast algorithm for moment computation. *Pattern Recognition 26*, 11 (1993), 1619–1621.

[86] Poularikas, A. D. *Signals and Systems.* In The transforms and applications handbook [87], 1996, ch. 1, pp. 1–94.

[87] Poularikas, A. D. *The Transforms and applications handbook.* The Electrical engineering handbook series. CRC Press Inc., Boca Raton, Florida, 1996.

[88] Press, W. H., Teukolsky, S. A., Vetterling, W. T., and Flannery, B. P. *Numerical recipes in C. The art of scientific computing.*, second ed. Cambridge University Press, 1992. Reprinted with corrections 1995.

[89] Prokop, R. J., and Reeves, A. P. A survey of moment-based techniques for unoccluded object representation and recognition. *Computer Vision, Graphics, and Image Processing: Graphical Models and Image Processing 54*, 5 (Sept. 1992), 438–460.

[90] Reeves, A. P., Prokop, R. J., Andrews, S. E., and Kuhl, F. P. Three-dimensional shape analysis using moments and Fourier descriptors. *IEEE Transactions on Pattern Analysis and Machine Intelligence 10*, 6 (Nov. 1988), 937–943.

[91] Reiss, T. H. The revised fundamental theorem of moment invariants. *IEEE Transactions on Pattern Analysis and Machine Intelligence 13*, 8 (Aug. 1991), 830–834.

[92] Reitboeck, H. J., and Altmann, J. A model for size- and rotation-invariant pattern processing in the visual system. *Biological Cybernetics 51* (1984), 113–121.

[93] Rodriguez, G., and Seatzu, S. Approximation methods for the finite moment problem. *Numerical Algorithms 5* (1993), 391–405.

[94] Ros, J. Reconstrucció d'imatges a partir d'un conjunt reduït de moments geomètrics. Master's thesis, TSC Dep., ETSETB, Universitat Politècnica de Catalunya, May 1998.

[95] Rosenfeld, A., and Kak, A. C. *Digital picture processing*, second ed., vol. 1. Academic Press Inc., Orlando, 1982.

[96] Sadjadi, F. A., and Hall, E. L. Three-dimensional moment invariants. *IEEE Transactions on Pattern Analysis and Machine Intelligence 2*, 2 (Mar. 1980), 127–136.

[97] Sardana, H. K., Daemi, M. F., and Ibrahim, M. K. Global description of edge patterns using moments. *Pattern Recognition 27*, 1 (1994), 109–118.

[98] Schmid, C., and Mohr, R. Combining greyvalue invariants with local constraints for object recognition. In *Proc. of the IEEE Int. Conf. on Computer Vision and Pattern Recognition* (San Francisco, CA, June 18-20, 1996), pp. 872–877.

[99] Shen, D., and Ip, H. H. S. Generalized affine invariant image normalization. *IEEE Transactions on Pattern Analysis and Machine Intelligence 19*, 5 (May 1997), 431–440.

[100] Shen, J., and Shen, D. Orthogonal Legendre moments and their calculation. In *Proceedings of the 13th IEEE Int. Conf. on Image Processing* (Vienna, Aug.25-29, 1996), vol. 1, pp. 241–245.

[101] Shen, L., and Sheng, Y. Noncentral image moments for invariant pattern recognition. *Optical Engineering 34*, 11 (Nov. 1995), 3181–3186.

[102] Shen, Y., and Lejeune, C. Invariant pattern recognition using Fourier-Mellin transforms and neural networks. *Journal of Optics 22*, 5 (1991), 223–228.

[103] Siu, W.-C., Lau, A. W.-F., Wong, W.-H., and Lam, K.-M. An analysis on the realisation of two-dimensional image moments. In *Proceedings of the IEEE Int. Conf. on Circuits and Systems* (San Diego, CA, May 1992), pp. 722–725.

[104] Super, B. J., and Bovik, A. C. Shape from texture using local spectral moments. *IEEE Transactions on Pattern Analysis and Machine Intelligence 17*, 4 (Apr. 1995), 333–343.

[105] Talenti, G. Recovering a function from a finite number of moments. *Inverse problems 3* (1987), 501–517.

[106] Teague, M. R. Image analysis via the general theory of moments. *Journal of the Optical Society of America 70*, 8 (Aug. 1980), 920–930.

[107] Teague, M. R. Optical calculation of irradiance moments. *Applied Optics 19*, 8 (Apr. 1980), 1353–1356.

[108] Teh, C.-H., and Chin, R. T. On image analysis by the method of moments. *IEEE Transactions on Pattern Analysis and Machine Intelligence 10*, 4 (July 1988), 496–513.

[109] Tuceryan, M. Moment based texture segmentation. In *Proceedings of the 11th Int. Conf. on Pattern Recognition* (The Hague, The Netherlands, Aug.-30, Sept.-3, 1992), vol. 3, IEEE Computer Soc. Press, pp. 45–48.

[110] Wang, S.-S., Chen, P.-C., and Lin, W.-G. Invariant pattern recognition by moment Fourier descriptor. *Pattern Recognition 27*, 12 (1994), 1735–1742.

[111] Wong, W.-H., Siu, W.-C., and Lam, K.-M. Generation of moment invariants and their uses for character recognition. *Pattern Recognition Letters 16* (Feb. 1995), 115–123.

[112] Wood, J. Invariant pattern recognition: a review. *Pattern Recognition 29*, 1 (1996), 1–17.

[113] Yang, L., and Albregtsen, F. Fast computation of invariant geometric moments: A new method giving correct results. In *Proceedings of the 12th Int. Conf. on Pattern Recognition* (Jerusalem, Israel, Oct.9-13, 1994), vol. 1, pp. 201–204.

[114] Yang, L., and Albregtsen, F. Fast and exact computation of cartesian geometric moments using discrete Green's theorem. *Pattern Recognition 29*, 7 (1996), 1061–1073. Also available at http://www.ifi.uio.no/ lurenya/publications.html.

[115] Yang, L., Albregtsen, F., and Taxt, T. Fast computation of three-dimensional geometric moments using a discrete divergence theorem and a generalization to higher dimensions. *Computer Vision, Graphics, and Image Processing: Graphical Models and Image Processing 59*, 2 (1997), 97–108. Also available at http://www.ifi.uio.no/ lurenya/publications.html.

[116] Yu, T.-H., and Mitra, S. K. Efficient subband analysis of images by the method of moments. *Journal of Electronic Imaging 1*, 1 (Jan. 1992), 68–72.

[117] Zakaria, M. F., Vroomen, L. J., Zsombor-Murray, P. J. A., and van Kessel, J. M. H. M. Fast algorithm for the computation of moment invariants. *Pattern Recognition 20*, 6 (1987), 639–643.

[118] Zhao, D., and Chen, J. Affine curve moment invariants for shape recognition. *Pattern Recognition 30*, 6 (1997), 895–901.

[119] Zhou, F., and Kornerup, P. Computing moments by prefix sums. In *IEEE Int. Conf. on Image Processing* (Lausanne, Switzerland, Sept.16-19 1996), vol. 3, pp. 619–622. Also available at http://www.imada.ou.dk/ kornerup/research.html.

[120] Zongker, D., and Jain, A. Algorithms for feature selection: An evaluation. In *Proceedings of the Int. Conf. on Pattern Recognition* (Vienna, Austria, Aug. 25-29, 1996), vol. 2, pp. 18–22.